POLITECNICO DI TORINO

Collegio di Ingegneria Chimica e dei Materiali

Corso di Laurea Magistrale
in Ingegneria Chimica e dei Processi Sostenibili

Tesi di Laurea Magistrale

Spray freeze-drying of pharmaceuticals

Relatori

prof. Roberto Pisano
prof. Kyuya Nakagawa

Candidato

Gabriele Ruggiero

Dicembre 2019

Index

Sommario esteso

Perché eliminare l'acqua è così importante?

L'acqua è indubbiamente l'elemento più abbondante in natura essendo presente nel corpo umano e in tanti prodotti di utilizzo quotidiano: dal cibo, ai cosmetici ai prodotti farmaceutici. Il contenuto di acqua però, se eccessivo, può portare a una degradazione del prodotto che la contiene. L'acqua è presente in due forme diverse: acqua legata e acqua libera. La prima è la frazione di acqua totale relativa ai vari componenti del materiale, e quindi non essendo disponibile come solvente non influenza in alcun modo la stabilità del prodotto stesso. La seconda non è legata ad altre molecole e viene trattenuta negli interstizi del prodotto a causa della tensione superficiale. L'acqua libera è essenziale per la maggior parte dei processi metabolici dei microrganismi e favorisce reazioni chimiche indesiderate. È quindi evidente che la stabilità non dipende dalla quantità totale di acqua presente, ma solo dal contenuto di acqua libera e dalla sua attività. L'attività dell'acqua, $a_w = P_v/P_{sat}$ dove Pv è la tensione di vapore dell'acqua nel prodotto ad una certa temperatura e P_{sat} è la tensione di vapore dell'acqua pura alla stessa temperatura, influenza infatti sia l'attività microbica dei prodotti sopra menzionati che la loro stabilità chimica e fisica andando così a minare la conservabilità dei prodotti alimentari, cosmetici e farmaceutici. La shelf-life, definita come il periodo di tempo durante il quale un prodotto rimane sicuro, mantenendo le proprietà chimiche, fisiche e microbiologiche desiderate, è fortemente influenzata da, a_w. Essere in grado di misurare e controllare l'attività dell'acqua, significa poter: a) prevedere quali microorganismi saranno potenziali fonti di deterioramento e infezione, b) mantenere la stabilità chimica dei prodotti, c) minimizzare le reazioni di imbrunimento non enzimatico e le reazioni spontanee di ossidazione lipidica auto catalitica, d) prolungare l'attività di enzimi e vitamine, ed e) ottimizzare le proprietà fisiche dei prodotti come la migrazione dell'umidità, la consistenza e la shelf life.
Da qui l'esigenza di poter sviluppare tecnologie per ridurre il contenuto di acqua quando necessario.

Tecnologie di essiccamento

L'essiccamento o disidratazione è, per definizione, l'eliminazione dell'acqua tramite evaporazione, da un prodotto solido o liquido, allo scopo di ottenere un contenuto d'acqua sufficientemente basso. L'eliminazione dell'acqua per essiccamento comprende sempre due processi simultanei che coinvolgono il vapore acqueo: il trasferimento di calore per l'evaporazione dell'acqua al prodotto in essiccamento e il trasporto dei vapori d'acqua formatisi al di fuori del prodotto stesso. Pur essendo utilizzati fin dall'antichità, essendo in grado di rimuovere efficacemente l'acqua, i processi di essiccamento di base hanno mostrato molti limiti come:

- la notevole quantità di spazio necessario per eseguire il processo
- l'elevato numero di operazioni discontinue
- la limitata efficienza termica
- i possibili fenomeni ossidativi sul prodotto dovuti all'uso di aria e ,soprattutto, molto spesso l'uso di aria calda per l'evaporazione dell'acqua non è adatto con prodotti deperibili sensibili alla temperature.
- il calore fornito al prodotto favorisce l'evaporazione dell'acqua, riducendone il contenuto può avere profondi effetti sulla qualità dei prodotti disidratati.

Per questo motivo ha preso sempre più piede un tipo di essiccamento che assicura la riduzione del contenuto di acqua, eliminandola non tramite evaporazione ma sublimazione.

Liofilizzazione

Con il termine liofilizzazione (freeze-drying) si definisce un processo in cui si rimuovono, attraverso sublimazione, le molecole di solvente, quasi sempre acqua, presenti in un dato materiale. Il processo di essiccamento è condotto in condizioni di bassa temperatura e alto vuoto, le quali consentono la processabilità di tutti quei prodotti che sono termo-sensibili. La temperatura del prodotto durante il processo di essiccamento è inferiore agli 0° C (-20/-40 °C), mentre la pressione operativa è inferiore alla tensione di vapore del solvente a quella determinata temperatura (5-100 Pa). Tale processo ha un ampio impiego nell'industria farmaceutica in quanto, a queste condizioni estremamente cautelative, i processi chimici e biologici che possono portare alla denaturazione del prodotto si fermano, non intaccando le proprietà biologiche e terapeutiche. Questo è però possibile solo se si utilizzano degli eccipienti, sostanze che proteggono le molecole più sensibili dagli stress indotti dal processo di liofilizzazione stesso. Come già detto la liofilizzazione è il processo più comunemente utilizzato oggi (principalmente in campo farmaceutico) per produrre farmaci allo stato solido al fine di stabilizzare quindi, tutti quei principi attivi che non lo sono in fase liquida.
La liofilizzazione permette di ottenere molteplici vantaggi quali: la stabilità dei principi attivi, la facilità di stoccaggio, anche a temperatura ambiente, e di somministrazione del liofilizzato, la possibilità di condurre il processo in ambienti privi di contaminanti (ambienti sterilizzati, a temperature molto basse e in condizioni di vuoto spinto), e la possibilità di reidratare il componente essiccato in tempi brevi.

Le fasi della liofilizzazione

Il processo di liofilizzazione prevede tre fasi: il congelamento (solidificazione del campione), essicamento primario (sublimazione del ghiaccio), essicamento secondario (rimozione per desorbimento delle molecole di solvente non solidificate poiché legate alle molecole di soluto). Durante il congelamento la temperatura del prodotto viene abbassata fino a raggiungere un valore tra -40°C/-50°C in modo da far permettere la formazione di ghiaccio, che inizia sottoforma di nucleazione, continuando poi con la crescita dei cristalli. È estremamente importante che il campione sia completamente congelato prima di tirare il vuoto e iniziare il processo di essiccazione degli step successivi. Il prodotto non congelato infatti può espandersi all'esterno del contenitore se posto sottovuoto e collassare per l'aumento di temperatura delle fasi successive al congelamento.
Durante l'essicamento primario viene innescata la sublimazione, così da rimuovere il ghiaccio formatosi, andando a ridurre la pressione nella camera al di sotto della tensione di saturazione del solvente, e aumentando la temperatura così da sopperire al calore rimosso dalla sublimazione. Alla fine di questa prima fase il contenuto di umidità residua del liofilizzato è tipicamente attorno al 5-10%. Questo perché è ancora presente una parte di acqua non congelata, e ancora legata al soluto che viene però ridotta durante la fase di essicamento secondario. In quest'ultimo step rispetto all'essicamento primario, la temperatura viene ulteriormente aumentata ed è relativamente breve rispetto alle prime portando alla fine il contenuto di acqua al 1-2% rispetto alla massa di materiale secco.

Nonostante sia largamente usato per diverse applicazioni poiché, rispetto al normale processo di disidratazione, la liofilizzazione non espone componenti labili al calore, assicura un ottimo comportamento di reidratazione ed è adatto al trattamento di prodotti di alta qualità; questo metodo presenta comunque dei limiti:
- riscaldare il prodotto a temperature troppo elevate può causare la fusione o il collasso del prodotto;
- il sovraccarico del condensatore causato dal troppo vapore che una volta formatosi viene catturato sulla sua superfice;
- il soffocamento del vapore, il vapore viene prodotto ad una velocità superiore a quella che può passare attraverso la porta tra la camera del prodotto e il condensatore, creando un aumento della pressione.

Spray freeze drying (SFD)

La liofilizzazione spray-freeze-drying (SFD) è una tecnica di liofilizzazione che produce prodotti in polvere includendo i vantaggi dei prodotti liofilizzati convenzionali. L'SFD ha potenziali applicazioni in prodotti di alto valore grazie al maggior mantenimento, rispetto ad altre tecniche di essiccamento, della struttura del prodotto e della qualità e ritenzione di composti volatili e bioattivi. Il mantenimento di queste caratteristiche fa distinguere lo SFD nonostante i costi e la complessità. Questa tecnologia aggiunge, alle fasi tradizionali della liofilizzazione, uno step iniziale. Un processo di SFD si esplica nel modo seguente:

- Atomizzazione della soluzione liquida o della sospensione;
- Congelamento delle goccioline in un liquido o vapore criogenico;
- Sublimazione del ghiaccio e desorbimento dell'acqua legata.

Lo sviluppo del processo e le fasi principali (spraying, freezing e drying) sono illustrate in figura 1.

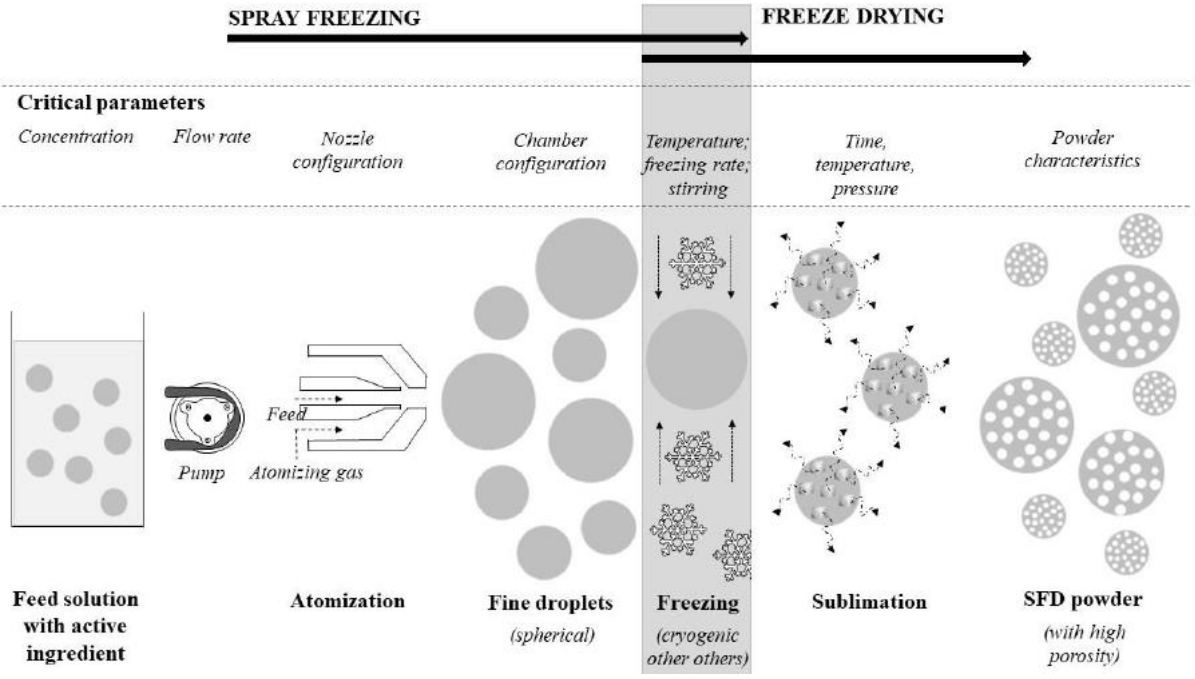

Figura 1: Illustrazione del processo di SFD (Vishali *et al.*, 2019).

Modellizzazione del processo di congelamento

Il primo step della liofilizzazione, ossia il congelamento, è la parte più delicata da sviluppare, in quanto determina le proprietà più importanti del liofilizzato quali la struttura e la morfologia. Da qui l'esigenza di derivare un modello che permetta di prevedere le ripercussioni del processo di congelamento sul prodotto finale. Tra le tante, la caratteristica che più interessa monitorare è il crystal size: cioè la dimensione dei pori lasciati dal ghiaccio a seguito della sublimazione.
La dimensione dei cristalli di solvente è di massima importanza per quelle soluzioni farmaceutiche che devono essere liofilizzate (la maggior parte dei farmaci è infatti insolubile in solventi polari e necessitano quindi di essere disidratati) perché influenza fortemente sia la dinamica del prodotto, cioè la temperatura massima raggiunta dal prodotto congelato durante l'essiccamento e il tempo di lavorazione oltre che la capacità degli additivi di preservare il principio attivo contro il congelamento e le sollecitazioni di essiccamento. Come ulteriore esempio, la dimensione dei cristalli di ghiaccio ha un forte impatto sulla proprietà organolettiche degli alimenti surgelati, mentre nel caso di leghe metalliche di cristallo le dimensioni dei pori influisce notevolmente sulle proprietà meccaniche del materiale. Trattandosi di una miscela acqua-soluto essa non congela a 0°C a pressione atmosferica, come suggerisce la termodinamica; per avere il *congelamento* della miscela si deve infatti raffreddare al di sotto della temperatura eutettica (Te), se si è in presenza di un soluto cristallino, oppure al di sotto della temperatura di transizione vetrosa (Tg), se si ha invece un soluto amorfo. In generale possono essere presenti entrambe le tipologie di soluto, e in questo caso si deve tener conto del fatto che i soluti amorfi congelano solo al di sotto della Tg.
Una prima influenza sulla dimensione dei cristalli è data dalla velocità di raffreddamento:

- Un raffreddamento lento ($< 0.5\ ^\circ C min$) comporta bassa velocità di congelamento, e quindi la formazione di grandi cristalli di ghiaccio che hanno più tempo per crescere, ed una concentrazione del soluto uniforme.

- Un Raffreddamento veloce (5-300 $^\circ C min$) comporta piccoli cristalli di ghiaccio essendo la loro formazione più rapida, che impediscono la fuoriuscita dell'acqua non congelata e allungano il tempo di essicamento. La concentrazione di soluto non è uniforme soluto si concentrerà solo in alcune regioni della soluzione. Alcune molecole di acqua non riescono a muoversi verso i nuclei e si comporteranno come un solido, rimanendo intrappolate tra i cristalli, seppur ancora allo stato liquido.

Risulta quindi essenziale poter conoscere nel dettaglio quello che succede durante il congelamento. In generale, tale trasformazione è costituita da tre fasi principali (figura 2), la fase di supercooling (A-B), in cui la formulazione liquida viene raffreddata dalla sua temperatura iniziale T_0 alla temperatura del punto di congelamento; il cambiamento di fase (B-C), quando il primo nucleo di ghiaccio inizia a formarsi e successivamente cresce; e la fase di solidificazione (da C in poi), in cui tutta l'acqua cristallizzabile viene separata come ghiaccio. La figura 2 mostra chiaramente l'evoluzione della temperatura (monitorata tramite termocoppie) di una formulazione liquida farmaceutica sottoposta a congelamento.

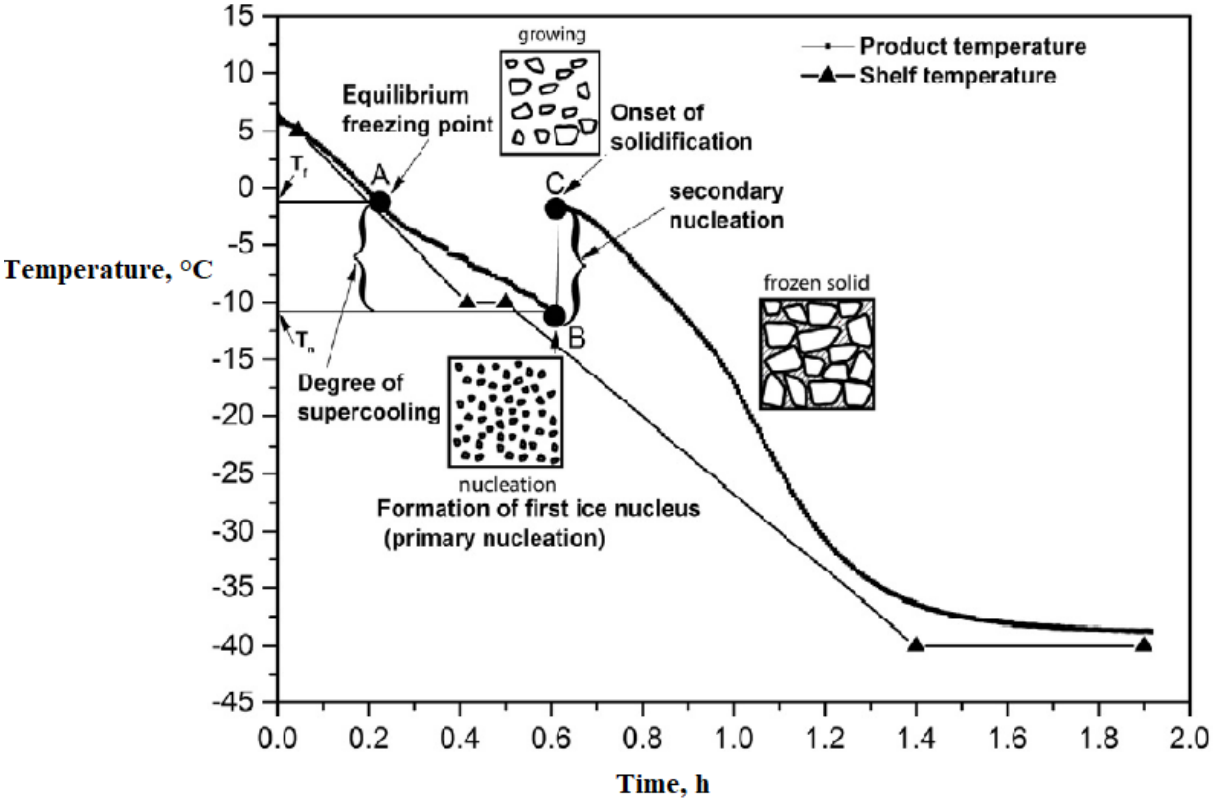

Figura 2: Le tre fasi del congelamento mostrate sul profilo della temperatura nel tempo. Dal punto di vista termodinamico, la soluzione dovrebbe congelare non appena la sua temperatura raggiunge il punto di equilibrio. In realtà, questo cambiamento di fase è evidente solo quando la sua temperatura è inferiore al valore di equilibrio, questo fenomeno viene chiamato supercooling (A-B). Una volta avvenuta la nucleazione, cioè l'aggregazione di molecole d'acqua in gruppi stabili, la cristallizzazione del ghiaccio avviene rapidamente all'interno dell'intero volume del sistema, (B-C). Durante questa fase, i gruppi d'acqua sono disposti in modo periodico che definisce la struttura cristallina. Una volta che i cristalli si sono formati, essi crescono progressivamente per aggiunta di molecole d'acqua sulla loro interfaccia (Cin poi), la fase di crescita cristallina.

Per un efficace sviluppo di processo e scale-up è stata sviluppata una modellazione matematica. L'obiettivo è quello di poter predire la dimensione dei cristalli finali; in letteratura ci sono molte leggi empiriche che condividono la stessa struttura e legano la velocità di congelamento con la dimensione media dei cristalli tramite due parametri: la velocità del fronte di congelamento ν (m/s) e il gradiente di temperatura della zona congelata θ (K/m). Tali modelli sono però empirici, cambiando da applicazione ad applicazione: in questo lavoro è stato derivato un modello il più generale possibile così da poter essere applicato a diversi scenari noti soltanto i due parametri sopra citati. Questi vengono calcolati tramite la simulazione di un processo di congelamento usando il programma COMSOL (vers 5.3).
Dato che lo SFD produce particelle di piccole dimensioni e più o meno sferiche il volume di controllo considerato è un guscio sferico di volume $dV = 4\pi r^2$ dr e superficie $dS = \pi r dr$. Su questo viene fatto un bilancio entalpico, tenendo in considerazione i due termini sorgente dati dal calore di cristallizzazione e quello di nucleazione:

$$\begin{pmatrix} heat\ removed\ by \\ the\ frozen\ product \end{pmatrix} + \begin{pmatrix} heat\ generated\ by \\ crystallization \end{pmatrix} + \begin{pmatrix} enthalpy\ change\ due\ to \\ new\ interface\ generation \end{pmatrix} = 0$$

Per i dettagli della derivazione vedere il capitolo 2 del manoscritto, il risultato finale del modello dopo opportune semplificazioni e modifiche è:

$$D_{p,i} = 4m\theta_i * \gamma a_{S,i} v_i \Big/ \left[\varrho_{ice} \left(m\theta_i * v_i \Delta H_f - 4k_f \theta_i^* \pi r^2 \Delta r \sum_{i=1}^{n} \theta_i^* \right) \right]$$

Per il calcolo di v e θ è stata svolta una simulazione su COMSOL vers. 5.3. La particella modellizzata è stata assunta come perfettamente sferica, le principali assunzioni sono sotto riportate:

- Particella sferica di raggio 50 µm.
- Coordinate sferiche per studiare il sistema
- Composta di pura acqua.
- Temperatura iniziale di 293 K.
- Come mezzo congelante è stato simulata aria a 223K
- Come meccanismo di trasferimento di calore la sola convezione, qualsiasi contributo dovuto all'irraggiamento è stato trascurato.
- Date le dimensioni della particella, nonostante sia coinvolto un cambiamento di fase come coefficiente di scambio termico h è stato calcolato quello di acqua liquida pari *1.67552, W/(m^2*K)*.
- Temperatura di nucleazione pari a 263K.
- La mesh scelta è quella densa triangolare non strutturata, date le ridotte dimensioni della particella e la velocità nel congelamento.

Come condizioni al contorno:

$$\begin{cases} I.C \;\; at\; t \leq 0 & T = T_0 & for\; all\; r, \theta, \varphi \\ B.C \;\; at\; r = R & J|_{r=R} = h(T_{air} - T|_R) & for\; all\; t, \theta, \varphi \\ B.C\; at\; r = 0 & \dfrac{\partial T}{\partial r} = 0 & for\; all\; t, \theta, \varphi \end{cases}$$

Da queste simulazioni sono stati ottenuti i profili termici della particella per la determinazione di v e θ. Con questi è stato possibile calcolare il D_p andando a simulare particelle di varie dimensioni (figura 3). Si può notare l'andamento del diametro medio dei pori, nello specifico di come questo aumenti all'aumentare della particella in esame. Inoltre, è possibile osservare che esiste una relazione lineare, purché la gocciolina sia sufficientemente piccola, cioè con d < 9 mm (per le gocce più grandi, questo non è più vero).
Perciò è stata ottenuta la relazione lineare utilizzabile per il confronto con i dati sperimentali (figura 4), valida però per particelle più piccole di 1cm, che permette di prevedere noto il diametro particellare quello dei pori presenti nel prodotto finale. Essendo l'azoto il fluido più utilizzato per il congelamento (e anche quello usato nelle prove sperimentali) è stata ripetuta la stessa procedura di simulazione utilizzando però azoto a 80K. Così è stato possibile ottenere la relazione lineare da confrontare in seguito con i risultati ottenuti a Kyoto (Eq 1).

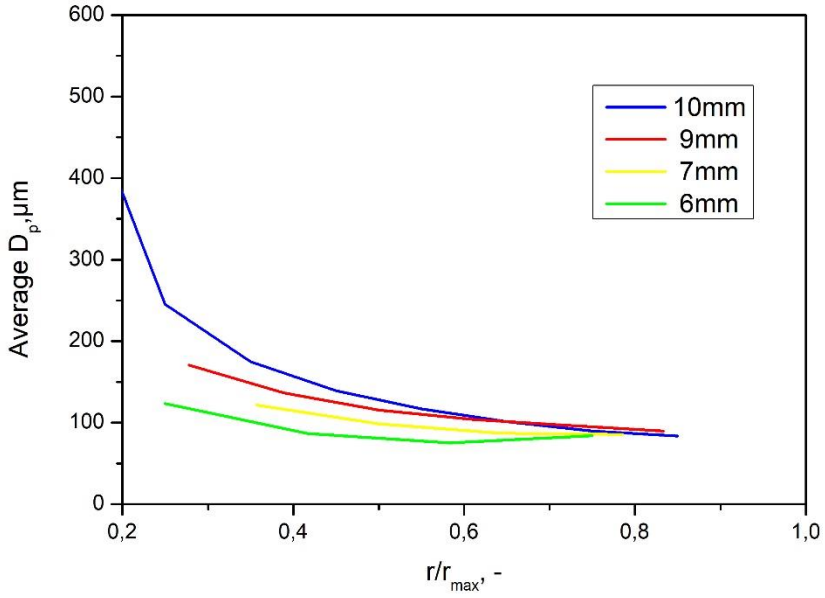

Figura 3: andamento di D_p al variare del raggio della particella.

La relazione ottenuta è:

$$D_p = 3.82d \qquad (1)$$

Convalida sperimentale

Nel laboratorio dell'università di Kyoto sono state svolte le prove sperimentali. L'obiettivo è stato quello di ricreare un processo di SFD e di calcolare sperimentalmente il diametro medio dei pori ottenuti nel liofilizzato. Per ottenere questo sono state preparate 3 soluzioni acquose contenenti soluti tipicamente liofilizzati nelle applicazioni farmaceutiche perché usati per proteggere i principi attivi di interesse.
Tutte e tre le soluzioni sono state preparate a partire da acqua distillata:

1. Soluzione A: 10%$_{w/w}$ of mannitolo.
2. Soluzione B: 15%$_{w/w}$ of mannitolo.
3. Soluzione C: 5%$_{w/w}$ di trealosio e 5%$_{w/w}$ di albumina.

Le tre soluzioni dopo essere state preparate sono state atomizzate sperimentando due diverse tecnologie (figura 4):

1. L'atomizzazione pneumatica ottenuta tramite un aerografo; il flusso di aria pressurizzata incontra, in prossimità dell'orifizio, la corrente liquida disperdendola cosi in fini particelle.
2. L'atomizzazione vibrazionale ottenuta tramite una siringa fatta vibrare da un motore; l'alimentazione liquida arrivata sulla punta dell'ago viene frantumata in fini gocce dal moto vibrante imposto.

Figura 4: Immagine dei meccanismi usati per atomizzare le soluzioni. Meccanismo 1 sulla sinistra, meccanismo 2 sulla destra.

I due metodi differiscono per forma e dimensione delle particelle ottenute: il metodo1 porta alla formazione di diametri dell'ordine dei µm (1-100 µm) inutilizzabile per la misura dei pori mentre il metodo 2 crea particelle più larghe dell'ordine dei mm (1-5 mm) utilizzate per la determinazione dei pori.
Per il congelamento, come già detto, è stato utilizzato dell'azoto liquido; questo è stato versato all'interno di un vassoio rettangolare in cui le particelle sono state fatte cadere. Una volta congelate sono state raccolte e inserite nell'essiccatore.
Come essiccatore ne è stato usato uno costruito dal professor Nakagawa in cui il condensatore e la camera di essiccamento sono disposti nello stesso spazio (figura 5).

Figura 5: Essiccatore usato a Kyoto.

Il vuoto era assicurato da una pompa collegata direttamente con il dispositivo. Riguardo il tempo di essiccamento invece, a causa della sua natura di laboratorio e quindi data l'impossibilità di poter intervenire a riguardo, è stato applicato sempre lo stesso(12h). Il condensatore è stato mantenuto a -60°C e poi aumentato a +5°C mentre lo shelf da -25°C a +20°C. Per poter calcolare la loro dimensione i campioni delle tre soluzioni descritte sono stati sottoposti al microscopio a scansione di elettroni (SEM). Le foto così ottenute sono state usate per calcolarne la distribuzione e ottenere un valore medio. Le distribuzioni sono mostrate in figura 7.

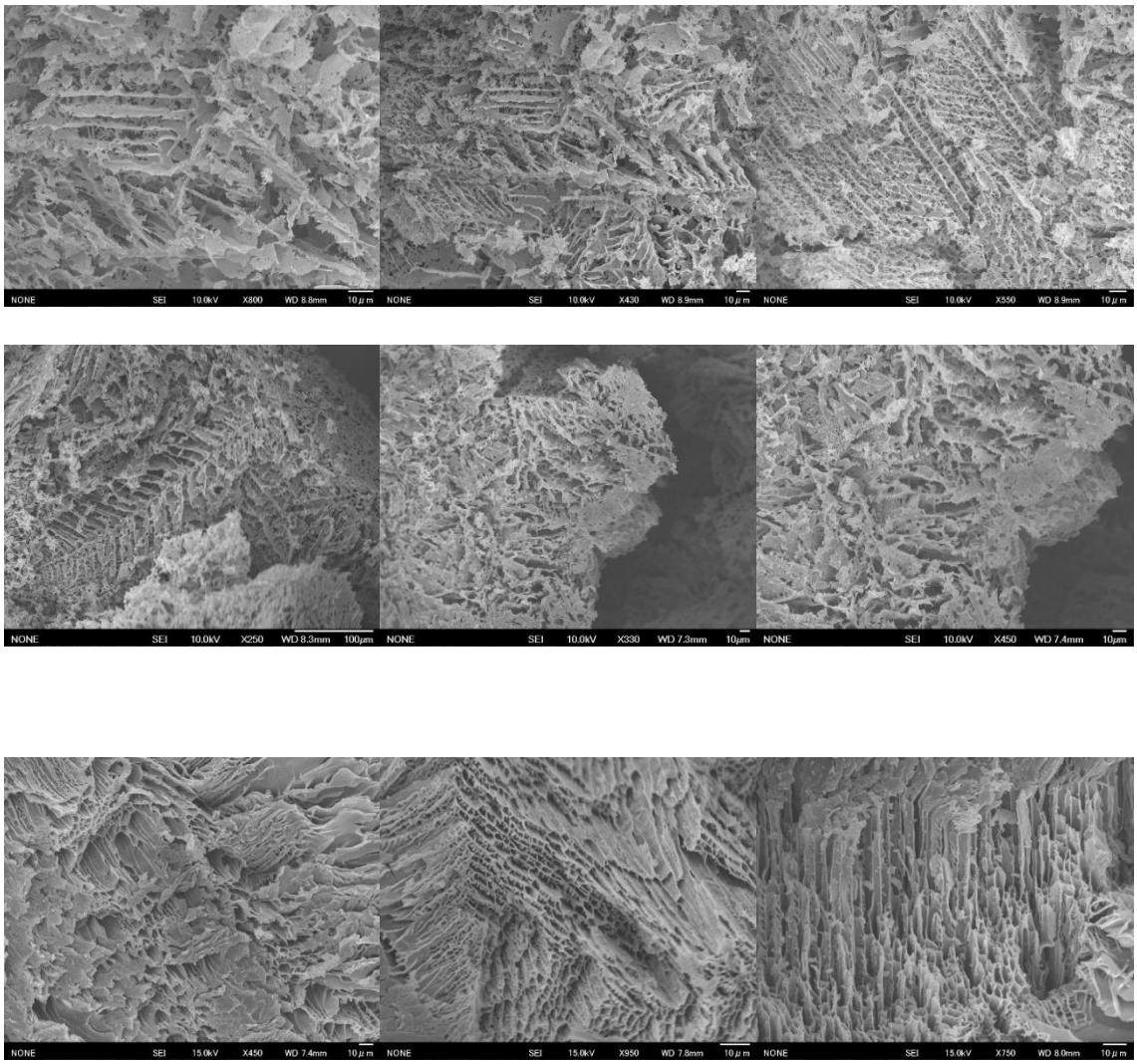

Figura 6: Immagini SEM usate per il calcolo del diametro dei pori. Sono presentate 3 foto per ogni concentrazione, in ordine le soluzioni A, B, C.

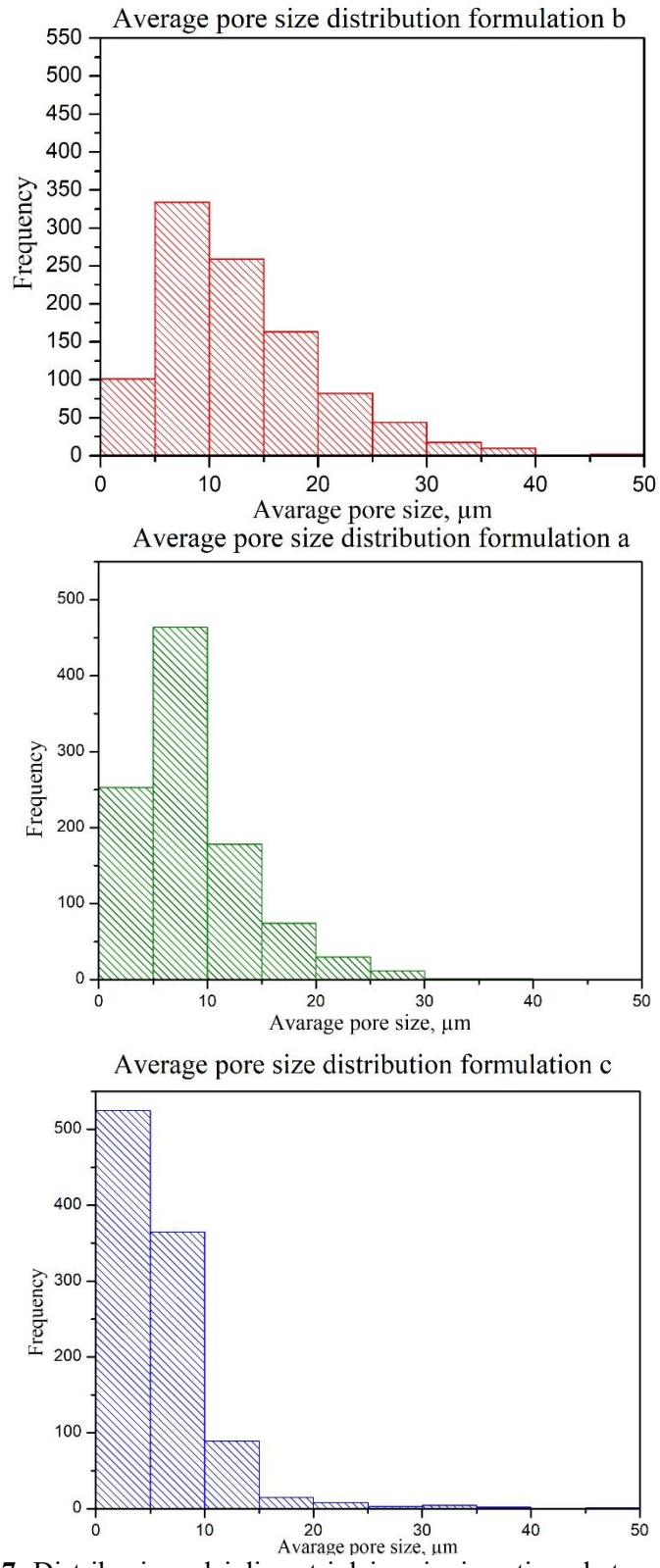

Figure 7: Distribuzione dei diametri dei pori misurati per le tre soluzioni.

I valori dei diametri trovati sono i seguenti 8.7 µm per la soluzione A, 12.7 µm per la B e 6.1 µm per la C. Come è possibile notare dalle distribuzioni la soluzione C mostra dei pori più omogenei e piccoli risultando quindi più vantaggiosa in termini di controllo del prodotto finale.

Per la convalida del modello è stata misurata una particella dalla formulazione C, con un d=1.5mm; usando la relazione lineare Eq 1 è possibile ottenere la dimensione dei pori corrispondenti: D_p = 5.73 µm. Questo è un valore molto simile a quello ottenuto sperimentalmente (6.12 µm). Nonostante la leggera discrepanza e la necessità di una convalida sperimentale più estesa, i primi risultati mostrano le potenzialità del modello nel predire la morfologia delle particelle congelate, a partire dalla dimensione delle gocce e temperatura del fluido criogenico, e quindi del comportamento delle stesse durante la fase di essiccamento primario.

Questo è un altro punto di forza nell'ottica di sviluppare un processo in continuo aumentando la produttività senza compromettere la soluzione trattata e assicurando l'uniformità del prodotto finale.

Chapter 1
Introduction

1.1 Why drying?

Water is essential to life, providing a universal solvent to support biochemical activities within cells hence enabling metabolism to continue and sustains all living processes. Quite simply, in the absence of water, life as we define it will cease, resulting in a state of death or dormancy in live cells or inhibiting biochemical activity in cellular extracts. Water is indeed the most abundant chemical compound on Earth, covering 71.12% of the planet surface and being the main constituent of the human body. It is also contained in many everyday products but often such presence is unwanted as it leads to the degradation of the products themselves in a short time. If we consider food the water content is variable depending on the production and kind of product but in general has to be monitored and removed if the content exceeds same critical value. Hence, there is increasing interest in developing conservation techniques to increase the duration of stocks, reduce packaging costs, reduce the weight of the products facilitating their transport and storage by removing water. Such techniques include drying, lyophilization and then, a quite recent method, spray freeze drying.

1.2 Water and its activity

Water is present in two distinct forms: bound water and free water. The first is that fraction of total water related to the various components of the food, is therefore not available as solvent and, consequently, does not affect the stability of the product. The second is not bound to other molecules and is held in the interstices of the substance due to surface tension only. Free water is essential for most of their metabolic processes of microorganisms and promotes undesirable chemical reactions. It is therefore clear that stability of a food does not depend on the total amount of water present, but only on content of free water and on its activity. Shelf life is defined as the time during which a product will remain safe, maintaining desired chemical, physical and microbiological properties still complying with nutritional labelling. Water activity, $a_w = P_v/P_{sa}$ where P_v is vapor tension of water in the product at a certain temperature e P_{sat} is the vapour tension of pure water at the same temperature, influences in fact both the microbial activity of the products mentioned above and their chemical and physical stability. Water activity strongly influences the shelf life of food, cosmetic and pharmaceutical products strongly affecting these three aspects. Chemical reactivity is altered as the water acts as a solvent by modifying the mobility of the reagent substances, thus affecting viscosity. a_w also influences non-enzymatic harness, lipid oxidation, vitamin degradation, enzyme reactions, protein denaturation, starch gelatinisation, starch retrogradation. Since a_w describes the state of thermodynamic energy of water within a system, there is a close relationship between a_w, physical stability and shelf life of a product. The major cause of deteriorative physical changes and texture loss in food (Oetjen and Haseley, 2004) is moisture migration. This could be caused by different levels of a_w between components or a component and the ambient humidity, resulting in a moisture migration. Everything depends on the value of a_w for the two components X and Y. If both have the same a_w value, there will be no exchange of moisture: it is the case of hygroscopic excipients used with pharmaceutical products sensitive to moisture. With the same principle, if two components with the same percentage of moisture are mixed, but with

different value of a_w, the system will experience an exchange of moisture until a balance of the value of a_w is reached. Regarding the microbiological proliferation, mould and microbial growth are the most dangerous threats to shelf life. Controlling water activity can inhibit or preclude microbial growth, extend shelf life, and allow some products to be safely stored without refrigeration. For each microorganism there is a specific water activity level (named critic) below which that microorganism cannot grow, so it is important to carefully tune it in order to avoid undesired growth. One or a combination of any of these factors can lead to faster deterioration and a shortened product shelf life. Non-enzymic browning reactions increase with increasing a_w to a maximum at 0.6 to 0.7 a_w (Troller and Christian, 1978). Lipid oxidation has a minimum at about 0.2 to 0.3 as a_w. Moisture migration is a major cause of deteriorative physical changes and texture loss in food. Water activity is a function of temperature, thus shipping and storage temperature changes water activities effect on the microbial, chemical and physical properties. It is important to determine critical water activity levels for a product and how sensitive it is to changes in water activity. Optimum chemical stability is generally found near the monolayer moisture content, as determined from moisture absorption isotherms. Changes in water activity by absorption of water when a product is exposed to a high humidity environment or loss of water when placed in a low humidity environment brings about undesirable changes in products and shortens shelf life. These changes can be physical, such as loss of crispness in dry products, caking and clumping of powders, or moist products losing water to become tough and chewy (Kawasaki, Shimanouchi and Kimura, 2019). In order to stabilize labile products, it is therefore necessary to immobilize or reduce the water content of stored samples. Hence the interest, since ancient times, in developing conservation techniques to increase the duration of stocks, reduce packaging costs, reduce the weight of the products facilitating their transport and storage. Industries and researchers develop new technologies seeking to meet three main objectives: economic (reduction of costs), environmental (reduction of energy consumption), product quality (preservation of organoleptic characteristics and nutritional of the fresh food (Valdenegro M *et al.*, 2013).

1.3 Drying

Drying is the most ancient methods of perishable goods (mainly used for food) preservation known to mankind. Preservation of meat, fish, coffee beans and food plants by drying in the sun or in the naturally dry air has been practiced since the origin of mankind and is still a vital operation in the life of many rural communities and industries (Doymaz, 2004). Drying or dehydration is, by definition, the removal of water by evaporation, from a solid or liquid food, with the purpose of obtaining a solid product sufficiently low in water content (Jennings, 1999). Drying is a much more costly process than other food preservation techniques, as it requires large quantities of energy; for this reason, it is important to work in optimal conditions with the aim of limit its energy consumption still ensuring the main technological objectives of perishable material dehydration which are:

- Preservation as a result of depression of water activity;
- Reduction in weight and volume;
- Transformation of a food to a form more convenient to store, package, transport and use; for example, transformation of liquids such as milk, eggs, fruit and vegetable juices, or coffee extract, to a dry powder that can be reconstituted to the original form by addition of water (instant products);
- Preservation in food goods of a desirable feature such as a certain flavour, crispiness, chewiness, etc., during the creation of new food (e.g., transformation of grapes to raisins); or in pharmaceutical products of a specific active principle.

The removal of water by drying always includes two simultaneous processes involving water vapour: the transfer of heat for the evaporation of water to the product under drying and transport of the water vapours formed away from the product itself. Drying (Banga and Paul Singh, 1994) is, therefore, an operation based on a simultaneous heat and mass transfer, where the rate limiting mechanism may be superficial evaporation or internal transport of water, depending on the process conditions used. Depending on how heat and mass are transferred, industrial drying processes can be grouped into two categories: convective drying and conductive (boiling) drying.

- Convective drying: a hot and dry gas (usually air, in this case named air drying) is used to supply the heat necessary for evaporation and to remove the water vapor from the surface of the product intended to dry (Figure 1.1). Both heat and mass exchanges between the gas and the particle are essentially convective transfers, although conduction and radiation may also be involved to some extent.

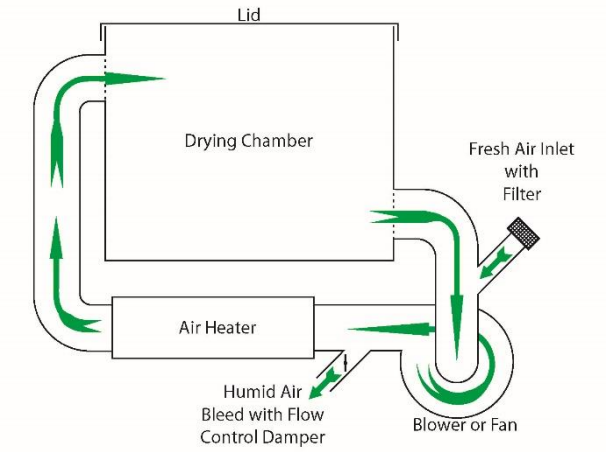

Figure 1.1: Air drying process plant scheme. Figure reprinted from https://techblog.ctgclean.com (last access 2/09/2019) with modifications.

- Conductive (boiling) drying: The moist-like product is brought in contact with a hot surface (or in specific applications with superheated steam). The water in the food is "boiled-off" (Figure 1.2). Boiling drying is tantamount to evaporation to dryness. Fall into this drying category: vacuum drying, drum drying, and drying in superheated steam.

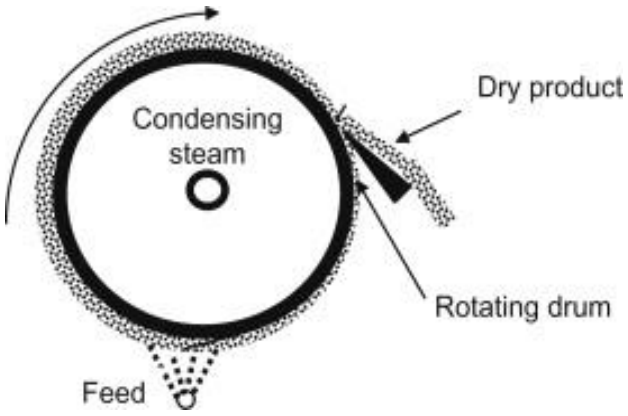

Figure 1.2: Boiling drying process plant scheme. Figure reprinted from https://techblog.ctgclean.com(last access: 2/09/2019), with modifications.

Although being used from ancient times and being capable of removing water effectively, drying basic processes have shown many limitations such as the significant amount of space required to carry out the process, the high number of discontinuous drying, the limited thermal efficiency, the possible oxidative phenomena on the product due to the use of air and most of all really often the use of hot air for water evaporation is not suitable with perishable temperature sensible goods. The heat given to the product promotes water evaporation, reducing the water content but may have profound effects of the quality of dehydrated products. Texture, structure, appearance, colour, flavour, taste, and nutritional value are all subject to change as a result of the drying. For that reason, the technological advance has investigated different methods of removing water from goods developing the freeze-drying (lyophilization) technology, that is another method of water removal based on the sublimation of water from a frozen material under high vacuum in order to avoid unwanted changes in characteristics and structure of the treated product.

1.4 Lyophilization

Freeze-drying (FD) or lyophilization consists of removing water from a liquid, pasty or solid product by freezing and sublimation under vacuum. When water is heated in the solid state and at very low pressure, it sublimates and passes into the gaseous state (water vapour). This water vapor that is released from the solid product is trapped on a condenser or trap. The peculiar aspect of FD, that makes it different from other dehydration techniques, is that dehydration takes place while the product is in a frozen state and under a vacuum.). However due to the low pressure at which the FD process is carried out, water vapor has a very large specific volume. In order to remove such big volumes of vapor in gaseous state, the vacuum pump must have unrealistically large displacement capacity. To overcome this problem, the vapours are condensed as ice crystals on the surface of condensers kept at extremely low temperature. These conditions stabilize the product, minimizing the effects of oxidation and other degradation processes, not altering its quality once freeze-dried. It is the only drying method that perfectly preserves the molecular structure of the temperature sensitive products (Cleland, Powell and Shire, 1993). For example, in case of proteins the molecules after the process are totally preserved in their native state, the vitamins are not destroyed, the different freeze-dried micro-organisms are intact (Sonner, Maa and Lee, 2002). FD is, however, an expensive method of dehydration, feasible only in the case of high value-added products and whenever the superior quality of the product justifies the higher production cost (Sadikoglu, Ozdemir and Seker, 2006). The phase diagram of pure water (Figure 1.3) indicates that sublimation of ice can occur only if the vapor pressure and temperature are below those of the triple point of water below 612 Pa and 0.01°C, respectively

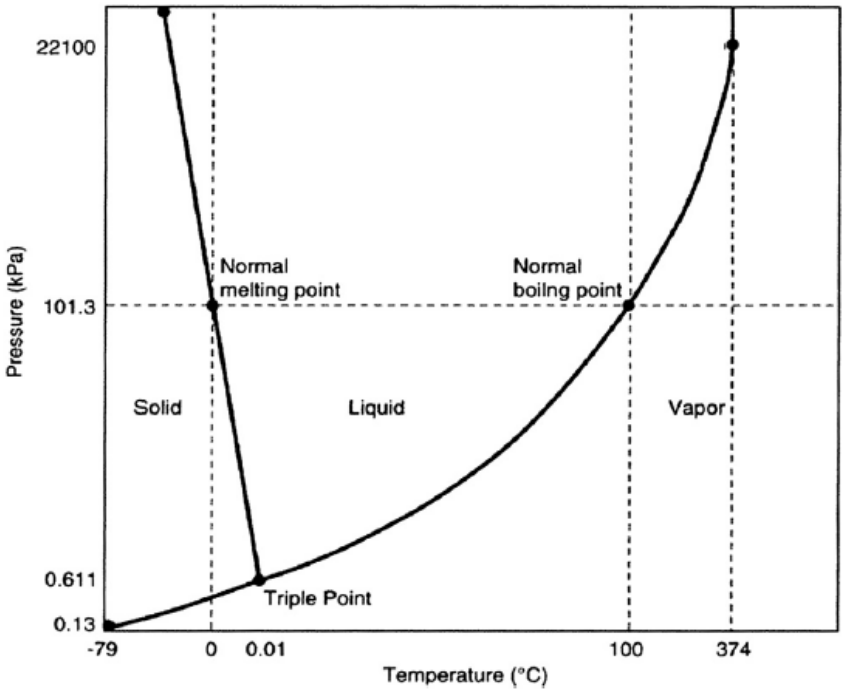

Figure 1.3: Phase diagram of water. Figure reprinted from http://scienzaduepuntozero.pbworks.com (last access: 2/09/2019), with modifications.

.

From a theoretical point of view, FD could be carried out at atmospheric pressure. If the partial pressure of water is very low, when for example the air is very dry, sublimation of ice can occur. The atmospheric freeze drying occurs in nature, for example, when snow "disappears" without melting in cold, dry weather(Claussen *et al.*, 2007). In practice, however, freeze drying is carried out at very low total pressure (typically 10–50 Pa). Typically, FD is carried to a final moisture content of 1%–3%. Lyophilization requires the design of a working process or cycle also known as a "recipe". Each specific product or formulation that is lyophilized requires the development of a freeze-drying process that is based on the unique characteristics of the product itself, the amount of product and the container used. There is no universal "safe" set of parameters, the "recipe", that will work with every product (Fissore and Barresi, 2011).

1.5 The freeze-drying process steps

Regardless of the application of the FD process, there are 4 basic steps:

1. Freezing;
2. Primary Drying (ice sublimation);
3. Secondary Drying (moisture desorption).

1.5.1 Freezing

Since FD provides for a change in the matter state from the solid to the gaseous phase, material to be freeze dried must first be adequately frozen. Freezing step is when the sample is frozen to a temperature below its "eutectic point" , T_e, freezing point, at which all the material is in a frozen state (Kasper and Friess, 2011). This is typically in the range of -40 to -60°C, whereas certain applications can go as low as -60 to -80°C. In fact for a crystalline product the transition from liquid to solid of water takes place if the temperature is brought below a critical value called eutectic temperature T_e, while for an amorphous solid the transition takes place only

below the transition temperature T_g glass, which is strongly dependent on the water content, in particular decreases with increasing the activity of the water (Nireesha *et al.*, 2013). The method of freezing and the final temperature of the frozen product can affect the ability to successfully freeze dry the material. Rapid cooling results in small ice crystals, useful in preserving structures to be examined microscopically, but resulting in a product that is more difficult to freeze dry. Slower cooling results in larger ice crystals and less restrictive channels in the matrix during the drying process. For example, for cells, bacteria etc. it is generally preferable for the freezing rate to be high, to obtain a significant number of small crystals rather than a small number of large crystals, which may damage the structure of the solid. Products freeze in two ways, depending on the makeup of the product. Most products that are subjected to freeze drying consist primarily of water, the solvent, and the materials dissolved or suspended in the water, the solute. Most samples that are to be freeze dried are eutectics which are a mixture of substances that freeze at lower temperatures than the surrounding water. When the aqueous suspension is cooled, changes occur in the solute concentrations of the product matrix. As cooling proceeds, the water is separated from the solutes as it changes to ice, creating more concentrated areas of solute. These pockets of concentrated materials have a lower freezing temperature than the water. The mixture of various concentration of solutes with the solvent constitutes the eutectic of the suspension. Only when all the eutectic mixture is frozen is the suspension properly turns into ice. This is called the eutectic temperature. It is very important in FD to freeze the product to below the eutectic temperature before beginning the drying process since small pockets of unfrozen material remaining in the product can expand and compromise the structural stability of the freeze-dried product. Another class of frozen product is a suspension that undergoes glass formation during the freezing process. Instead of forming eutectics, the entire suspension becomes increasingly viscous as the temperature is lowered. Finally, the product freezes at the glass transition point forming a vitreous solid, this type of product is extremely difficult to freeze dry. The kinetic aspect of freezing according to the values of temperature with respect to time. The products to be lyophilised are composed generally from solutions concentred whose freezing is different from pure water. At the beginning, the solution is at room temperature (Figure 1.4); subtracting heat temperature goes down linearly until it begins to form ice with consequential emission of latent heat of crystallization (A). Continuing to cool the temperature decreases in until the eutectic point is reached and the mixture solidifies; since a phase transition occur the temperature stays constant (B); continuing to subtract heat, there will be a linear cooling because there are no longer any state changes (Fissore, Pisano and Barresi, 2019).

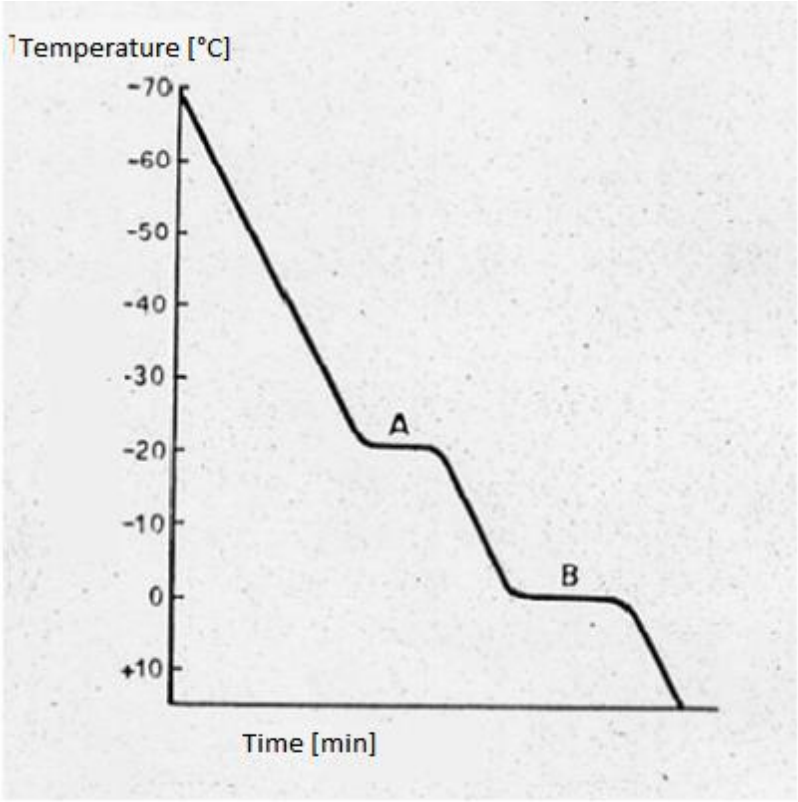

Figure 1.4: Temperature profile during freezing. Figure reprinted from https://pim-resources.coleparmer.com/ (last access: 2/09/2019), with modifications

Once the freezing point (eutectic point) of the product is determined, the optimal rate of freeze must also be determined since the properties of the lyophilised material strictly depend on the method used to freeze the solution. The solidification is the result of two consecutive phenomena: the nucleation of the crystal of ice and the growth of the same. If the solidification takes place in a time for which growth is faster than nucleation: larger crystals are obtained, creating a structure with wider pores during the next drying, reducing the resistance to steam transport during sublimation. In some cases, it is recommended a quick freezing, to get small ice crystals, which impact less on product quality (Holzwarth *et al.*, 2012), with speed of cooling of 0.5-1°C/min (Oetijen and Haseley, 2004). Typically, this is advantageous for the optimization of FD cycles but may not result in the best product in terms of rehydration (reconstitution). On the other hand, a fast-freezing rate will result in a product that turns inactive at a faster rate and has a smaller crystalline structure, which in turn results in it being more granulated and therefore easier to reconstitute, even if it takes longer to freeze dry. During freezing, the freeze dryer works as a freezer, in that no vacuum is applied. Freezing could also be done separately from the dryer. The freezing step is of paramount importance, as it determines the ice morphology and pore size distribution, which is essential for success later in the process. This seems rather elementary, but it is often the least understood and investigated step of the process.

1.5.2 Primary Drying

During primary drying, ice sublimates (turning directly into vapor) under ultra-low pressure, typically around 0,01 hPa (mBar) or lower, depending on the freezing temperature of the sample

and at cooler temperatures, safely below the maximum allowable product temperature. The driving force of sublimation is the difference between the ice vapor pressure, that depends on the product temperature, and the partial pressure of water inside the drying chamber. The vacuum speeds up the process by removing air molecules to allow sample vapor molecules to move easier from the sample, through the chamber and into the condenser. Typically, shelf temperatures during primary drying are ramped from –30 to +20°C during the process time, which can vary from a few hours to several days. The shelf temperatures indirectly influence the temperature of the sample by conducting heat (contact to the shelf) as well as the radiating of heat from the shelf above. During the primary drying phase, it is essential to heat the product as much as possible (without passing the eutectic point) in order to maximize the ice vapor pressure and hence the driving force for mass transfer However, it is important to remember that the heat input constraints are often caused by the product's own thermal characteristics. If a product has a eutectic temperature of -10°C, then the product may be taken to a temperature of -15°C. All three methods of heat transfer - conduction, convection and radiation, must be considered when freeze drying a product. When using a vial chamber system (shown in Figure 1.5) is it possible to control the energy input to the product via temperature and pressure control. These controls allow to optimize the FD cycle. Primary drying is typically the part of the process that takes the longest and is therefore subject to optimization such as adjusting the temperature and pressure in order to bring the product as close as possible to its collapse conditions, but without overcoming this upper bound(Patel, Doen and Pikal, 2010).

Figure 1.5: Vial freeze dried products. Figure reprinted from https://www.cleanroomtechnology.com/ (last access: 2/09/2019), with modifications

1.5.3 Secondary drying

During this step, in addition to the free ice that is sublimed during primary drying, there remains a substantial amount of water molecules that are bound to the product (that is why the water being removed, desorbed, during this desorption step is referred to as "bound" (Prestrelski *et al.*, 1993). Since all the free ice has been removed in primary drying, the product temperature can now be increased considerably shelf temperature is, however, usually never raised above +42°C, as biological samples contain proteins that would denaturize as a result of this. Vacuum is at this point very high (low pressure) as no- or very few vapor molecules are present. This part of the FD cycle typically represents less than half of the total cycle but is highly essential for the final moisture content of the sample. Indeed, secondary drying is continued until the

product has acceptable moisture content for long term storage. Depending on the application, moisture content in fully dried products is typically between 0.5% and 3%. In most cases, the drier the product is, the longer its shelf life will be. However, certain complex biological products may become too dried for optimum storage results and the secondary drying process should be controlled accordingly. In the pharmaceutical field, in order to have the most stable product possible, the water content at the end of this phase must be less than 1% (Sarciaux *et al.*, 1999); but this must be balanced with the need for the temperature in the hottest part of the sample not to exceed the spontaneous combustion temperature (scorch temperature) of the freeze-dried product, above which reactions of inactivation of the drug may occur. The ideal process is therefore able to combine conditions of low thermal stress with conditions of high-water removal. This can only be obtained using FD chambers equipped with stoppering arrangements for sealing the vials with, e.g., rubber stoppers that close under vacuum, or by equalizing the chamber vacuum with an inert gas, such as anhydrous nitrogen. Typically, cell cultures, pharmaceuticals and diagnostic kits are subject to this low level of residual water content. Methods such as the Karl Fisher Titration Test or weighing the sample pre and post process may be used as a check of the residual moisture content. From a reconstitution point of view, it is not advantageous to aim for a lower residual moisture level than required, as it will get increasingly longer and more difficult. Once the product is determined to be at the end of its cycle it must be removed from the freeze dryer. If bulk chambers are used, the system is brought to atmospheric conditions by "bleeding" air or nitrogen into the chamber before unloading the trays. Product processed in this manner will absorb the water vapor that it meets. Consequently, this product should be processed or stored as quickly as possible. When drying the vials, they are usually closed off under vacuum (or back pressurized with N_2 to atmospheric conditions), meaning that they do not require as quick treatment and only need appropriate storage. Secondary drying starts during the primary phase, but at elevate temperatures desorption proceeds much more quickly. Secondary drying rates are dependent on the product temperature. System vacuum may be continued at the same level used during primary drying; lower vacuum levels will not improve secondary drying times. Amorphous products may require that the temperature increase from primary to secondary drying is controlled at a slow ramp rate to avoid collapse. without fear of melting or collapse. The amount of bound, or residual water, in the product is dependent on the amount of time the product remains in the secondary drying phase. The removal is controlled and optimized by increasing the shelf temperature to its allowable maximum value. In fact have in the 90s have been shown how secondary drying only depends on the temperature of the chamber instead of the pressure (Pikal *et al.*, 1990).

1.5.4 A traditional cycle

A typical sublimation cycle is shown lingering on both pressure and temperature profiles in Figure 1.6. The product is first cooled to a temperature lower than its eutectic point (Point A). The collector is cooled to a temperature approximately 20° C cooler than the product temperature, generally around -50 to -105° C. The product, as already stated, is freeze dried at a temperature slightly lower than its eutectic or collapse temperature (Point B) since the colder the product, the longer the time required to complete primary drying, and the colder the collector temperature required to adequately freeze dry the product. After the product is adequately frozen and the collector temperature achieved, the system is evacuated using a vacuum pump (Point C). At this point, primary drying of the product begins and continues until the entire frozen matrix appears dry. Heat input to the product may be achieved by several means such as increasing the shelf temperature in the case of tray drying or using a liquid bath for manifold drying. While the collector and vacuum pump create the conditions for allowing

sublimation to occur, heat input is really the driving force behind the whole process. Heat input to the sample can be enhanced by controlling the pressure in the system at some level above the ultimate capability of the vacuum pump. freeze dryers incorporate vacuum control systems that automatically regulate the pressure to the pre-set level. This improves the sublimation rate, reducing process time and associated energy costs. Care must be taken to prevent the pressure within the system from exceeding the ice vapor pressure of the product or melting of the sample may occur.

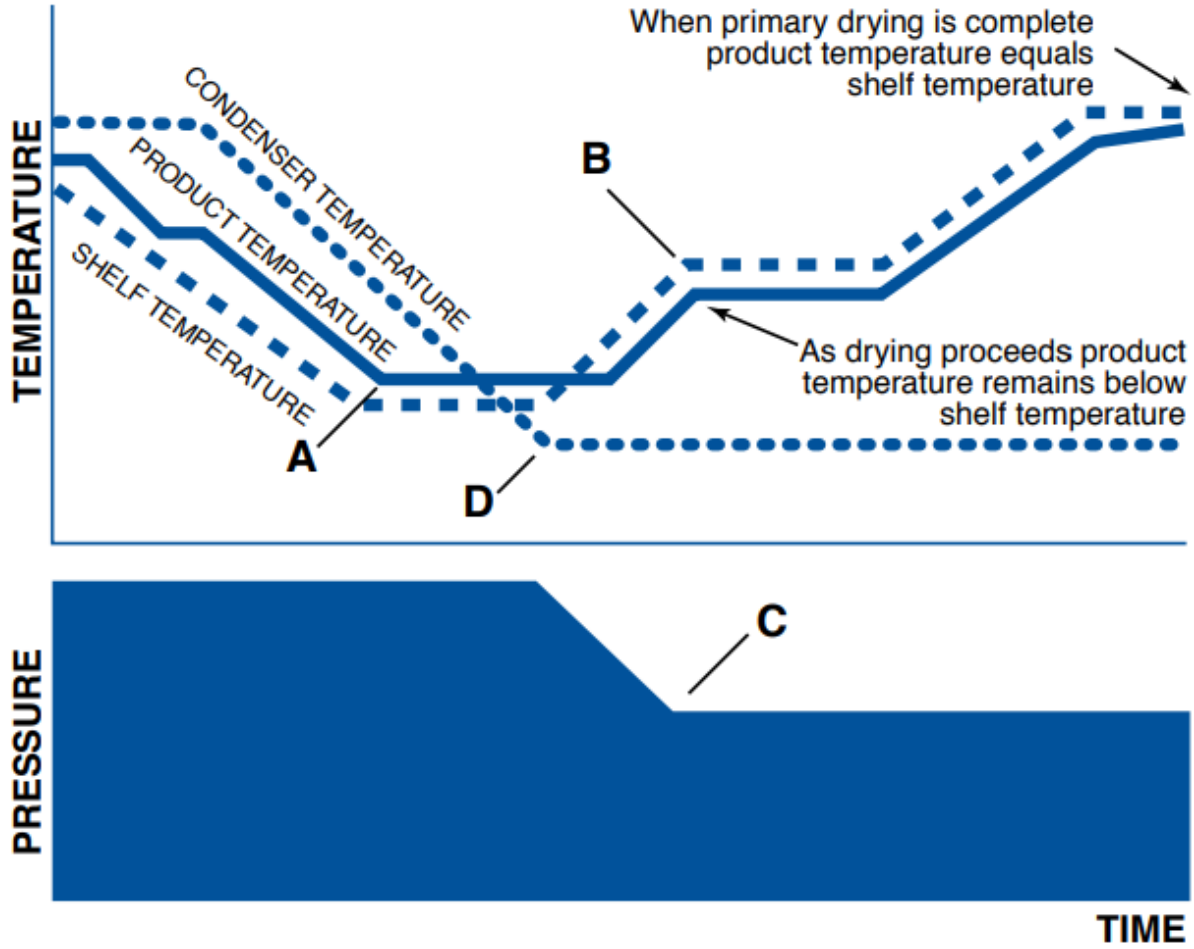

Figure 1.6: Example of a FD cycles following the profiles of both temperature and pressure. Figure reprinted from https://www.drugdiscoverytrends.com/ (last access: 2/09/2019), with modifications.

Despite being used very often for several applications because, compared to the normal drying process FD preserves heat labile components, ensures a very good rehydration behaviour and it is suitable for treating high quality product, this method has same limitations such as:

- Heating the product too high in temperature can cause melt-back or product collapse;
- Condenser overload caused by too much vapor hitting the condenser;
    - Too much vapor creation
    - Too much surface area
    - Too small a condenser area
    - Insufficient refrigeration

- Vapor choking – the vapor is produced at a rate faster than it can get through the vapor port, the port between the product chamber and the condenser, creating an increase in chamber pressure.

1.6 Spray Freeze Drying

Spray freeze drying (SFD) is a technique wherein an atomized liquid spray is sprayed into a cryogenic medium, and the spray droplets are quickly frozen. Once frozen, these frozen droplets are lyophilized (freeze-dried) to remove the frozen solvent and leave particles behind. This technique is used as an alternative to conventional spray drying for thermo-sensitive compounds that have particular issues with the heated chamber and/or gas used in conventional spray drying but are retained or reacted as desired with the combination of flash freezing and lyophilization. SFD is thus a unique drying technique as it is a combination of both spray drying and freeze drying (Mujumdar, Huang and Dong Chen, 2010). Such a technique is of p interest in the pharmaceutical and food industries, as well as to produce ceramic powders, and perhaps other fields where conventional spray drying, or spray pyrolysis may be typically used. SFD can also be used to produce microspheres or other microparticles of various morphologies and compositions. It was obtained by the continuous research of different approaches have been proposed by various researchers to reduce the costs of conventional freeze drying. Spray freeze-drying is a three-step semi-continuous process that addresses the limitations of conventional technologies for biologics processing. It takes its concept from attempts to reduce drying time of a conventional FD process by first atomizing a liquid food into a suitable low temperature zone (maintained usually with a cryogen such as liquid nitrogen). Following this, sublimation of the frozen particles occurred under atmospheric pressure. Logically, reduction in product dimensions improves heat transfer and associated mass transfer, and hence, freezing and FD times reduce. The three major steps involved include (Figure 1.7): dispersion of bulk liquid solution into droplets, solidification of droplets by direct contact with the cold fluid, and sublimation of the solidified droplets at a very low temperature and pressure. In SFD technique, atomization is the primary step in which the liquid is broken down into smaller droplets. For the atomization process, two-fluid, and three-fluid, four-fluid and ultrasonic nozzles can be used(Her *et al.*, 2010). Amongst different types of nozzles used, ultrasonic nozzle was reported to have good control over the particle size and four fluid nozzles were found to be suitable for drugs with poor aqueous solubility. Apart from that, atomization plays a critical role in determining the particle size distribution of the sprayed droplets. Factors influencing atomization include feed viscosity, atomization energy, the feed flow rate and surface tension. Therefore, in order to achieve smaller droplet size, high atomization pressures are required. After atomization, freezing is carried out below the sub-zero temperatures in the presence of a cryogenic fluid such as liquid or gaseous nitrogen.

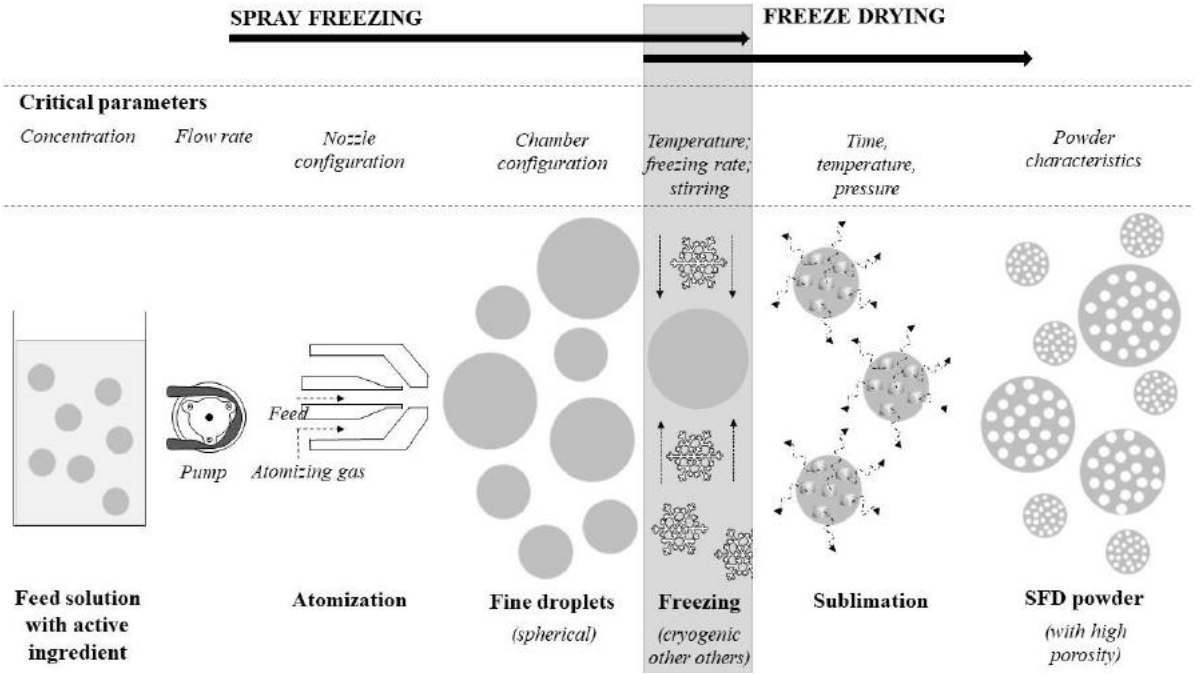

Figure1.7: Overall view of SFD process. (Vishali *et al.*, 2019)

1.7. Motivation of this thesis

This work aims to contribute to the development of a model used to predict the freezing step at which undergo the products spray-freeze-dried. What is of interest is being able to know and model the ice crystal size that corresponds to the void left in the dried process. At first a mathematical model has been obtained and solved using a software and then it has been validated with experimental data. The first part has been carried out at Polytechnic of Turin and the experimental one at Kyoto University of technology.

Among the three different phases of an SFD process, this work focuses on freezing which is, despite the apparent simplicity, the most difficult to tune and predict. What is very hard is understanding how it affects the characteristics of the final product obtained; above all interest is focused on the dimension of the ice crystals obtained once the product is frozen

The prediction of the average size of solvent crystals formed during freezing of a solution is a major issue in various fields as food, chemical, and pharmaceutical industries. Hence the importance to be able to tune the crystal size by finding a correlation between the thermal history during the freezing step of the product processed and the average size of solvent crystal.

From literature there are many examples of derivation of this correlation and most of them are primarily empiric due to the difficulty of knowing physical parameter a priori. This work offers two different approaches whit the same aim, the impact of freezing conditions on the average size of ice crystals and, thus, of pores.

In the first part of this thesis, attention was focused on the derivation of a mechanistic model that describes the freezing process of droplets in direct contact with a cryogenic gas. The

results have then been compared with experimental data obtained during the second part of the thesis, which has been carried out at the Department of Chemical Engineering of Kyoto University.

In this chapter, the theoretical base of the lyophilization has been explained comparing the main drying methods existing and highlighting the major features of SFD process as the most advantageous among the others.

In chapter 2 the most important aspects relating to the process of freezing are discussed. We focus, starting from an enthalpic balance, on the mathematical modeling which correlates the average size of crystals in a dried material to the freezing front rate and the temperature gradient in the frozen area. Parameters obtained from the simulation of the freezing process in COMSOL vers.5.3 for a spherical particle in contact with a cryogenic fluid (what happens in an SFD process)

In chapter 3 the experimental part carried out in Kyoto is explained. There an SFD the process was simulated using different formulations and atomizers to freeze the particles obtained into liquid nitrogen. The hence obtained sample was dried by using a drier built by Nakagawa's team and then subjected to different analyses to characterize the dried formulation.

In chapter 4 the results obtained from the experimental test are presented with the information obtained from the dried sample. Thus, the experimental data have been compared to the theoretical one for the determination of the average crystal size.

Chapter 2

Mathematical modelling of the spray freezing process

For pharmaceutical applications, much attention has been given to the problem of predicting the average size of solvent crystals formed during the freezing of solutions containing active principles. The crystal size, that is the void left by the ice sublimated, is crucial for the characteristics of the final dried product. All the already proposed methods are based on empirical laws and are variable depending on the operational condition; in this chapter a mechanistic model is derived to give physical theoretical background on the relationship between solvent crystal size, the velocity of the freezing front R, and temperature gradients G which was postulated by the empirical laws. To obtain these parameters is required to understand the freezing process: on COMSOL (vers 5.3) freezing has been simulated on a spherical particle in order to obtain the thermal history of the body. From the results of the simulations the parameters are calculated and a theoretical law for the crystal size obtained.

2.1 The fundamentals of freezing

Among the three phases of an SFD process, this work focuses on the freezing of droplets. Freezing conditions tremendously impact on the ice crystal morphology, size, and size distribution, which influence several quality attributes of the dried product as well as its behaviour during drying. In fact, the frozen product morphology influences its resistance to vapor flow, specific surface area, primary and secondary drying rates, crystallinity, and its ability to be retreated without suffering of severe drawbacks. Therefore, it is of upmost importance to understand the correlation between freezing conditions and product morphology. Among all the features which characterized a frozen product the crystal size is certainly the most important. In general, freezing consists of three main stages, the supercooling stage(A-B), in which the liquid formulation is cooled down from its initial temperature T_0 to the freezing point temperature; (B-C) the phase change stage, when the first ice nucleus start to form and subsequently grows; and (C) solidification stage, in which all the crystallizable water is separated as ice (Evans, 2009). These three phases can be identified in Figure 2.1, which clearly shows the evolution of temperature (monitored through thermocouples) of a pharmaceutical liquid formulation subjected to freezing.

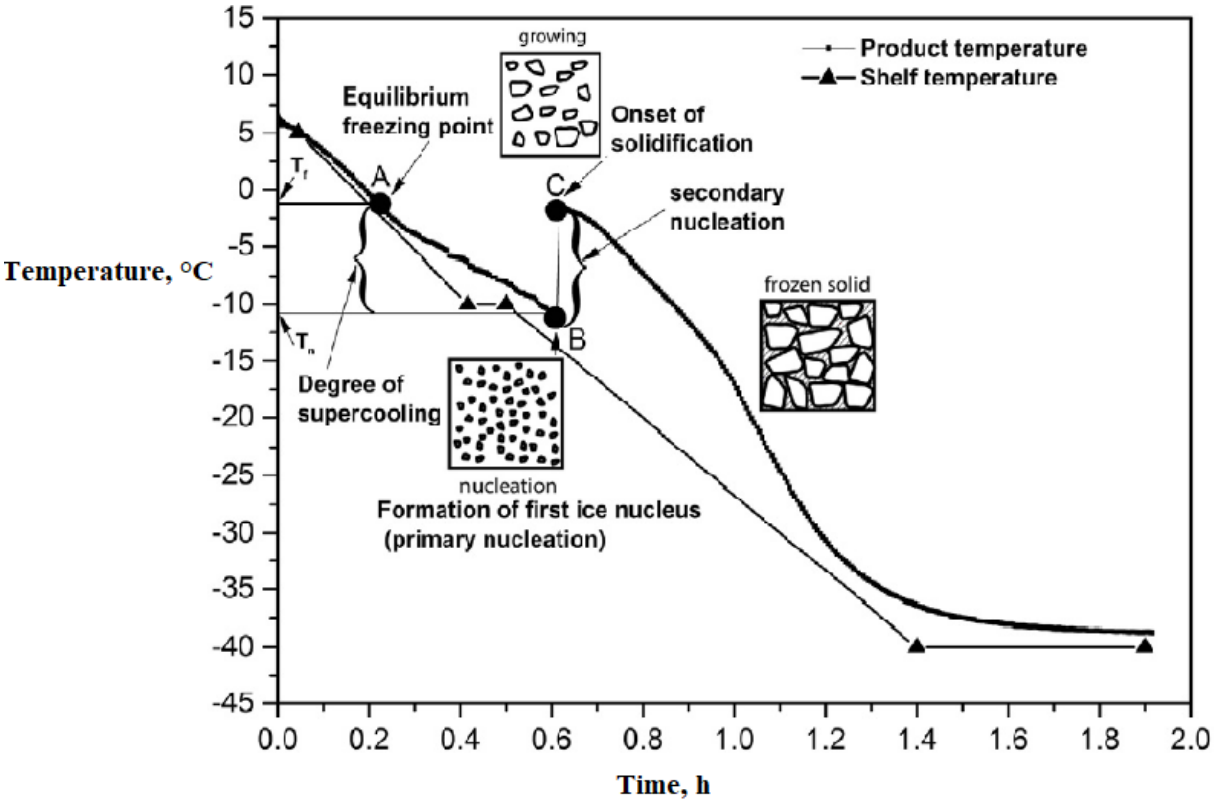

Figure 2.1: The three phases of freezing shown on the temperature profile over time. From a thermodynamic point of view, the solution should freeze as soon as its temperature reaches the equilibrium state. However, this phase change is only evident when the temperature is below the equilibrium value, which is called supercooling (A-B). Once nucleation has occurred, i.e. the aggregation of water molecules into stable groups, the crystallization of the ice occurs rapidly within the entire volume of the system, (B-C). During this phase, the water groups are periodically arranged to define the crystalline structure. Once the crystals have formed, they progressively grow by adding water molecules to their interface (Chin then), the crystalline growth phase.

2.1.1. Cooling of the liquid

During the cooling phase, the temperature of the solution is progressively reduced till the first, stable ice nucleus is formed. The value of temperature at which this happens is defined as nucleation temperature and is denoted as T_n. When an aqueous system is cooled at atmospheric pressure, freezing is not spontaneously occurring at the equilibrium freezing point, but the solution retains its liquid state to a certain degree. For an aqueous system the equilibrium freezing requires both the availability of an ice crystal nucleus and the absence of appreciable temperature differences within the system. When either of these two conditions is not fulfilled, supercooling occurs. Supercooling is therefore the ability of an aqueous system to maintain its liquid state below its equilibrium freezing point. It is a nonequilibrium and metastable state during which long-living hydrogen bonds are established between water molecules that arrange themselves to form clusters with similar molecular arrangements to ice crystals. Since these clusters are not stable, but break up rapidly, supercooling is energetically unfavourable. This breaking process continues until an adequate number of molecules are associated in all the three dimensions to form a thermodynamically stable aggregate, known as critical nucleus, which acts as a suitable surface for crystal growth. The equilibrium freezing point of a pharmaceutical formulation is shown in Figure 2.1 as point A. Because of supercooling, freezing does not start at point A, but the liquid state is retained by the solution until point B when the first, stable ice nucleus is formed. The segment AB represents the supercooling of the liquid and the

corresponding temperature difference is the degree of supercooling. It is quite variable and affected by several factors, such as container surface area, process conditions, presence of extraneous particles, filling volume and contact area between sample and container.

2.1.2 *Ice crystal growth*

Once a formulation reaches its ice nucleation temperature T_n, point B of Figure 2.1, the phase change from liquid to solid starts and the first ice nucleus appears. This phenomenon is also known as primary nucleation. This process is extremely fast and interests the entire volume of the system. Primary nucleation is immediately followed by secondary nucleation (from point B to C in Fig. 1) which basically consists in the addiction of ice nucleation sites. During this phase in fact a crystal structure is obtained by the arrangement of water-clusters in a periodic manner. Once formed, the ice crystals grow by the progressive addition of water molecules onto their interface (crystal growth phase). The ice crystals formation is an exothermic process so, in order to allow the process to continue, the heat released during this phase must be removed. This is ensured by the supercooled solution, which is at a fixed degree below the equilibrium freezing temperature. During the process, the supercooled solution absorbs a limited amount of heat leading to a quick increase of temperature of the solution to its equilibrium freezing temperature where there is no more formation of ice crystals, point C of Figure 2.1. How much heat has been absorbed during the secondary nucleation phase determines the total number of ice crystals formed, which depends on the degree of supercooling. The higher is the degree of supercooling, the bigger is the amount of heat to be absorbed during the exothermic crystallization process and this grants the formation of many ice crystals.
The mass fraction of water that undergoes the phase change crystallizing during nucleation (X_{ice}) can be calculated according to Equation 2.1, in which the extent of supercooling is used to absorb the heat of crystallization up to the equilibrium freezing point:

$$X_{ice} = \frac{m_{wn}}{m_{wf}} = \frac{(T_f - T_n)C_{pw}}{\left(1 - {C}/{C_g'}\right)\Delta H_f} \tag{2.1}$$

Where, m_{wn} is the mass of water crystallized at nucleation, m_{wf} is the mass of freezable water, T_f is the equilibrium freezing temperature of water, T_n is the ice nucleation temperature, C_{pw} is the heat capacity of water (around 4.2 J/g.K), C is the solutes mass fraction, C_g' is the solutes in the maximally freeze concentrated state mass fraction and ΔH_f is the latent heat of fusion of water (334 J/g). The total amount of both crystallizable and unfrozen water is influenced not by the nucleation temperature, but by the composition of the solution. Moreover, the freezing rate, that is the rate of ice crystal growth, depends on the degree of supercooling. The higher is the degree of supercooling (which implies the lower is the ice nucleation temperature), the faster is the ice crystal growth rate. This is because the shelves of the freeze dryer, which are relatively colder, remove the heat generated during ice formation faster. Both the rate of releasing of latent heat during the phase change and the rate of mass transfer (the rate of water molecules to diffuse from the solution to the crystal lattice and counter-diffusion of solutes away from the growing crystal surface) tune the growth. The rate of crystal growth (G) can be expressed as a function of degree of supercooling, as shown in Equation 2.2:

$$G = \beta(\Delta T_S)^n \tag{2.2}$$

Where, $\Delta T_S = T_f - T_n$ (degree of supercooling), and β and n are experimental constants. On the other hand, if the degree of supercooling of a certain solution is low, meaning a small temperature difference between the equilibrium freezing temperature and the nucleation point, the supercooled water can absorb a very small amount of heat of crystallization. Leading to an instantaneous freezing of only a small fraction of freezable water and, hence, to the formation of just a few ice crystals. Furthermore, the low degree of supercooling causes the ice crystal growth rate to be slow, as the driving force for removing the crystallization heat of the relatively warmer freeze dryer shelves is low. Ice crystal morphology is strongly influenced by the degree of supercooling. Generally, three different types of ice crystal morphologies can be found in a solution undergoing freezing: (1) at low degree of supercooling, the water molecules have sufficient time to arrange themselves to form regular hexagonal crystals, called dendrites, since the freezing rate is slower; (2) at high degree of supercooling, being the freezing rate so fast, the water molecules arrange randomly around the ice nuclei, creating irregular dendrites or needle-like crystals; (3) at high cooling rates, many ice spears can originate from the core of crystallization without side branches, called spherulites. Specifically, samples frozen at high degree of supercooling (i.e., colder nucleation temperature) yield crystal filaments, whereas samples frozen low degree of supercooling (i.e., warmer nucleation temperature) yield dendritic structures (Mason, 1953).

2.1.3. The solidification phase

After the formation of stable ice nuclei, they continue to grow by the addition of water molecules to the interface, which is defined as solidification. In point C of Figure 2.1 the onset of solidification can be observed. During the solidification process, the concentration of the solution increases as more water is removed by ice crystal growth and this increase in concentration is independent of the initial concentration (it only depends on temperature). Crystalline formulations undergo eutectic freezing, in which the solute crystallizes below the eutectic temperature. During the eutectic freezing, the unfrozen water is released from the supersaturated solution as the solute continues crystallizing and this free water immigrates to the frozen water and further crystallizes. If 100% solute crystallization is assured, it could be concluded that all the available water is also frozen. This means that, during freeze-drying of a crystalline formulation, all the water can be removed by sublimation. Crystalline formulations can be freeze-dried a few degrees below their eutectic temperatures without the need for secondary drying. Amorphous formulations, on the other hand, undergo vitrification, in which the solute concentration continues to increase as more water freezes below the eutectic temperature. Freezing of water ceases when the freeze-concentrated solution changes from a rubbery to a glassy solid. Depending on the initial concentration of the solute, the unfrozen water in the glassy solid can be as high as 20%. Primary drying of amorphous formulations can be performed at a few degrees below T_e until all the frozen water is removed. At the end of primary drying, the water content of the dried product is still significantly high, which accounts for the unfrozen water. During the freeze-drying process, the unfrozen water is removed by a desorption process (more commonly known as secondary drying). During the secondary drying, the temperature of the formulation is increased to facilitate desorption of unfrozen water through the pores of the dried cake. It is, however, important to note here that the increase in temperature during the secondary drying should not lead to a temperature of the sample above the glass transition temperature, and hence the secondary drying curve should remain below the glass transition curve during the complete process

2.2 Mathematical formulation

The knowledge of the freezing step and its impact on the product quality and process performance is a critical requirement for a successful process development and scale-up. A mathematical formulation has been developed to achieve this goal. The governing equations and the physical system under analysis will be described in the following sections.

2.2.1 Case study

The system being investigated is described in this section. As discussed SFD process includes three main phases; in the first one, namely, spraying, the solution is atomized through different devices which influences the final size of the droplets obtained. For the mathematical model herein developed to describe the freezing step a perfectly spherical particle has been considered. After atomization, this particle needs to be frozen: a spontaneous freezing has been considered in this study, where the particle falls into liquid nitrogen in stationary condition. The spherical droplet is supposed to have radius *R* after atomization, and to remain spherical during the subsequent cooling and phase change. As the object being studied has a spherical shape, spherical coordinates (r, θ, φ) will be used to describe the system (Figure 2.2).

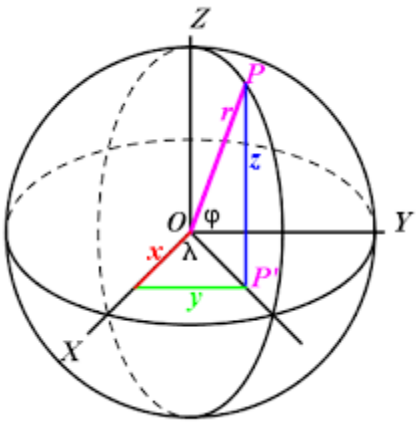

Figure 2.2: Spherical coordinates shown used in our model. Figure reprinted from http://www.scmncamogli.org/mortola/ (last access: 31/1072019), with modifications

2.2.2 Cooling

Once droplets enter in contact with cold gas, their temperature starts to decrease with a specific cooling rate: fast at the beginning of the operation and then gradually getting slower with time. During freezing the temperature of the droplets is reduced until the first crystal of ice is generated; this phenomenon occurs at a temperature, randomly distributed, named nucleation temperature T_n. The solution remains liquid before the formation of the first ice crystal. No phase change is observed until then, and the second Fourier's law (Equation 2.3) can hence be used to express the temperature evolution during cooling:

$$\varrho_l \; c_{p,l} \frac{\partial T}{\partial t} = \nabla \cdot k_l \nabla T \qquad (2.3)$$

Where ϱ_l , $c_{p,l}$ and k_l are the density, specific heat and thermal conductivity of the liquid phase, respectively; since no phase change occurs, these parameters are assumed to be constant.

Defining T_0 the initial temperature of the solution, h the overall heat transfer coefficient and T_{air} the temperature of the cooling media, the initial and boundary conditions can be written as shown in Equation 2.4:

$$\begin{cases} I.C \ \ at\ t \leq 0 & T = T_0 & for\ all\ r, \theta, \varphi \\ B.C \ \ at\ r = R & J|_{r=R} = h(T_{air} - T|_R) & for\ all\ t, \theta, \varphi \\ B.C\ at\ r = 0 & \dfrac{\partial T}{\partial r} = 0 & for\ all\ t, \theta, \varphi \end{cases} \tag{2.4}$$

2.2.3 Freezing

During freezing, a phase transition from liquid to solid occurs, and three zones corresponding to different physical states can hence be identified: a solid zone, i.e., the area in which ice has already been formed, a liquid zone, where cryo-concentration occurs, and an intermediate (mushy) zone, i.e., a suspension of ice in liquid with a given ice fraction X_{ice} (from 0 to 1).
The freezing phase modelling is based on Equation 2.5 that is a heat transfer balance within the product being frozen:

$$\varrho c_p \frac{\partial T}{\partial t} = \nabla(k \nabla T) + \ + Q_c \tag{2.5}$$

where c_p is the specific heat of the system, the first member of the equation represents the accumulation term while in the second member we find the conduction term and the source contributions Q_n and Q_c due to nucleation and crystals growth of ice respectively. As already stated, each particle can be divided into three distinct zones (Figure 2.3):

1. Liquid zone if $T > T_{max}$
2. Mushy zone if $T_{min} < T < T_{max}$
3. Solid zone if $T < T_{min}$

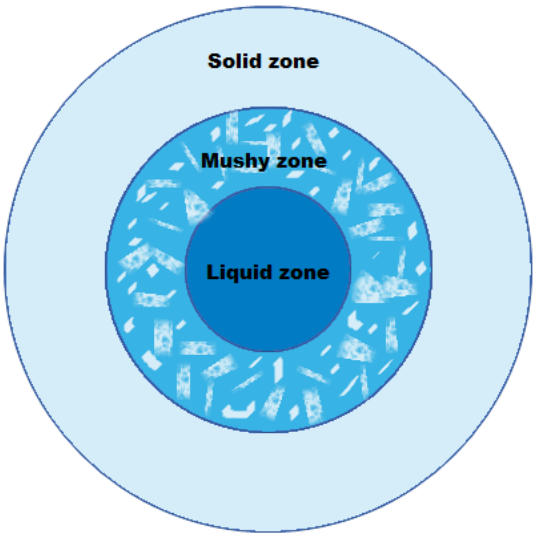

Figure 2.3: Scheme of the particle during freezing highlighting the three different zones that can be recognized**.**

The phase transition is confined within the mushy zone, therefore occurring in the range [T_{min}; T_{max}]. If the rate of heat release during nucleation Q_n, always positive, is proportional to the degree of supercooling ($T_f - T$) it is possible to write:

$$Qn = \Delta H_f k_n (T_f - T) \tag{2.6}$$

where k_n represents the rate of nucleation per unit of volume, and is a function of the freezing front velocity R, thus providing information about the nucleation kinetics,

$$k_n = \frac{\varrho R}{\xi (T_f - T^*)} \tag{2.7}$$

where ξ is the thickness of the undercooled zone, while $T^*$is the temperature of the undercooled liquid. The other source term, Q_c , represents the latent heat released upon ice crystallization; it also is always positive and can be described as a function of the ice fraction, X_{ice}, in the mushy zone:

$$Q_c = \Delta H_f \frac{\partial}{\partial t}(\varrho X_{ice}) \tag{2.8}$$

If we assume ρ to be constant, and equal to the average value between the density of water and ice, ϱ^*, it is possible to obtain Equation 2.9:

$$Q_c = \Delta H_f \varrho^* \frac{\partial X_{ice}}{\partial t} = \Delta H_f \varrho^* \frac{\partial X_{ice}}{\partial T} \frac{\partial T}{\partial t} \tag{2.9}$$

Then, we further assume the ice crystal rate to be completely tuned by the heat transfer and the ice fraction X_{ice} within the mushy zone to be linearly varying with temperature for small values of the temperature gradient. In this way the equation can be re-arranged as follows:

$$Q_c = \Delta H_f \varrho^* \frac{\Delta X_{ice}}{\Delta T} \frac{\partial T}{\partial t} \tag{2.10}$$

where ΔT is the temperature variation in the intermediate zone. This source term can be included into the accumulation term by using the following expression for the specific apparent heat $c_{p,app}$:

$$c_{p,app} = \begin{cases} c_{p,s} \quad for\ T < T_{min} \\ \frac{c_{p,l} + c_{p,s}}{2} + \frac{\Delta H_f}{\Delta T} \Delta X_{ice} \quad for\ T_{min} < T < T_{max} \\ c_{p,l} \quad for\ T > T_{max} \end{cases} \tag{2.11}$$

where $c_{p,l}$ and $c_{p,s}$ are defined as the specific heat of water and ice respectively. With these assumptions, Equation 2.12 holds true:

$$\varrho^* c_{p,app} \frac{\partial T}{\partial t} = \nabla (k \nabla T) + Q_n \tag{2.12}$$

2.3 Prediction of the final product structure

In the literature various researchers have worked on mathematical models to describe the temperature profile of a solution being frozen. Knowing that, in fact, it is possible to predict the ice crystals size within the product. This last calculation is however commonly based on empirical models, which are therefore limited to small range of possible applications.
In early 1991 Bald proposed an empirical formula, Equation 2.13, to correlate the average crystal size to the cooling rate $\frac{\partial T}{\partial t}$:

$$D_p = \alpha \left(\frac{\partial T}{\partial t}\right)^{-\beta} \tag{2.13}$$

where D_p is the average crystal size, or equivalently, the average pore size since the two coincide in freeze-drying process, while β and α are fitting parameters.
Woinet et al. (1998) proposed a model which highlights the molecular diffusion of water as the main cause of ice growth. In this case, the ice crystal size, D_p, is related to the initial freezing front position S, the degree of supercooling ΔT and the diffusion coefficient D_s of the solute,

$$D_p = \sqrt{\frac{16 S^2 \Delta T D_s}{X(T - T_s)}} \tag{2.14}$$

A wide class of models, which share the same structure, has also been proposed (Equation 2.15). They highlight the correlation between D_p, the freezing front rate (v) and the temperature gradients in the frozen zone (θ),

$$D_p = \alpha v^{\lambda_1} \theta^{\lambda_2} \tag{2.15}$$

where α is a product-specific parameter obtained from regression of experimental data, and λ_1 and λ_2 depend on the application considered. Examples of different correlations is listed in Table 2.1 (Arsiccio, Barresi and Pisano, 2017).

Table 2.1: Empirical formulas for crystal sizing.

Application	Correlation	Reference
Metal solidification at low rate	$D_p \propto v^{-1}\theta^{-1}$	Kurz and Fischer-1
Freezing of apples	$D_p \propto v^{-0.5}\theta^{-0.5}$	Bomben and King
Freezing of pharma solution	$D_p \propto v^{-0.5}\theta^{-0.5}$	Nakagawa et al.
Alloy solidification at high rate	$D_p \propto v^{-0.25}\theta^{-0.25}$	Kochs et al.
Metal solidification at low rate	$D_p \propto v^{-0.25}$	Kurz and Fischer-2

In order to create a relationship as general as possible, capable to cover a wide range of conditions independently of the specific final application a mathematical model has also been developed. Knowing the temperature profile during freezing, the freezing front velocity and temperature gradients within the frozen zone can be estimated and used to compute the average ice crystal size. The model still employs a fitting parameter, which anyway has a well-defined meaning, and can easily be determined by regression of experimental data.

2.3.1 Predictive model

The model herein presented, once nucleation occurred, applies to the crystal growth phase, after the onset of nucleation. It corresponds to a lumped parameter model easily to be solved since the partial differential equations of the continuous time and space behaviour are transformed into ordinary differential equations with a finite number of parameters. Temperature is assumed to be constant both within the liquid layer and at the freezing front; its value at the freezing front is assumed to be equal to the equilibrium freezing temperature of the solvent. This assumption is realistic if we consider that temperature gradients within the frozen zone are orders of magnitude greater than those within the liquid zone. For deriving the model, the control volume is divided into the three zones previously described, namely, solid, mushy and liquid. Given the spherical shape of our system, our control domain will be a spherical shell of volume *dV* and surface *dS*

$$dV = 4\pi r^2 dr \tag{2.16}$$

$$dS = \pi r dr \tag{2.17}$$

We can consider *dr* as the fraction of the mushy zone where crystal growth is occurring. So, the control domain considered changes its position during the process, as it follows the mushy zone

from the external surface towards the core of the particle. We further assume that the ice crystals are cylinders with diameter D_p and with an inclination with respect to the radial direction, r, described by the angle δ. δ is linked to tortuosity τ of the porous structure resulting by the lyophilization process, $\tau = cos\delta^{-1}$. Since the term τ will cancel out during the mathematical derivation of the model, the specific inclination will not affect the results obtained. While the crystal growth process continues, the freezing front moves along the particle and, thus, the radial interval dr considered, correspondingly changes its position as it follows the freezing front. Thus, it is necessary to discretize the particle radius into a finite number n of intervals having extension Δr and the number and diameter of the crystals within the i-th of these intervals, as well as the other variables which change during the process, will be denoted with subscript i (Pisano and Capozzi, 2017).
The enthalpy balance for the control volume is now derived; it can be written, for the lumped parameters model herein considered, as:

$$\begin{pmatrix} heat\ removed\ by \\ the\ frozen\ product \end{pmatrix} + \begin{pmatrix} heat\ generated\ by \\ crystallization \end{pmatrix} + \begin{pmatrix} enthalpy\ change\ due\ to \\ new\ interface\ generation \end{pmatrix} = 0$$

$$-k_f \theta_i 4\pi r^2 + \frac{dV_{ice,i}}{dt}\, \varrho_{ice} \Delta H_f - \frac{dS_{ice,i}}{dt} \gamma = 0 \qquad (2.18)$$

where k_f and θ are the thermal conductivity and temperature gradient within the frozen zone respectively, V_{ice} and S_{ice} the ice crystals volume and surface, respectively. Considering that the heat flux at the external boundary of the spherical particle must be continuous, it is possible to write,

$$k_f \theta_i = K_{v,f} \Delta T \qquad (2.19)$$

Where ΔT is the temperature difference between the external gas and the product being frozen, while K_v is an overall heat transfer coefficient,

$$K_{v,f} = \frac{1}{1/_h + i\Delta r/_{k_f}} \qquad (2.20)$$

By integrating Equation 2.18, from time 0 to time Δt_i, that is the time interval necessary for the mushy zone to move ahead of Δr we obtain

$$-k_i \theta_i^* 4\pi r^2 \Delta t_i + \Delta V_{ice,i} \varrho_{ice} \Delta H_f - \Delta S_{ice,i} \gamma = 0 \qquad (2.21)$$

where θ_i^* is the average temperature gradient during Δt_i. A further assumption is that the initial volume and surface of crystal nuclei is completely negligible compared to their final values and thus,

$$\Delta V_{ice,i} = N_i\, \pi\, \frac{D_{p,i}^2}{4}\, \tau\, \Delta r \qquad (2.22)$$

$$\Delta S_{ice,i} = N_i\, \pi\, D_{p,i}\, \tau\, \Delta r\, a_{S,i} \qquad (2.23)$$

with N_i being the total number of nuclei, and $D_{p,i}$ the average size of ice crystals. The term $a_{S,i}$, in Equation 2.23, accounts for the real ice crystals habit and surface morphology and is equal to the ratio between the real surface area and the fictitious one which is calculated assuming that the ice crystals are cylinders of length Δr,

$$a_{S,i} = \frac{real\ surface\ area}{N_i\,\pi\,D_{p,i}\,\Delta r\,\tau} \tag{2.24}$$

$a_{S,i}$ is, more specifically, the product of two different terms: b_1, assumed to be constant, is the coefficient related to the ice crystals habit, while $b_{2,i}$ considers the surface irregularities and can be assumed to be inversely proportional to the total surface area of crystals. Indeed, the larger the total surface area is, the smaller the contribution given by surface irregularities is. Therefore, $a_{S,i}$ reads as,

$$a_{S,i} = b_1 b_{2,i} \tag{2.25}$$

If we substitute Equation 2.22 and Equation 2.23 into Equation 2.21 and divide both members by Δt_i, we obtain Equation 2.26

$$-k_i\theta_i^* 4\pi r^2 + N_i\pi\frac{D_{p,i}^2}{4}\varrho_{ice}\tau v_i\Delta H_f - N_i\pi D_{p,i}\tau v_i\gamma a_{S,i} = 0 \tag{2.26}$$

where v is the freezing front rate.
The mass of ice crystallized in $\frac{1}{4}\pi D^2\Delta r$ is assumed to be directly proportional to θ^*. In fact, if the temperature gradient increases, the heat released by ice crystallization and, in its turns, the heat to be removed to avoid any temperature increase increases as well. This assumption has stronger physical motivations than simply assuming the average ice crystals size to be proportional to θ^{λ_2}. It follows that,

$$N_i\pi\frac{D_{p,i}^2}{4}\varrho_{ice}\tau\Delta r = a\theta_i^* \tag{2.27}$$

where a is a proportionality coefficient. The following expression, Equation 2.28, can hence be obtained

$$N_i\pi D_{p,i}\tau v_i\gamma a_{S,i} = -k_i\theta_i^* 4\pi r^2 + \frac{\Delta H_f}{\Lambda r}a\theta_i^* v_i \tag{2.28}$$

which establishes that the rate of generation of crystals surface area in the control volume increases with the temperature gradients within the frozen zone, and thus with the total mass of ice formed, and with the freezing front velocity.
For a given volume of liquid being frozen, the following mass balance equation is valid,

$$\sum_{i=1}^{n} N_i\,\pi\frac{D_{p,i}^2}{4}\varrho_{ice}\tau\Delta r = \phi m \tag{2.29}$$

where m is the total mass of water in the solution, and ϕ is a coefficient with a value close or equal to 1 and considers the mass of water which remains in the amorphous phase without crystallizing. Since in crystalline materials almost all the water gets frozen, it can be assumed

that ϕ is 1. In the case of amorphous solutes, the solid solution phase usually contains between 15% and 50% of unfrozen water, but except for very concentrated solutions the value of ϕ is anyway close to 1. In this work we assume that ϕ is equal to 1.
Combining Equations 2.27 and 2.29, a reads as,

$$a = \frac{m}{\sum_{i=1}^{n} \theta_i^*} \tag{2.30}$$

and, thus, Equation 2.27 reads as,

$$N_i \pi \frac{D_{p,i}^2}{4} \varrho_{ice} \tau \Delta r = m \frac{\theta_i^*}{\sum_{i=1}^{n} \theta_i^*} \tag{2.31}$$

Substituting Equation 2.31 into 2.26 and rearranging it,

$$D_{p,i} = 4m\theta_i * \gamma a_{S,i} v_i \Big/ \left[\varrho_{ice} \left(m\theta_i * v_i \Delta H_f - 4k_f \theta_i^* \pi r^2 \Delta r \sum_{i=1}^{n} \theta_i^* \right) \right] \tag{2.32}$$

This equation correlates $D_{p,i}$ with the freezing front velocity (v) and the temperature gradient (θ). However, freezing, as already stated, is only an apparently simple process. The phenomena at its basis are very complex and its detailed description would imply non-ordinary approaches such as the phase-filed approach (Berberović *et al.*, 2018).
Despite that, the average size of ice crystals seems to be satisfactory described by two parameters, v and θ. Here, the proposed model indirectly accounts for other factors such as nucleation temperature, cooling rate, and product geometry which come into play during the calculations of θ and v. Thus, θ and v implicitly consider all the other relevant factors involved.
As previously stated, the a_S coefficient, which accounts for the real crystal habit and the surface irregularities, is the product of a constant term and of a term which is assumed to be inversely proportional to the surface area of crystals. Equation 2.27 states that the volume of ice crystallized in $\frac{1}{4}\pi D^2 \Delta z$ is proportional to θ^*. It follows that if the volume is proportional to θ^*, the surface area can be assumed to be proportional to $\theta^{2/3*}$. So, $a_{s,i}$ reads as,

$$a_{S,i} = b_1 b_{2,i} = \frac{b}{\theta_i^{*2/3}} \tag{2.33}$$

where b is determined by regression of experimental observations of D_p. The model here presented has been obtained from heat and mass balance equations and is, therefore, applicable over very different conditions. Despite it is a firt principle model, the model is not entirely theoretical, because the value of one parameter, γb, needs to be calculated from experimental data. Furthermore, this model requires that both v and θ are defined as inputs. For this purpose, the temperature profile during freezing is needed and a study on how the droplets undergo freezing has to be carried out.

2.4 Numerical methods

2.4.1 Software

The governing equations presented in the previous sections were solved by using COMSOL Multiphysics (vers.5.3). This is a simulation software working as a cross-platform finite element analysis and multiphysics solver. COMSOL provides conventional physics-based user interfaces, making it possible to solve systems of partial differential equations (PDEs).

2.4.2 Case of study and simulation set-up

In the interface offered by COMSOL a sphere has been created to simulate the behavior of the droplet undergoing freezing. As the system shows spherical symmetry, only half of the sphere has been created and studied. To facilitate the study, the particle has been assumed to be made of pure water and a cold flux of air has been considered as freezing medium.
The main parameters set in the simulations have been gathered in the following table:

Table 1.2: List of the input parameters used in COMSOL (vers.5.3)

Input parameters	Value, unit
k_{ice}	*2.56 W/(m*K)*
k_{air}	*0.026 W/m/K*
Cp_{ice}	*2.1E3 J/(kg*K)*
Cp_{gas}	*1616.6 J/(kg*K)*
M_{ice}	*18 g/mol*
M_w	*18 g/mol*
k_{H2O}	*0.6 W/m/K*
Cp_{H2O}	*4186, J/kg/K*
ρ_{H2O}	*1000 kg/m^3*
P_{ice}	*920 kg/m^3*
h_{nat}	*4.5 W/m^2/K*
T_eq	*273 K*
T_0	*293.15 K*
T_{AIR}	*223 K*
R	*50 µm*
h	*1.67552 W/(m^2*K)*
ΔH_f	*333500 J/kg*

2.4.3 Mesh

Due to the small dimension of the particles simulated in the model (100 µm) there is no need of a small mesh with a high number of cells. Aware of that, after different simulations we have decided to use a dense mesh to study the problem (Figure 2.4).

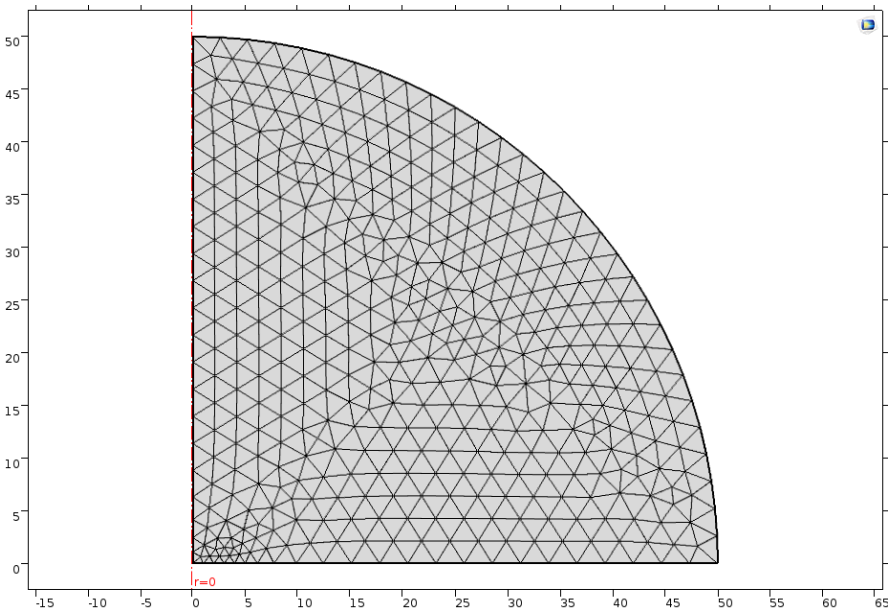

Figure 2.4: Image of the mesh used in the simulation.

2.4.4 Simulation parameters

An important parameter involved in a freezing process is the time of freezing, t_n, that is the moment at which the solution from liquid becomes solid. In literature a correlation(Eq 2.34), valid only for water as in our simulation, exist to calculate the time required to freeze a droplet (Grace *et al.*, 1978).

$$t_n = -\frac{r * c_{pw} * \rho_w}{3 * h} \ln \frac{T_n - T_f}{T_0 - T_f} \tag{2.34}$$

Where r is the radius, T_f is the temperature of the cryogenic fluid used, T_n the nucleation temperature and T_0 the temperature t t=0 and T_n the nucleation temperature.
It is hence interesting to see how the different parameters affect each other and the process in general (Figures 2.5-2.9), influencing for example the time, the temperature or the size of the reactor, assumed as column-shaped with a certain D_h hydraulic diameter.

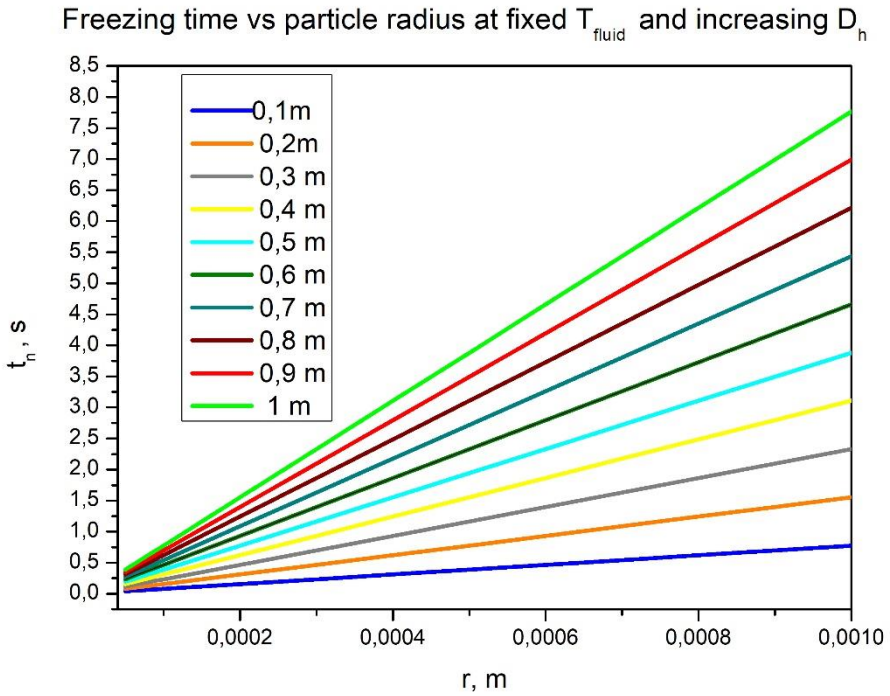

Figure 2.5: How t_n changes by varying the particle to freeze, for different reactor size but fixing the cryogenic fluid temperature.

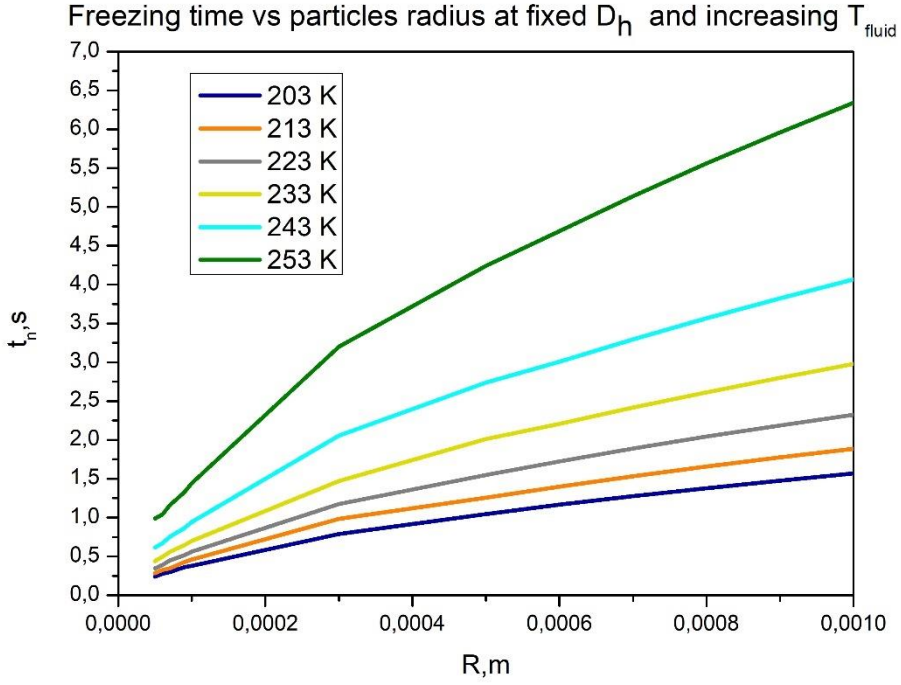

Figure 2.6: How t_n changes by varying the particle to freeze, for different cryogenic fluid temperatures but fixing the reactor size.

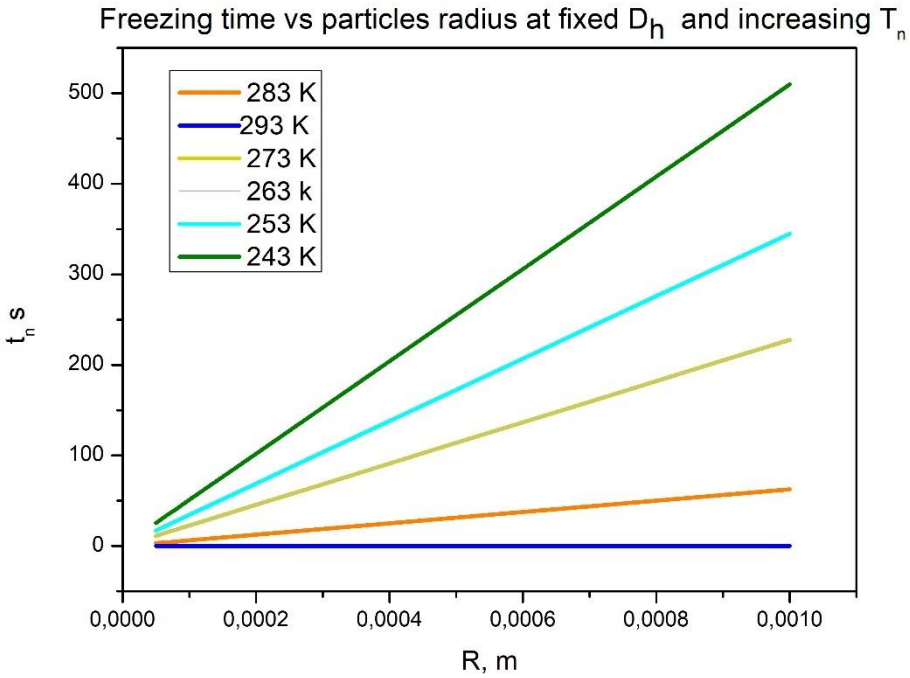

Figure 2.7: How t_n changes by varying the particle to freeze, for different nucleation temperature but fixing the reactor size.

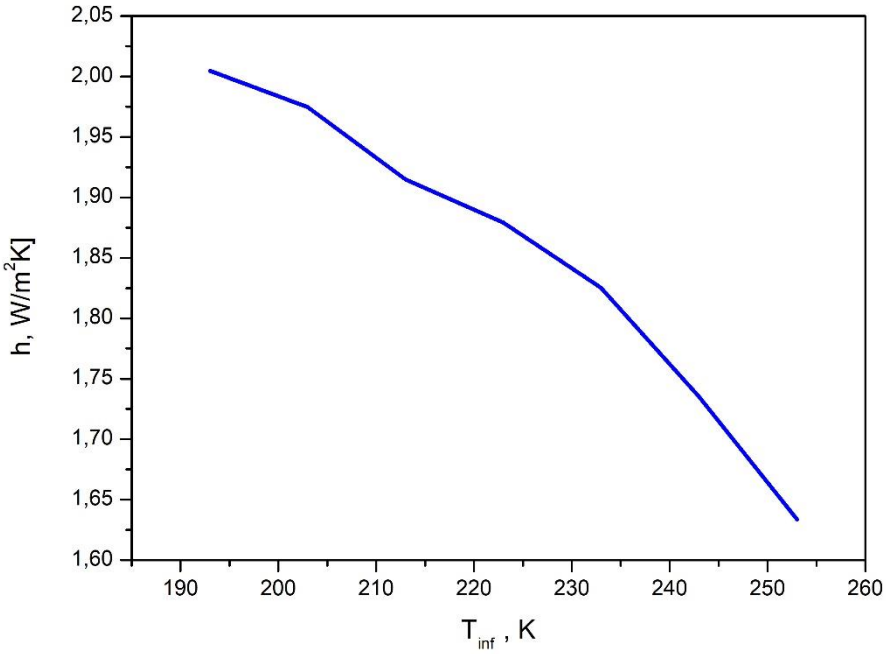

Figure 2.4: How h changes by varying cryogenic fluid used.

2.4.5 Determination of G and R

The mathematical model was used to predict the temperature profile within the particle to be frozen as well as its temperature at the external surface. An example of result is given in Figure 2.9 which has, as expected, the same trend observed in Figure 2.1.

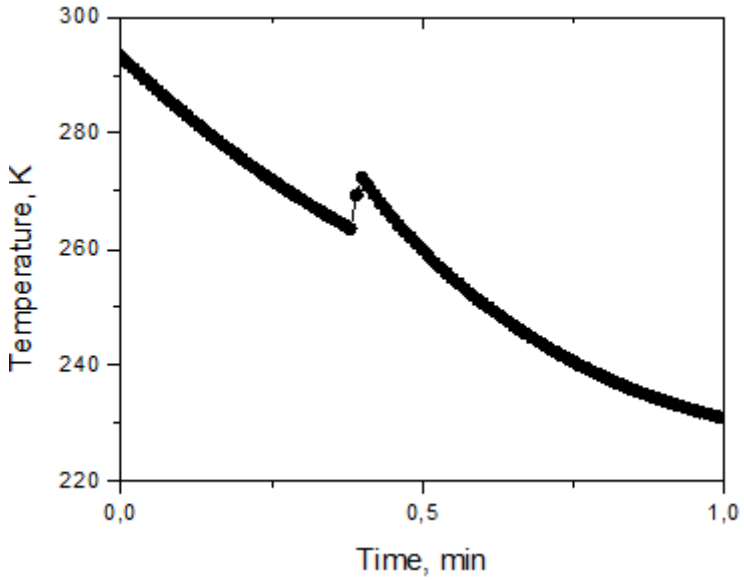

Figure 2.9: Example of the particle' temperature evolution, measured at its external surface during freezing by contact with cold air simulated on COMSOL. The body studied was a 50μm spherical droplet of water falling at 0.43 m/s in a column containing cold gas(air) at 223K.

The values of the freezing front rate *R* and the temperature gradient in the frozen zone *G* can be obtained once the temperature profile in the product is known during freezing. For the determination of *R*, it is necessary to have the temperature profile inside the product. However, freezing was so fast that the microdroplets instantaneously freeze and it was not possible to detect the movement of the freezing rate. Thus, we have simulated the freezing of larger droplets (having from 6 to 10 mm as diameter) and then exported that information to smaller ones. To detect the temperature profile within the droplet, various probes have been placed along its radius as shown in Figure 2.10.

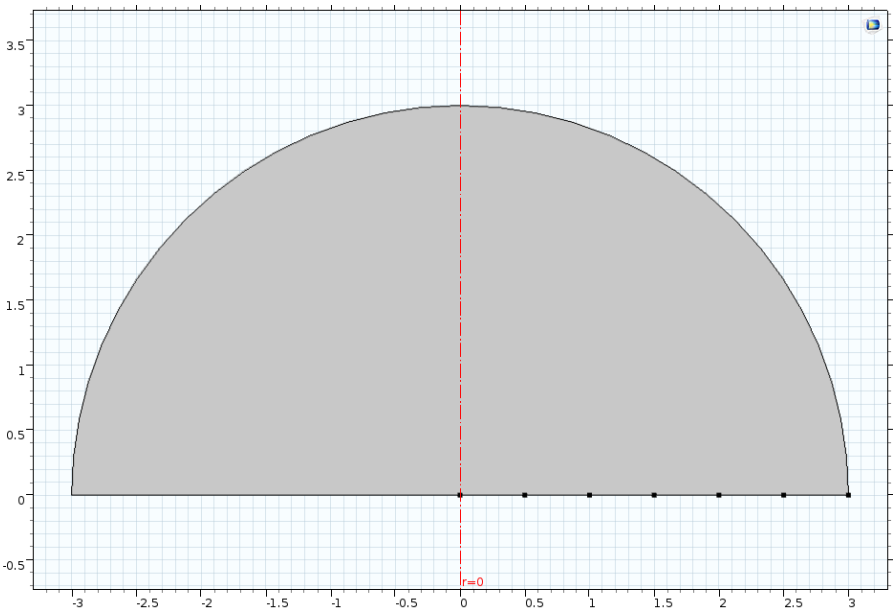

Figure 2.10: The black spots refer to the various probes placed along the radius of the droplet to track its temperature profile evolution.

The sensors have been placed equidistant and the values of temperature have been collected. To calculate *R*, the freezing front reaches a generic distance r at a certain t defined as t_s when the temperature at that position is equal to the equilibrium value (T_{eq}) of 273.5 K. Thus, it is possible to know the position of the freezing front over time. Freezing front rate *R* is defined as the ratio between the front variation of position Δr and the time spam in which this happens Δt_z:

$$R = \frac{\Delta r}{\Delta t_z}$$

t_s is recorded for each probe along the radius and so the Δt_z is so calculated by considering each couple of consequential sensors; Δr instead is fixed and equal to the distance between the probs equal to 0.5 mm. The temperature gradient of the frozen area *G* is calculated by detracting from T_{eq}, reached at a certain time by a prob, the temperature detected by the prior prob (which is already frozen since the freezing is moving from the external surface toward the core of the particle). Once obtained the value of *R* and *G* for different droplet diameters, their value has been substituted into equation 2.31 and the average size of ice crystals D_p is calculated. For each diameter simulated, the matching D_p is shown in Table 2.3. How D_p changes with the size of the drop is represented in Figure 2.11.

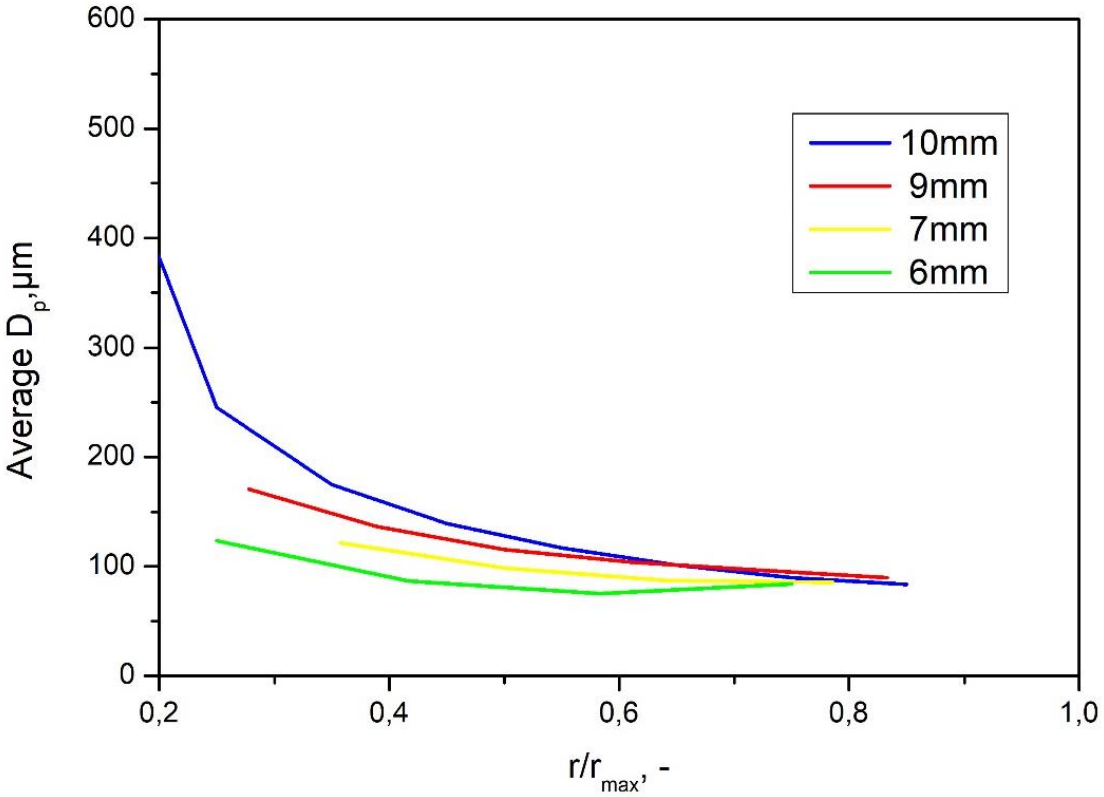

Figure 2.11: Trend of D_p changing radius of the particle simulated, using as cryogenic fluid cold air.

It is possible to notice how the crystal size and hence the porosity of the dried product increases increasing the diameter of the particle.

Table 2.3: The average values of D_p calculated for different diameters.

Diameters, mm	*Average D_p, µm*
10	209,886
9	114,821
7	96,9528
6	91,1748

It can be observed that there is a linear relationship, provided that the droplet is sufficiently small, that is smaller than 9 mm. For larger droplets, this correlation is not anymore linear. So, we have derived a linear relationship (Eq 2.35) that is valid for droplets smaller than 1 cm. The predicted values of D_p (µm) vs. the size (d, mm) of the droplet has been described as,

$$Dp = 13.61\mathrm{d} \tag{2.35}$$

This relationship is valid for small droplets, smaller than 1 cm. The simulation, as described in the input parameters section, used cold air (at 220K) to freeze the droplets. We have then decided to switch to nitrogen (at 80K) since it is the cryogenic fluid used to carry out SFD. Moreover, it will be the cooling media used in the experimental part performed in Kyoto. We have repeated the procedure explained above to calculate *R* e *G* for different diameters and the corresponding D_p. How D_p changes with the size of the particle is shown in Figure 2.12.

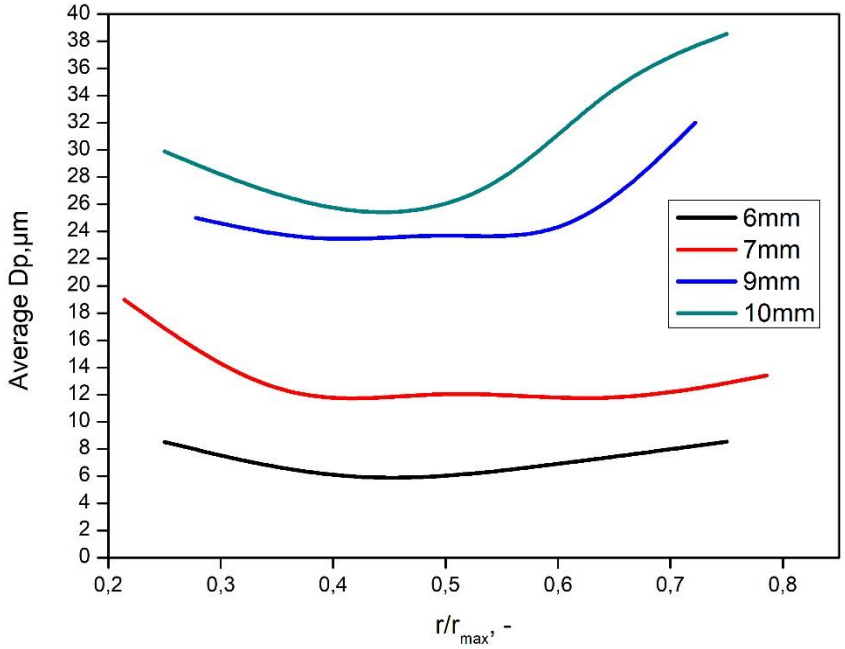

Figure 2.12: Trend of D_p changing radius of the particle simulated, using as cryogenic fluid nitrogen.

The same consideration already discussed can be repeated and a linear relationship, Eq. 2.36, can be written to express D_p as function of d:

$$D_p = 3.82d \tag{2.36}$$

Comparing Eq 2.36 with Eq 2.35 is evident how the pores obtained from air are bigger than the one obtained from nitrogen. It is coherent with the rate of freezing that the two fluid determine: being air hotter compared to nitrogen it will freeze the particle but slower giving time to the ice crystal to grow. Nitrogen, being colder, ensure a fast-freezing rate creating small crystals.

Chapter 3

Materials and methods

In this chapter the experimental work carried out at Kyoto University is described. Using a drier built by Nakagawa's team SFD processes have been performed: once prepared the formulation to freeze-dry two distinct atomization methods were experienced, then the dispersed particles have been frozen and subsequently dried. The samples hence obtained have been characterized in term of internal structure and surface, SEM, XRD and BET analyses in order to investigate the dried product structure and determine the average size of ice crystals. In fact, the pores detected in this manner can be related to the actual size of crystal since the void left in the particles derived by ice sublimation.

3.1 Materials

The experimental tests have been performed at Kyoto University using an in-house dryer realized by Prof. Nakagawa`s laboratory; the trials were run from August to November 2019. The apparatus allowed us to dry different formulations, but was not equipped with any devices to monitor the critical parameters of the process such as product temperature, drying time, residual moisture etc. Because of that, this experimental study was mainly focused on the spray freezing technology, while drying was essentially used to make the material stable for its morphological characterization. The key parameter used for the validation is the average pore size of the lyophilized matrix, which should correspond to the ice crystal size predicted by the model. A list of formulations and process conditions used in this study is given

3.1.2 Preparation of the formulations to be lyophilized

Since Prof. Nakagawa`s team did not have any experience on this subject, we decided to use a robust formulation as model product, that is, a mannitol-based formulation. Once we have consolidated the experimental apparatus and the manufacturing set-up, we have investigated more complex formulations that are more representative of real pharmaceutical formulations.
The use of bulking agents, such as mannitol and glycine, prevents appearance problems known as shrinkage and collapse(Johnson, Kirchhoff and Gaud, 2002). These excipients are not required in the liquid formulations but are added to increase the tonicity of the solution. Since the active substance for each container is very often too small (even a few mg) and the corresponding volume of solution would be difficult to measure accurately, this kind of excipient, which is non-toxic and free of any pharmacological activity, is necessary to give a good-looking lyophilizate. The benefit of using mannitol is that it crystallizes during freezing and permits drying processes at higher product temperatures, thus with higher sublimation rates relative to purely amorphous systems. Mannitol, however, is known to form different crystalline modifications which compromises reproducibility of product characteristics and storage stability due to phase transformations.
D-mannitol (Figure 3.1), the D-enantiomer of mannitol ($C_6H_{14}O_6$), is an osmotic diuretic that is metabolically inert in humans and occurs naturally, as a sugar or sugar alcohol, in fruits and vegetables. It elevates blood plasma osmolality, resulting in enhanced flow of water from tissues, including the brain and cerebrospinal fluid, into interstitial fluid and plasma. Mannitol may also be used for: the promotion of diuresis before irreversible renal failure becomes established, the promotion of urinary excretion of toxic substances, as an antiglaucoma agent, and as a renal function diagnostic aid.

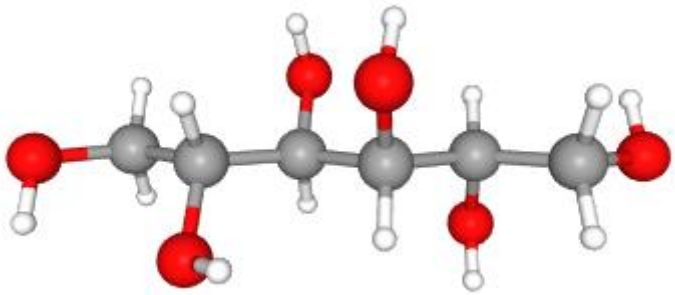

Figure 3.1: Molecular structure of mannitol. Reprinted from https://pubchem.ncbi.nlm.nih.gov/ (last access: 2/11/2019) with modifications.

Beside mannitol other solutes have been used to prepare the solution to dry, due to some results which will be explained in the results chapter. A different formulation has hence been used changing the solute from mannitol to a mix of two different components, limiting the solid content to 10% w/w. This percentage was made of:

- 5% w/w of trehalose
- 5% w/w of albumin

The new solution contained not only a sugar but also a protein (another common biomolecule often lyophilized). In Figure 3.2 the structures of the two solutes is shown.

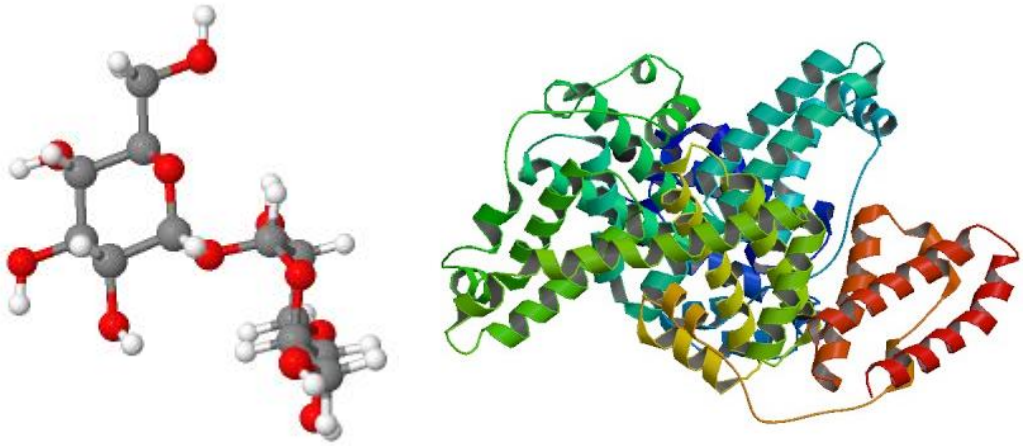

Figure 3.2: Structure of trehalose (on the left) and of albumin (on the right) Images reprinted from https://www.molinstincts.com (last access 22/11/19) with modifications.

D-Trehalose (C12H22O11) is a lyoprotectant that effectively maintains the conformation of proteins and other biomolecules during water removal due to the freeze drying. This non-reducing disaccharide (two glucose molecules linked by the anomeric carbon) provides the same type of protection during lyophilization that sucrose does with the great advantage that is less prone to cause sample collapse. This excipient is used in combination with albumin, which is the active ingredient that has to be stabilized also against the process stresses(Jena *et al.*, 2019). Bovine serum albumin (BSA) has been chosen for its sensitivity to freezing and dehydration. To carry out the drying, 3 aqueous formulations have been used, described in Table 3.1. All three formulations have been prepared starting from distillate water, the grams of the different solutes listed above, were added to the water and mixed using a spoon. Being both mannitol and trehalose/albumin totally soluble in water no magnetic stirring or filtration were needed; the solution hence obtained look different in colour since the two mannitol-based

look like water being completely transparent whereas the trehalose one is yellow coloured, it can be seen in Figure 3.3.

Table 2.1: Scheme of the solutions used with their composition.

Solutions	Composition	Purity of solutes	Manufacturer of the solutes
A	10% w/w of mannitol	99.0%	FUJIFILM Wako Pure Chemical Corporation
B	15% w/w of mannitol	99.0%	FUJIFILM Wako Pure Chemical Corporation
C	5% w/w of trehalose 5% w/w of albumin from bovine serum (ABS) pH 5.2	98% 98%	FUJIFILM Wako Pure Chemical Corporation

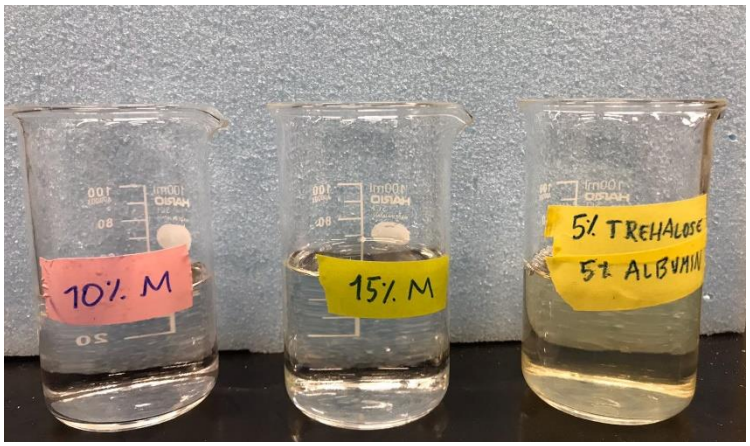

Figure 3.3: Formulations, described in Table 3.1) used for the SFD performance in Kyoto laboratory. From the left to the right, solution A, B, C.

3.2 Spraying

In this section, the atomization process of a pharmaceutical formulation will be investigated. The droplets will then fall into a cooling gas or liquid to make them frozen. The type of atomizer not only determines the energy required to form the spray blast but also their average size and distribution along with their trajectory and speed. The drop size establishes the heat transfer surface available and thus the drying rate. Hence, a successful prediction of droplet size enables one to tune the powder properties as desired. In the laboratory, among the multiple techniques to atomize a liquid stream, two have been tested:

1. Pneumatic atomization (solution atomized through a spray gun)

2. Vibration atomization (solution atomized through a needle let vibrate)

The two methods fundamentally differ in the size of the final particles: the first one atomizes the solution in fine and small particles (diameter ~ μm), making it impossible to distinguish from each other; on the other hand, the second technique atomizes the formulation into bigger and more spherical droplets (diameter ~ mm).

3.2.1 Pneumatic atomization

Pneumatic nozzles, also known as two-fluid nozzles, use compressed air or steam to atomize the fluid into fine droplets. Usually, the liquid stream and the air are mixed outside the body of the nozzle, rarely the mixing occurs inside the nozzle. The spray angle ranges from 20°C to 60°C and depends on the nozzle design. Figure 3.4 displays the working principle of the atomization and the device in the laboratory during the experimental phase, in our case a spray gun connected to a compressor has been used. It spray-gun HP-C Plus (obtained from ANEST IWATA Corporation, Japan). The nozzle shape was circular with a diameter of 0.3 mm.

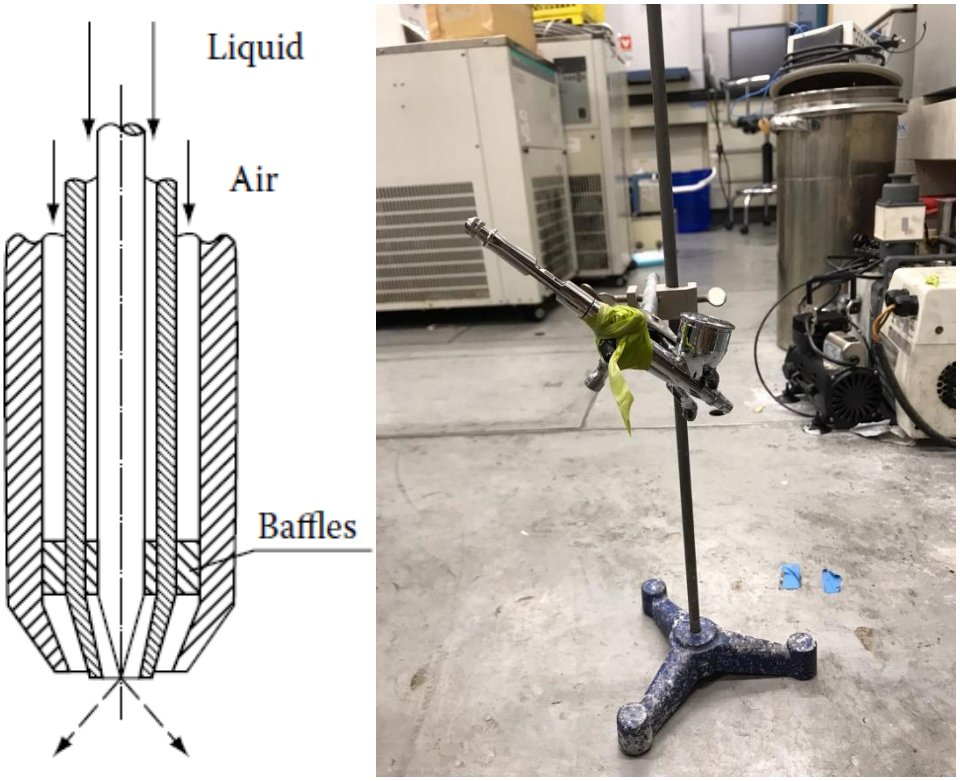

Figure 3.4: Pneumatic atomization technology; on the left the working principle, on the right the spray gun used in Kyoto.

From the spray gun shown in the picture, a powder was obtained. The sample was too small for any further analysis and, even varying the flow rate of air inside the atomizer, the dimension of the particles obtained was still too small. It was problematic for two main reasons: first of all, the model derived was not suitable for particles that small; second, the results from both nitrogen adsorption and SEM detections were not reliable enough, in fact the average diameter measured using imageJ vers 1.39, of the particles was 11,43 μm for solution a and 9.67 μm for solution b. For these reasons, the atomizing device was switched to a vibrating one.

3.2.2 Vibrating atomization

In this case, the breakup of a liquid stream into droplets can be brought about by periodically vibrating a liquid jet or liquid reservoir. In the laboratory at Kyoto University, we have used the simplest form of vibrating atomization droplet generator, that is, a hypodermic needle vibrating at its resonant frequency able to generate a stream of uniform droplets. The size and frequency of droplet generation are dependent on the needle diameter, resonant frequency, liquid flow rate, and amplitude of oscillation of the needle tip. The technique of periodical vibrations for droplet generation is based on the instability of a liquid jet emerging from a capillary tube or an orifice. If a liquid jet is emitted from an orifice under pressure, the jet is by nature unstable and will eventually disintegrate into droplets by the action of internal and/or external forces depending on the orifice diameter as well as flow conditions and properties of the liquid and surrounding medium. Droplets produced using periodic vibrations generally exhibit excellent mono-dispersity whether the vibrations are generated by a piezoelectric crystal, an engine or in general any sort of mechanical means. Figure 3.5 shows, compared to a theoretical description, the device used in the laboratory; it is made of a needle connected to an engine that gives the vibration. Our atomizer was hand-built made of a needle from e supermarket and an engine from an old machine. The liquid is fed through a plastic tube linked to a piston to ensure a flow rate of 1.1 ml/min. This flow rate was chosen from empirical observation in term of particle size that I did under the supervision of Prof. Nakagawa.

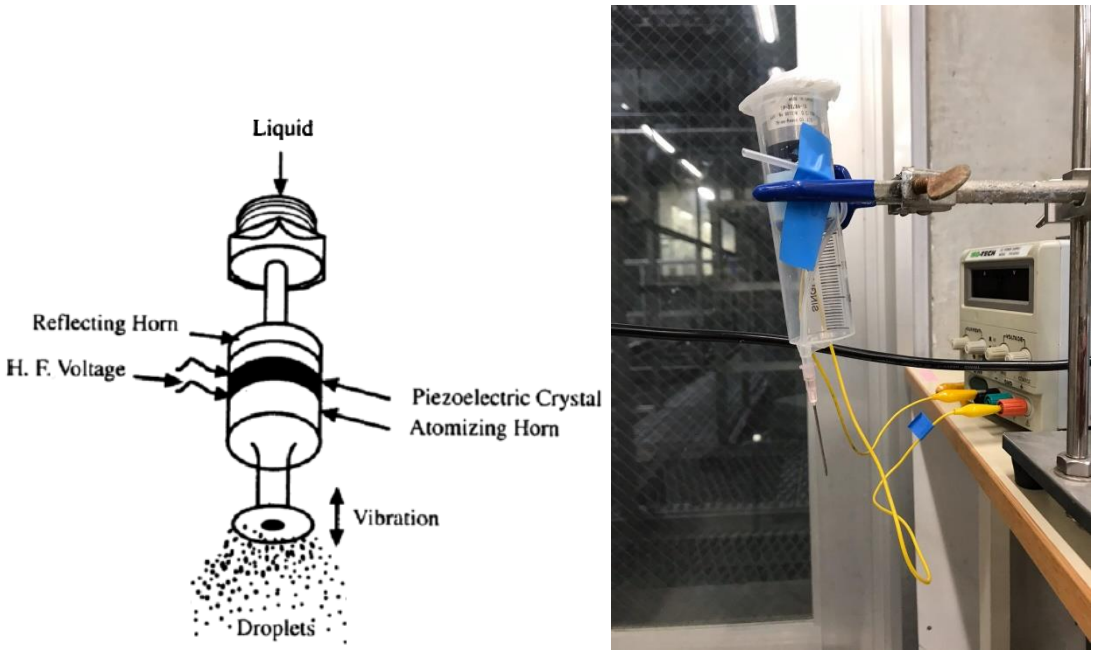

Figure 3.5: Vibrating atomization technology; on the left the working principle, on the right the device used in Kyoto

The droplets obtained were spherical and bigger thus was possible to both detect the pore size from SEM pictures and to use nitrogen adsorption to detect the surface area. In Figure 3.6 the particles after drying, from all three the formulations, atomized with the needle vibrating method.

Figure 3.6: Particles obtained with the vibrating atomization method. The particles look more spherical hence to facilitate the investigation of its internal surface.

3.3 Freezing

To freeze the liquid formulation, the droplets fall into a freezing media and then collected to undergo drying. The cryogenic fluid used to achieve this purpose is liquid nitrogen; it is poured into a rectangular tray (Figure 3.7) in order to create a enough height of fluid to compensate the natural evaporation of nitrogen itself and ensure droplets freezing. To collect the so frozen particles, aluminium foil and various Petri capsules were placed into the tray, see Figure 3.8. In this way, after the deposit of an adequate number of frozen samples, their collection was facilitated.

Figure 3.7: Tray used at Kyoto University containing liquid nitrogen to freeze the particles.

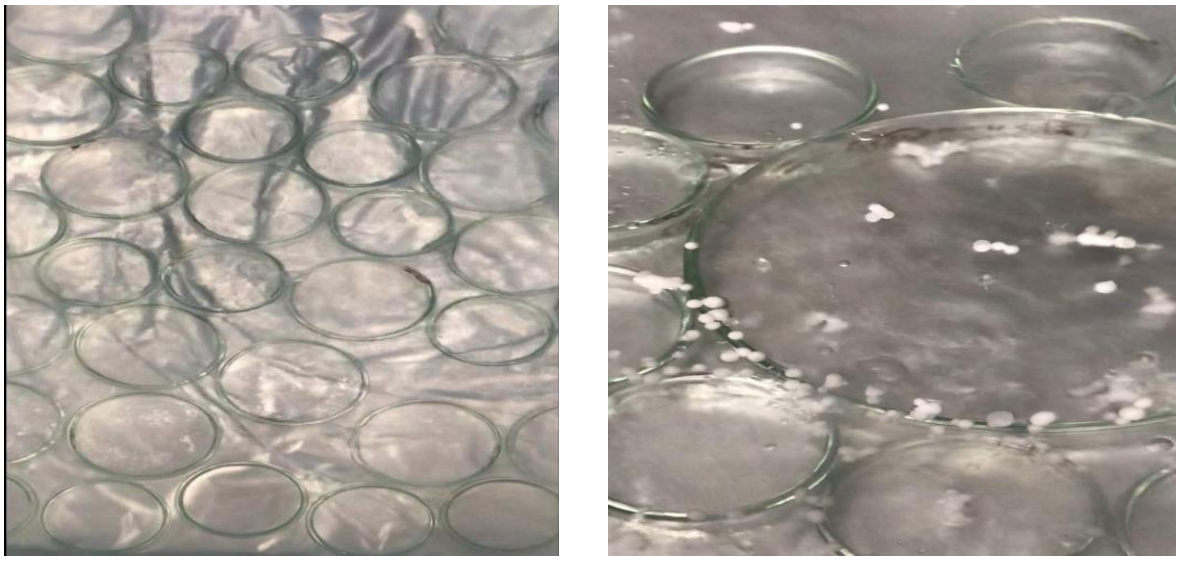

Figure 3.8: Detail of the tray used with the Petry capsules prominently on the left; on the right a close view of the particles being frozen.

3.4 Drying

After freezing, the sample was at first placed into a refrigerator working at -80 °C, for at least 30 min. In this way, the temperature of the particles reaches the same value, fixing any possible change during the collection of the sample hence avoiding ice melting. After that, the particles are located in the dryer chamber. As already stated above, the device depicted in Figure 3.9 has been built by Prof. Nakagawa group and it has not two different locations for the condenser and the drying chamber respectively, as it happens instead for the industrial-scale ones.

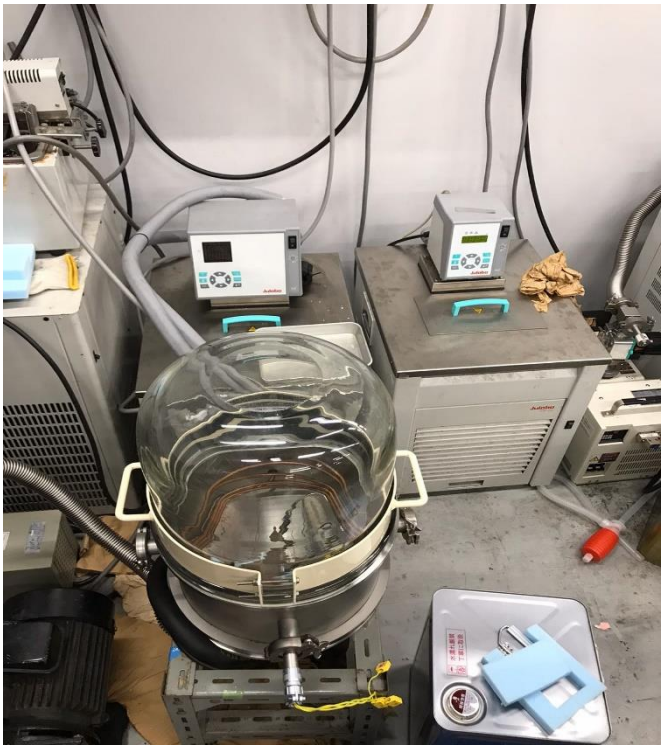

Figure 3.9: Drier used in Kyoto.

The freeze-dryer used consist of the basic elements: refrigeration system (i), a vacuum system (ii), product chamber or manifold (iii), and condenser (iv). The refrigeration system cools the condenser located inside the freeze-dryer. It cools both the shelves and the condenser in the product chamber to freeze the product. The vacuum system consists of a separate vacuum pump connected to an airtight condenser and an attached product chamber. The drying chamber is a vertical cylinder containing the condenser installed close to the shelve. The sample placed in the Petri disks received heat supplied through radiation or conduction to particles. The condenser attracts the vapours being sublimed off the product and condenses them back into a solid form (ice). Due to its lab-scale the condenser is located inside the product chamber (internal condenser, as shown in Figure 3.10) and not in a separate chamber (external condenser) connected to the product chamber by a vapor port. That is the reason why it was impossible to obtain any measurement of time or temperature during the drying.

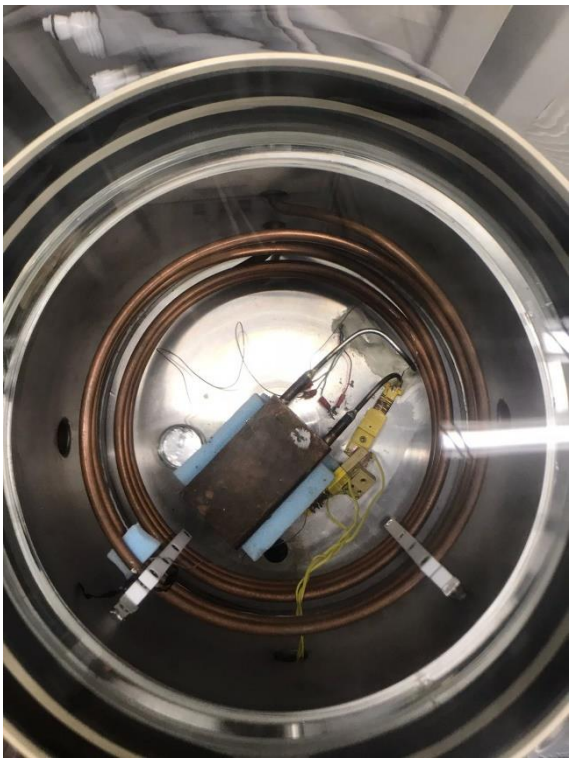

Figure 3.10: Image taken from inside the chamber: detail of the condenser and the shelf.

The condenser and the shelf are in the same chamber, they are maintained through a refrigeration fluid at constant temperature -20°C for the shelf and -60 °C for the condenser. This difference in temperature and partial pressure push the vapor to leave the particles decreasing the water content of it, the primary drying starts. After 12h, the time control was impossible to achieve due to the laboratory scale and nature of the drier, the temperature of the chamber is increased to allow the rest of the water to leave the particles the new temperatures are +20 °C for the shelf and + 5 °C for the condenser. These parameters are maintained for 1 h after that the pump is turned off, the vacuum released, and the dried powder collected and labelled.

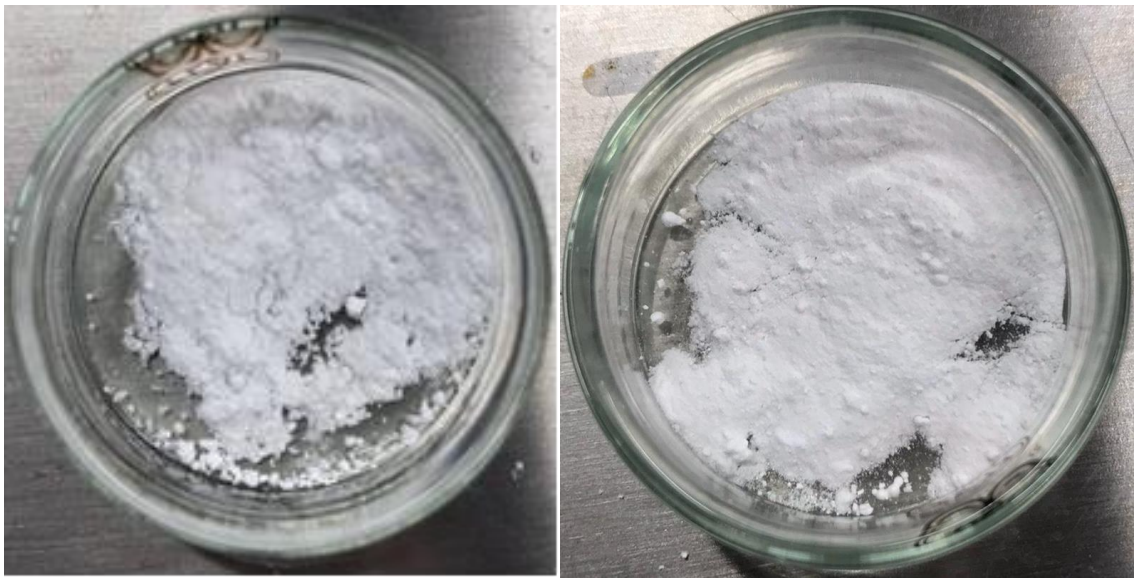

Figure 3.11: Lyophilized samples as obtained from a 10% w/w (left) and 15% w/w (right) mannitol solution. In both cases, particles were obtained by using a spray gun atomizer.

Figure 3.12: samples dried from a liquid solution 10% w/w (left) and 15% w/w (right) of mannitol. Both obtained atomizing with the vibrating needle.

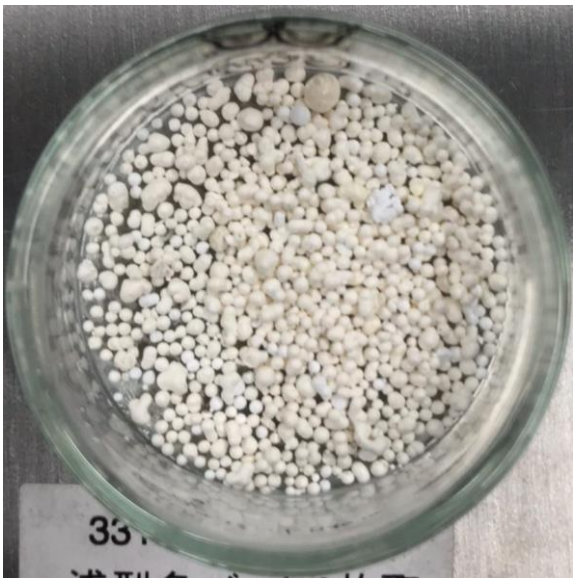

Figure 3.13: Sample dried from the liquid solution 5% w/w trehalose 5% w/w albumin atomized with the vibrating needle.

Figure 3.11- 3.13 shows the samples obtained after a complete SFD process for all the three the liquid solutions prepared and described in Table 3.1. Among the formulations prepared only solution a and b, the two mannitol-based, have been atomized with both the techniques described in paragraph 3.1; the solution c have been sprayed only with the vibrating needle since, as already stated, seems to give the most satisfying results in terms of particles morphology. In fact, a considerable difference in size and shape between the mannitol particles can be observed. The ones obtained with the vibrating method are larger and more spherical, the same features cannot be found in the particles obtained with the spray gun. In this last case, in fact, it was not possible to distinguish the different granules. The dimension varies from μm of the powder to various mm in the case of the spherical particles. The samples hence obtained has been further analysed in order to characterize the dried solutions trying to obtain an experimental measurement of its internal surface and pores size.
These data were obtained by three main methods:

- Scanning electron microscope (SEM)
- X-ray powder diffraction (XRD)
- Nitrogen adsorption

The results of these analyses are discussed in the following sections. Due to the humid weather in Kyoto the samples after drying were placed in a hermetic plastic bag with silica gel.

3.5 SEM analysis

The size of the ice crystals formed during freezing coincides with the size of the pores created after drying, they are in fact the void left by the ice after sublimation. An electron scanning microscope (SEM) was used to observe the shape and size of these pores, which provides a topographic analysis of the product itself. SEM works by using a beam of low-energy primary electrons (0,5-10 kV), which, interacting with the surface, scan the sample under analysis. This interaction then induces the emission of X-rays, back-scattered electrons and secondary electrons, the intensity of which depends on the surface topography of the sample. An image of the surface of the sample can, therefore, be reconstructed by measuring the intensity of the emitted secondary electrons as a function of the position of the primary beam of electrons in its

scanning movement. By increasing the magnification of the image, the energy of the incident beam of primary electrons will also increase; the higher the energy of the beam, the greater the probability of compromising the final product. Moreover, the intensity of the back-scattered electrons can be correlated with the atomic number of chemical elements present on the surface under analysis and therefore some qualitative indications on the elementary composition can be given. Before putting the sample in the SEM, the particles have been put on an adhesive tape with magnetic features so to be seen during the measurement. Once attached the samples have been further dried in a vacuum dryer working at -0.1 MPa for at least 2 h to remove any water molecules which could be re-adsorbed on the particles, it is a regular. After that, since the samples tested were non-conductive, they were subjected to metallization before being analysed with SEM. In fact, due to their non-conductive nature, particles surface acts as an electron trap. This accumulation of electrons on the external surface is named "charging" and leads to the creation of white areas on the sample which alter the image obtained. The material used in our case was gold, because of its high conductivity and the relatively small size of the grains, which allows to obtain high resolution images. The surface has hence been covered by a layer of nebulized gold on its surface to make it detectable by the electron beam. For the samples under analysis, 2 SEM images type were acquired from both the external and internal surface, in order to represent the morphology of the lyophilized product. Thanks to the images acquired, it was, therefore, possible to observe in a qualitative manner the average size of the pores obtaining a pore size distribution.
The evaluation procedure consists of manually determining, from SEM image of the different samples, the average diameter of a population of pores assuming a cylindric shape for the latter. Given the irregularity of these pores, only the diameter was measured as a characteristic quantity. The average diameter was then obtained by carrying out a weighted average of the average diameters obtained. Figures 3.14 and 3.15 show an example of some SEM images obtained for the mannitol-based solutions used for the evaluation of the diameters discussed above.

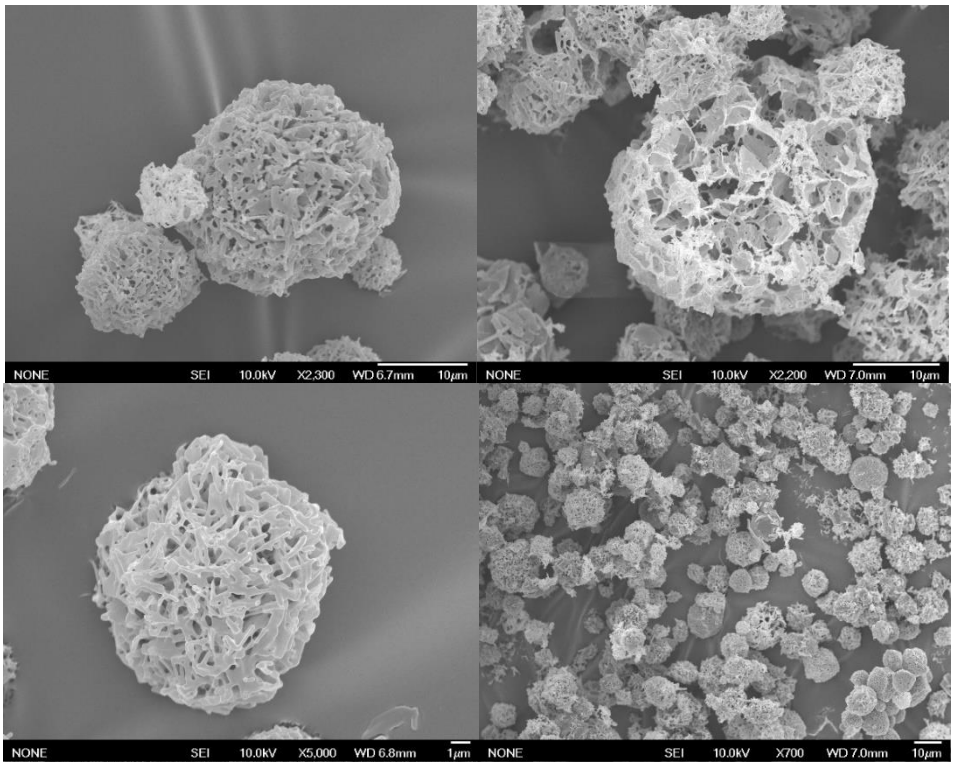

Figure 3.14: SEM images of a 10% w/w solution of mannitol atomized with the spray gun system and then lyophilized.

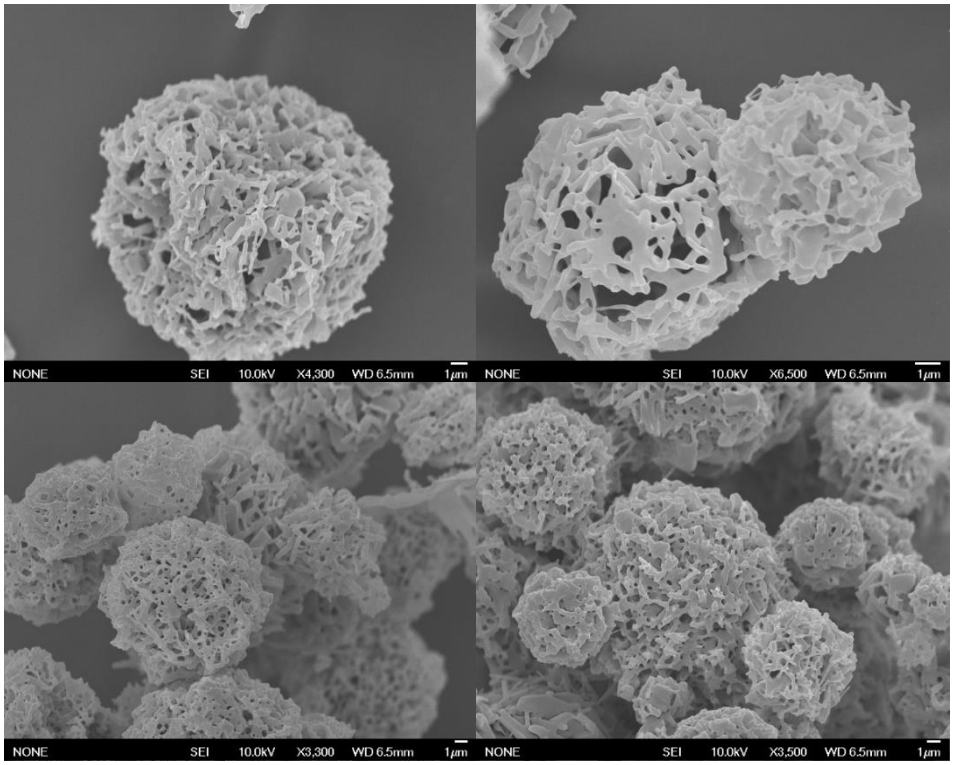

Figure 3.15: SEM images of a 15% w/w solution of mannitol atomized with the spray gun system and then lyophilized.

As shown in the images, the particles obtained with the spray gun are not perfectly spherical, the external surface looks rugged and irregular and the pore size detection is hard to achieve, some internal pores are shown (for both the concentration) in Figure 3.16. The powder has been shattered in order to cut the particle in half to access the cross-section and clearly see the pores in it.

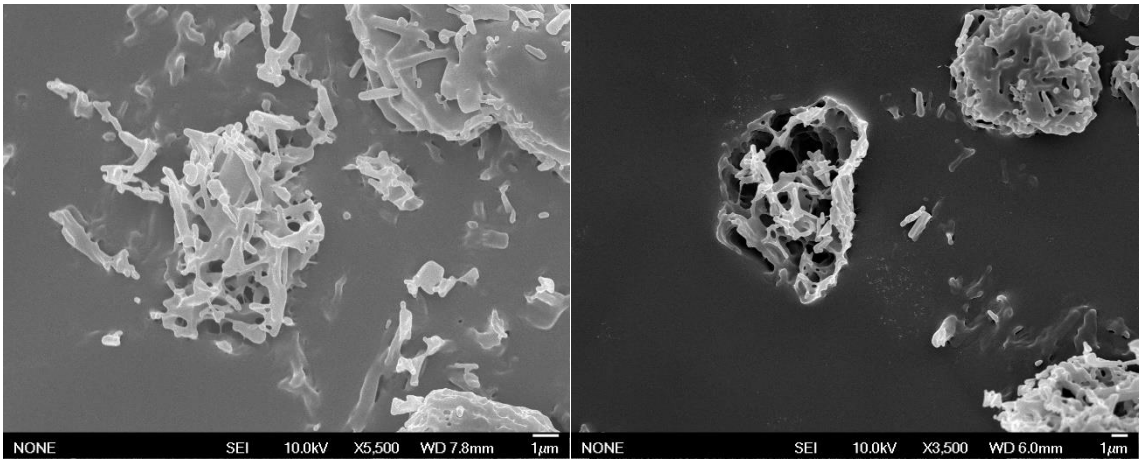

Figure 3.16: SEM images of broken particle from the two formulations of mannitol 10% w/w on the left 15% w/w on the right) atomized with the spray gun.

Despite the effort, it was impossible to collect a clear image of the cross-section notably enough for measuring the pores. That is the main reason why we choose to change the atomization technique hence the size and morphology of the particles obtained. It was easier to cut in half the particles and to measure the pores on its cross-section (Figure 3.17).

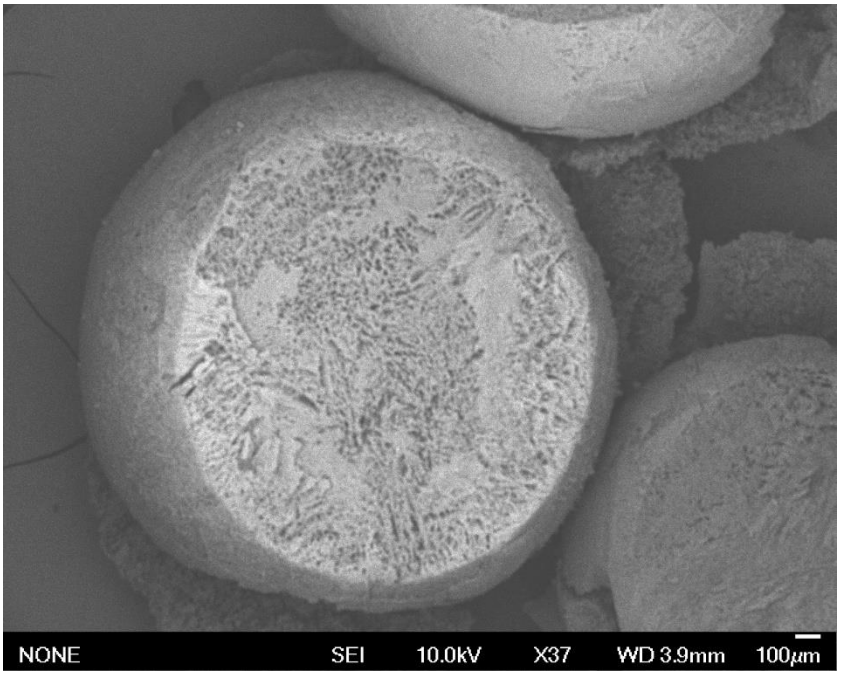

Figure 3.17: SEM image of a particle cut halved, to show an example of how the particles have been prepared before using SEM.

The SEM images of the three solutions atomized with the vibrating needle is shown in Figures 3.18 - 3.20, evidencing both external and internal surfaces for each sample.

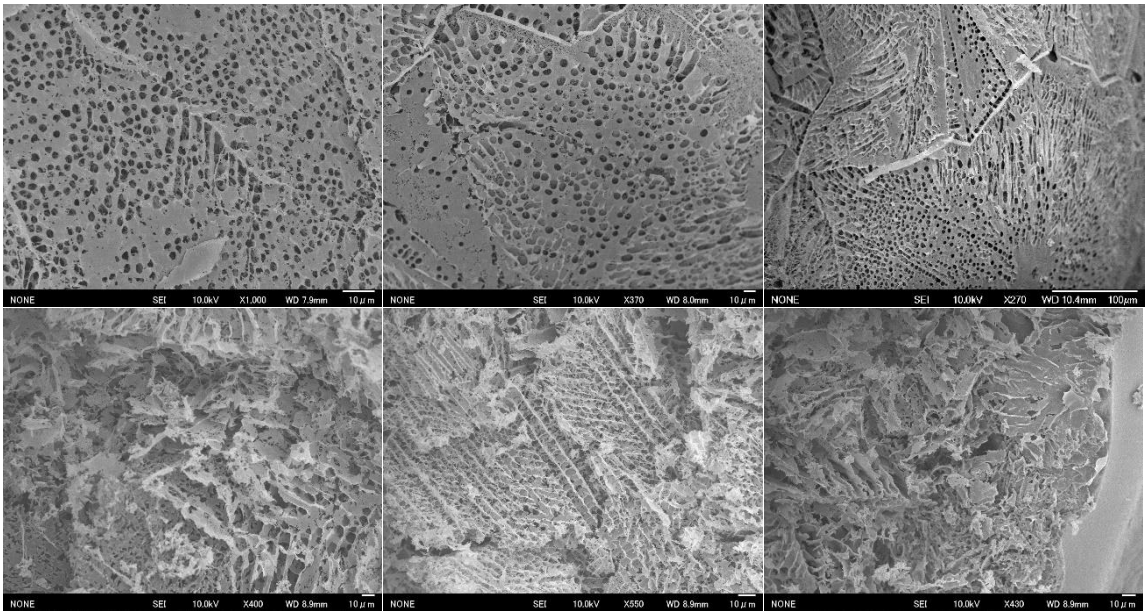

Figure 3.18: SEM images of 10% w/w solution of mannitol atomized with the vibrating needle. The images above show the external surface, the images below show instead the cross-section.

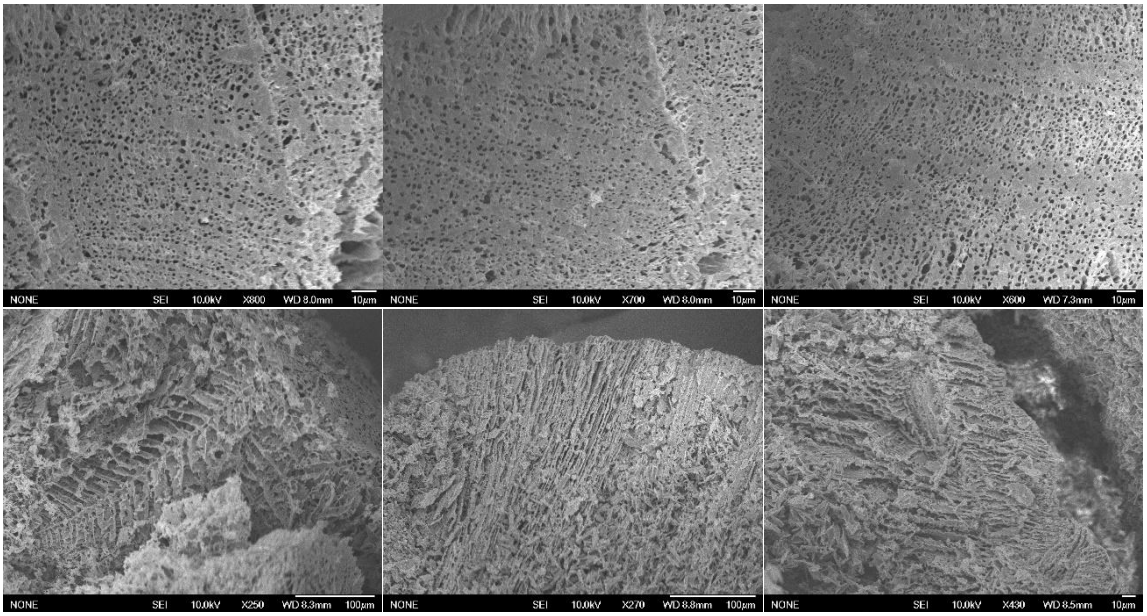

Figure 3.19: SEM images of 15% w/w solution of mannitol atomized with the vibrating needle. The images above show the external surface, the images below show instead the cross-section.

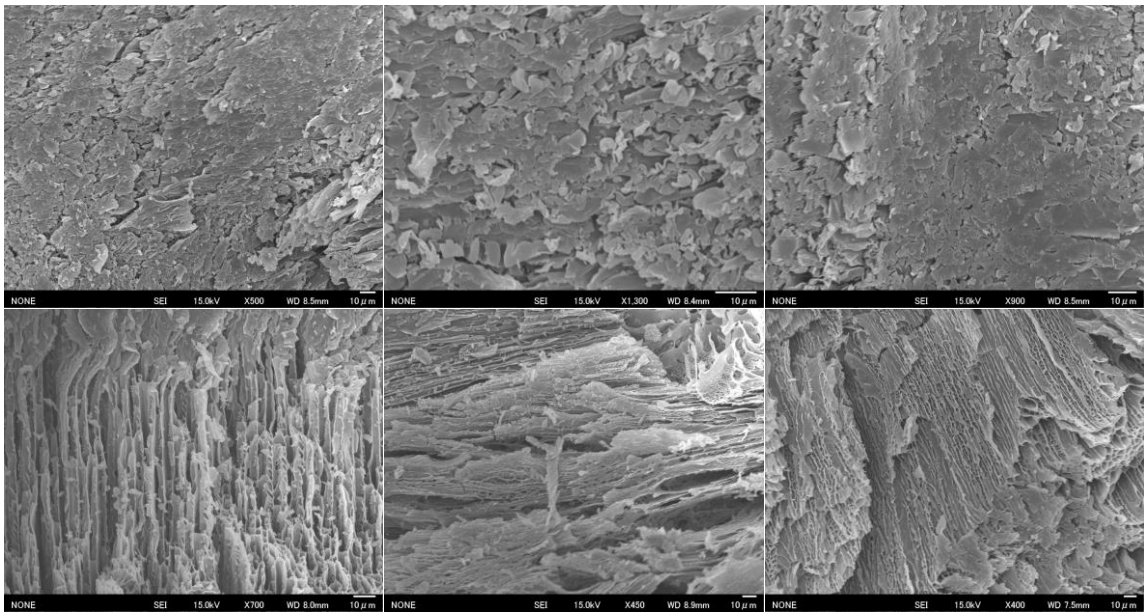

Figure 3.20: SEM images of 5% w/w trehalose 5% w/w albumin solution atomized with the vibrating needle. The images above show the external surface, the images below show instead the cross-section**.**

These pictures have then been processed using *ImageJ* program (vers1.39). This software in fact can be used to measure any length or area starting from an image by setting at first the scale. In our case it allows to directly detect the diameters of the pores by drawing a line to connect the edges of one pore (as shown in Figure 3.21). By repeating this procedure for all measurement needed it was possible to obtain a distribution and an average value.

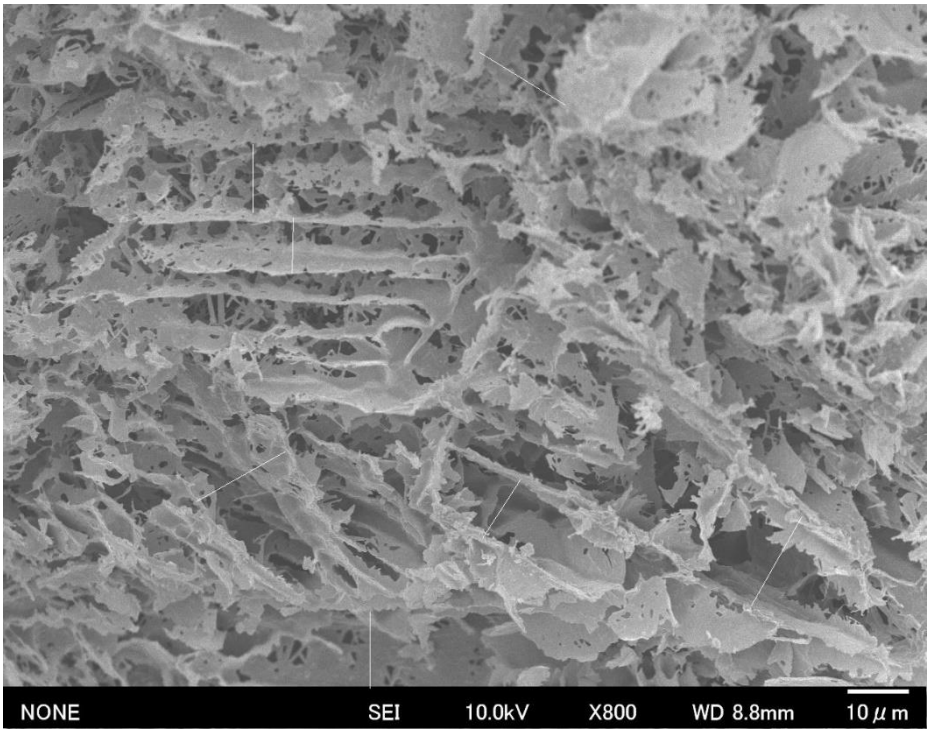

Figure 3.21: SEM images of a particle cross-section during the measurement (in white the length measured) of the pore size using ImageJ.

3.6 XRD analysis

The freezing process determine the preferred formation of different polymorphs which influence important features such as the reconstitution time, the storage stability and the protein stability. Mannitol has three different polymorphs: α, β, δ.The thermodynamic stable form of mannitol is the β one, while α and δ are metastable. That is why understanding the physical state of excipients is important and XRD measurement was used. X-ray powder diffraction (XRD) is a rapid analytical technique primarily used for phase identification of a crystalline material and can provide information on unit cell dimensions. The analysed material is finely ground, homogenized, and average bulk composition is determined. X-ray diffraction is based on constructive interference of monochromatic X-rays and a crystalline sample. These X-rays are generated by a cathode ray tube, filtered to produce monochromatic radiation, collimated to concentrate, and directed toward the sample. The interaction of the incident rays with the sample produces constructive interference (and a diffracted ray) when conditions satisfy Bragg's Law ($n\lambda=2d \sin\theta$). This law relates the wavelength of electromagnetic radiation to the diffraction angle and the lattice spacing in a crystalline sample. These diffracted X-rays are then detected, processed and counted. By scanning the sample through a range of 2θangles, all possible diffraction directions of the lattice should be attained due to the random orientation of the powdered material. Conversion of the diffraction peaks to d-spacings allows identification of the mineral because each mineral has a set of unique d-spacings. For this purpose, we have compared the d-spacings with standard reference patterns: some samples were analysed to compare them with the references pattern for mannitol through a qualitative analysis the spectra hence determined were compare with the position of the polymorphs (α, β, δ) peaks.

3.7 Nitrogen adsorption

The fundamental parameters to be evaluated from the samples under analysis are the exposed surface and the average size of the pores. They are usually deduced by measuring the adsorption isotherms, deducted by measuring the amount of gas adsorbed across a wide range of relative pressures at a constant temperature (typically liquid N_2, 77K). These curves represent the mass of gas adsorbed on the porous matrix as a function of the equilibrium pressure of the surrounding vapour. The process of BET measurement is shown in Figure 3.22. As all data are measured relative to P, that is the saturation pressure of adsorbate at the temperature of adsorption, which must also be calculated. It can either be measured initially for an empty tube (as in our case, to the device an empty vial has been connected) or it can be measured at the same time as the measurement described below is occurring in a third tube(Sing, 2001). The assumptions made for the measurement are:

- Homogeneous surface
- No lateral interactions between molecules
- Uppermost layer is in equilibrium with vapour phase
- All surface sites have same adsorption energy for adsorbate
- Adsorption on the adsorbent occurs in infinite layers
- The theory can be applied to each layer

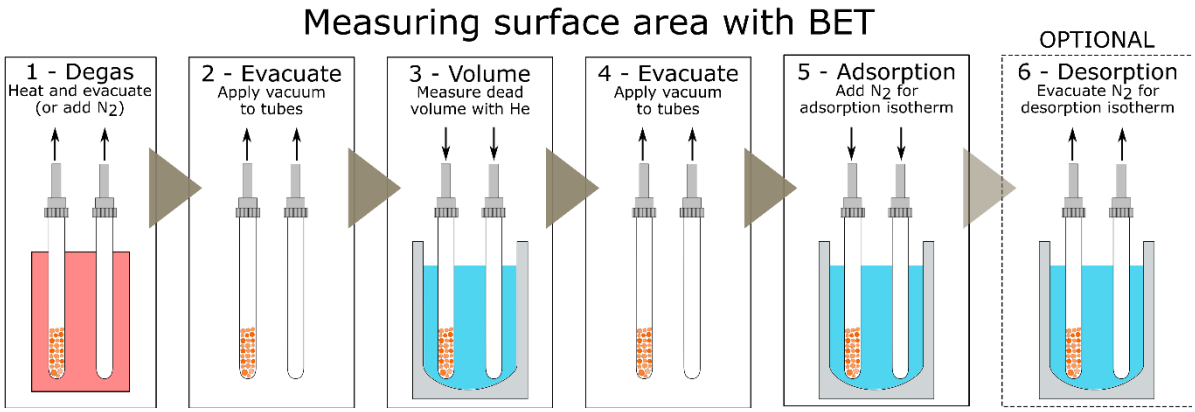

Figure 3.22: Measuring surface area with BET. Figure reprinted from https://andyjconnelly.wordpress.com/ (last access 23/11/19) with modifications.

In our case as a first attempt we tried to perform the analyses using Nitrogen but, regardless of the gas used, we realized that the sample must be pre-treated in order to remove any content of water. So, the samples were dried 2 hours under vacuum conditions at 80/90 °C. Once the pre-treatment is completed the samples are placed in the adsorption machine that is shown in Figure 3.23.

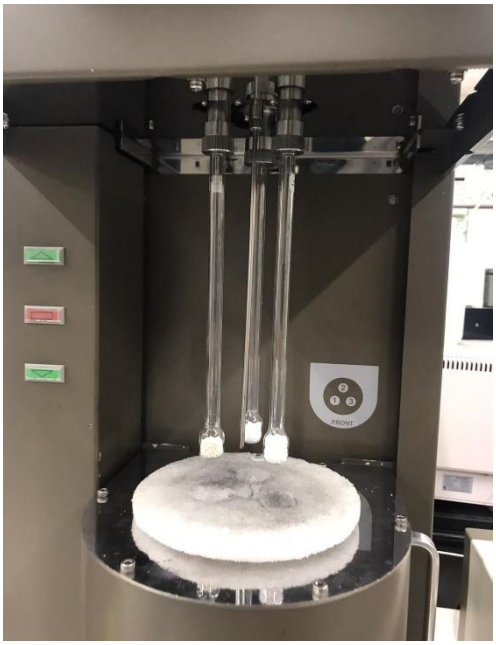

Figure3.23: Nitrogen adsorption analyser used in Kyoto, sample loaded after the removal of the water contained.

The machine simply records different pressures of gas in the sample cell due to adsorption and desorption. The instrument then calculates the amount (as STP volume) of gas adsorbed/desorbed. Surface area and pore size are then calculated by BELSORP vers.2. The results are presented as isotherms; there are six adsorption isotherms according to the IUPAC classification (see Figure 3.24). This classification of gas-solid adsorption isotherms, which covers the behaviour of a great number of adsorption system, associates to each gas-solid equilibria a certain range of pore size, shown in Figure 3.25.

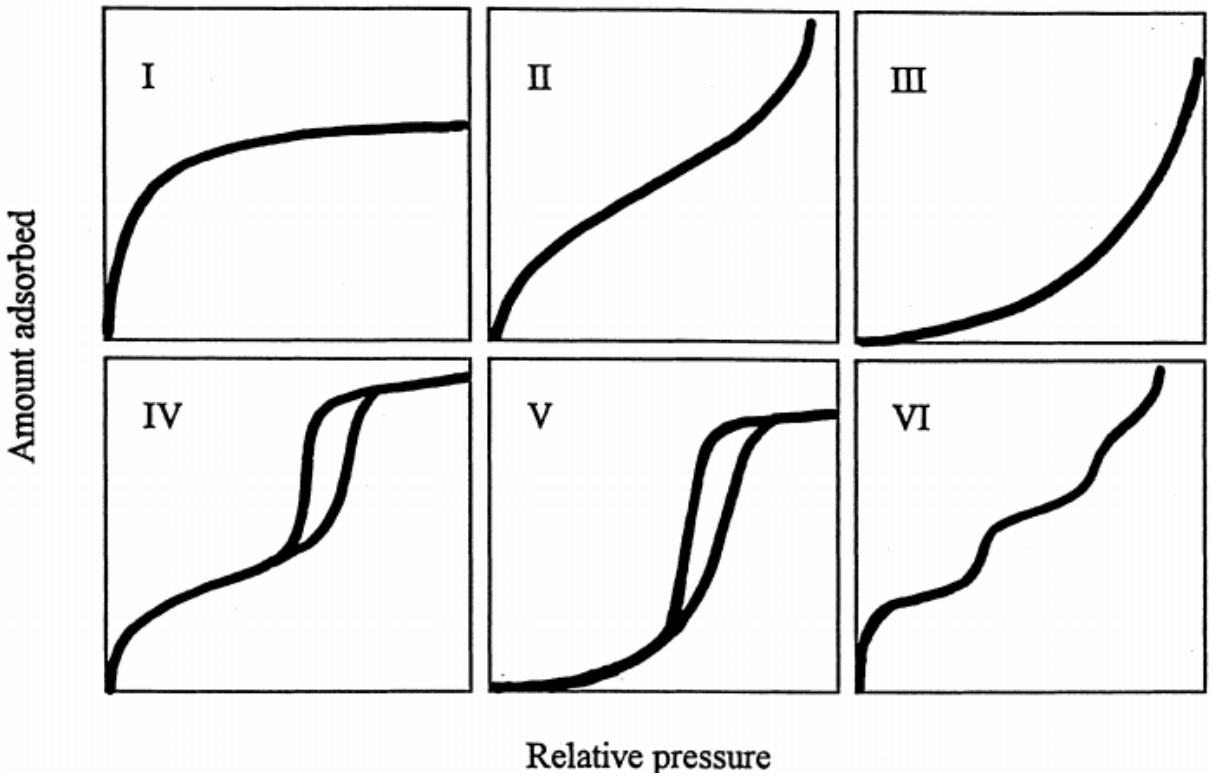

Figure 3.24: IUPAC classification of adsorption isotherms. Image reprinted from lafsi.fisica.unipd.it (last access 22/11/19) with modifications.

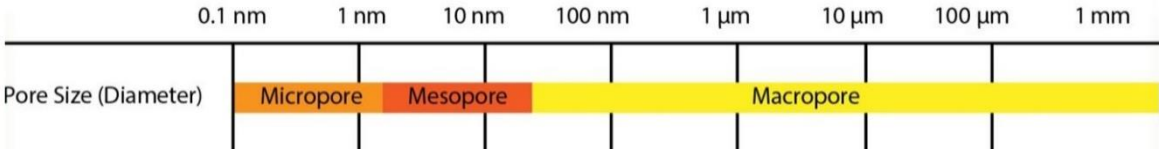

Figure 3.25: pore size classification. Image reprinted from andyjconnelly.wordpress.com (last access 22/11/19) with modifications.

Type I isotherm (concave to P/P_0 axis) approaches a limiting value as $P/P_0 \rightarrow 1$ and usually is used to describe adsorption on microporous adsorbents. Types II and III (convex to P/P_0 axis) describe adsorption on macroporous adsorbents with strong and weak adsorbate adsorbent interactions respectively. More over type IV and V represent mono-and multilayer adsorption plus capillary condensation while type VI, which was not included in the Brunauer classification, illustrates that the adsorption isotherms can have one or multiple steps(Donohue and Aranovich, 1998). We then decided to repeat all the measurements switching from nitrogen to argon; the device and working principle stay the same the only difference is the gas used and hence the adsorbed molecules dimension.

Chapter 4

Results

This chapter shows the experimental data collected at Kyoto University on the spray freeze-drying technology. Attention was focused on the impact of process conditions on particles morphology, shape and average pore size. Furthermore, the mathematical model, presented in Chapter 2 for the description of the freezing of droplets suspended into a cryogenic gas, is validated in terms of average pore size.

4.1 Spraying method

As already stated in Section 3.2, we have tested two spraying methods which, as will be discussed later, produced particles having different shape and size. As first attempt, we used a pneumatic atomizer. Figure 4.1 and 4.2 shows an example of particles so obtained. Such particles appear as fine powder since they were very small; their average size was 1-20µm. Results refer to two mannitol-based formulation having 10% w/w and 15% w/w as solid content. From SEM images, we have also calculated the particle size distribution using the software *ImageJ* (vers. 1.49). The results of this analysis are shown in Figures 4.3.

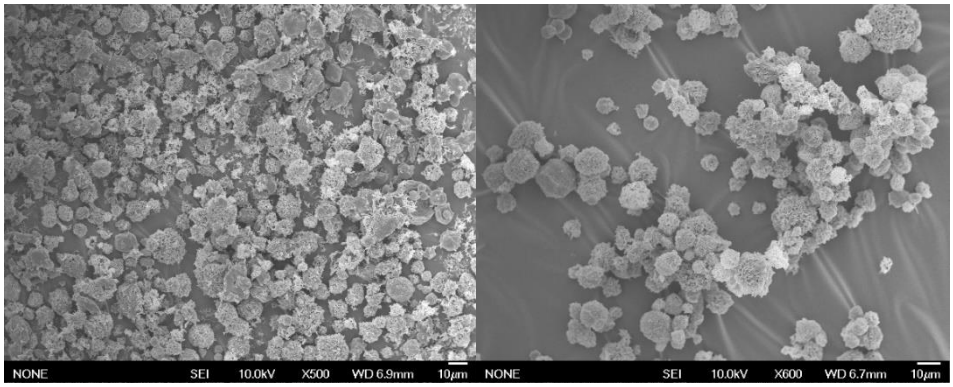

Figure 4.1: SEM images of the particle population obtained from10% w/w mannitol solution spray freeze dried atomized with the spray-gun.

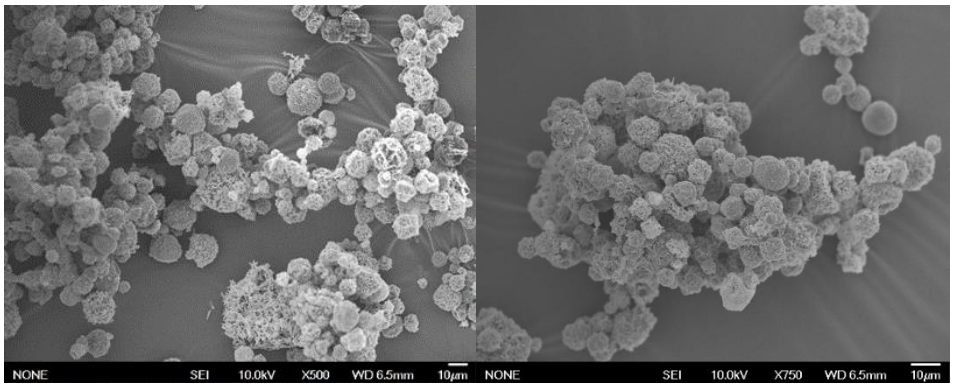

Figure 4.2: SEM images of the particle population obtained from 15% w/w mannitol solution spray-freeze dried atomized with the spray-gun.

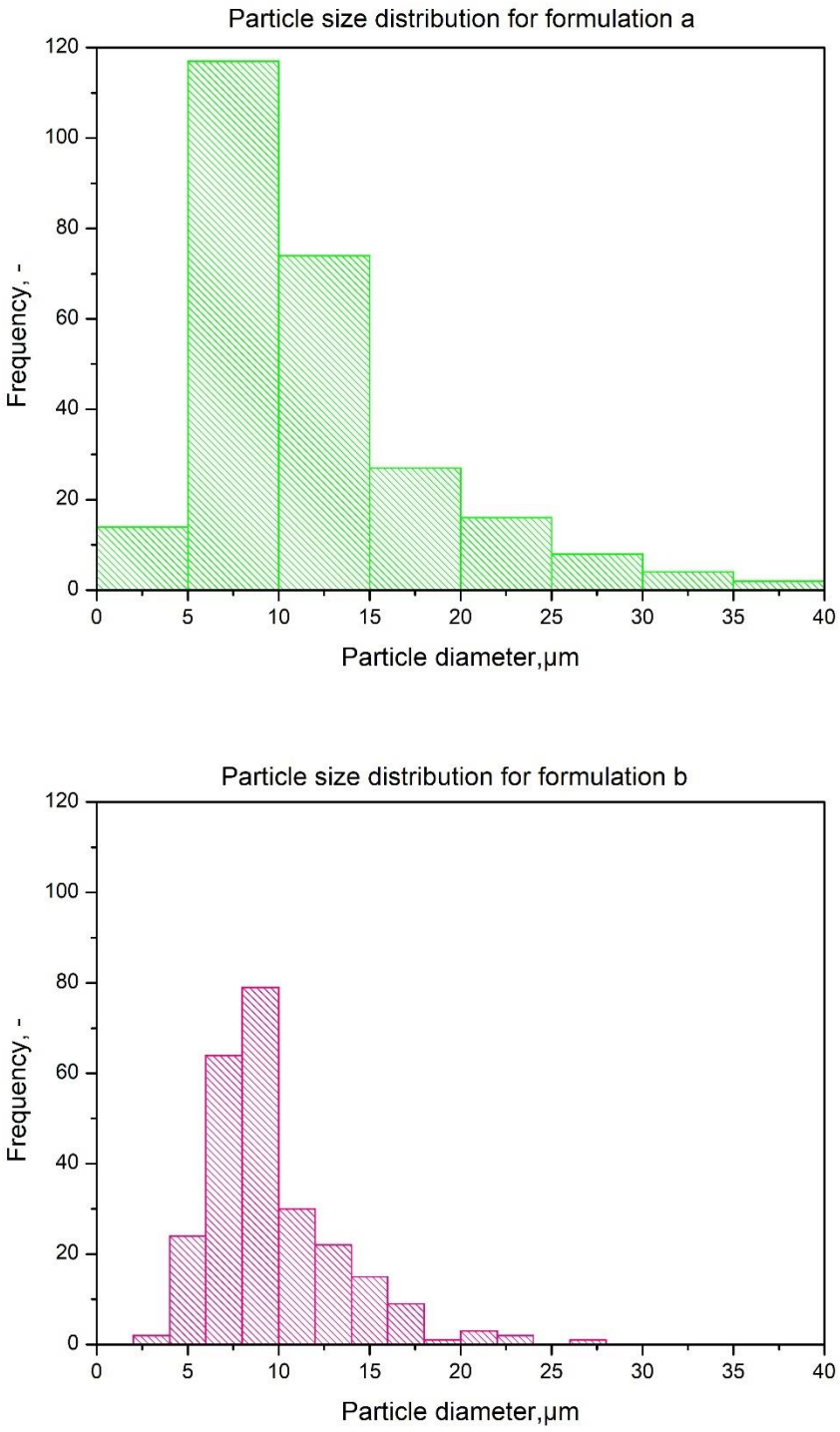

Figure 4.3: Particle size distribution for the two mannitol-based solutions atomized with the spray gun. The two distribution differ being the first one spreader than the second one which is narrow.

In Figure 4.3, it is possible to observe how the particles' diameters of solution A are bigger than of those observed for solution B and more disparate. The particles' distribution of solution B, on the other hand, was narrower indicating that the particles are more uniform than the previous case. Anyways the particles are generally small, and this is due the atomized device used which ensures a dispersion of the liquid stream into fine particles. For the same particles we have then

estimated, using ImageJ vers. 1.39, the size of 1754 particles. Then, we have calculated its average diameter and the results are shown in Table 4.1.

Table 4.1: Average particle size for both mannitol solutions.

Concentration,-	Average particles dimension, µm
10% w/w	11.43
15% w/w	9.67

The average diameter of formulation a is larger as expected but still too small for the required analysis. In fact, because of their small size, it was very difficult to obtain an estimation of the average pore size. We could not cut the particles along their radius. However, we could obtain information about their internal structure from SEM images of particles spontaneously broken during the manipulation of the powder. An example of result is given in Figure 4.4. However, the porous structure is very open and pores very interconnected, so it was very difficult to establish the borders of individual pores. Even where possible (when we were lucky and some particles spontaneously broke in the cross section) the measurement was not repeatable for an enough time. As second attempt, we tried to use a different atomizing system in order to produce larger particles which can better be characterized the results are notable in Figure 4.5.

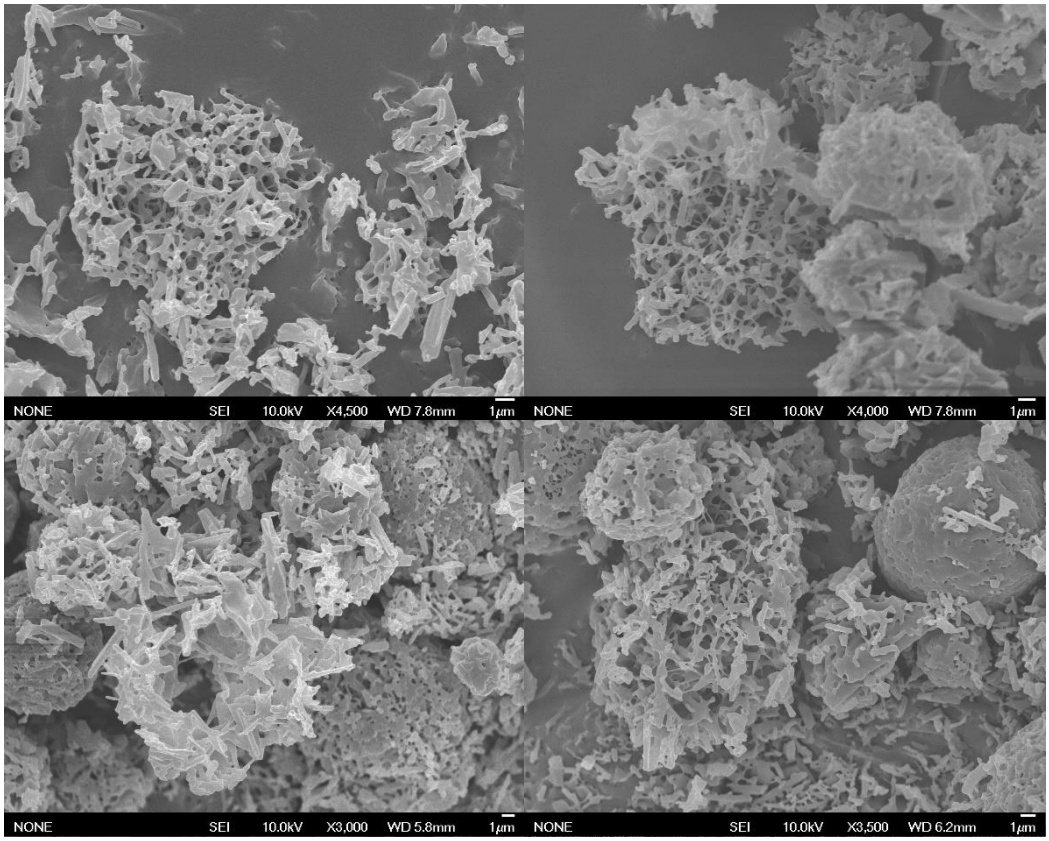

Figure 4.4: SEM images of some particles 10% w/w the two above,15% w/w the two below) broken by grindering the sample dried.

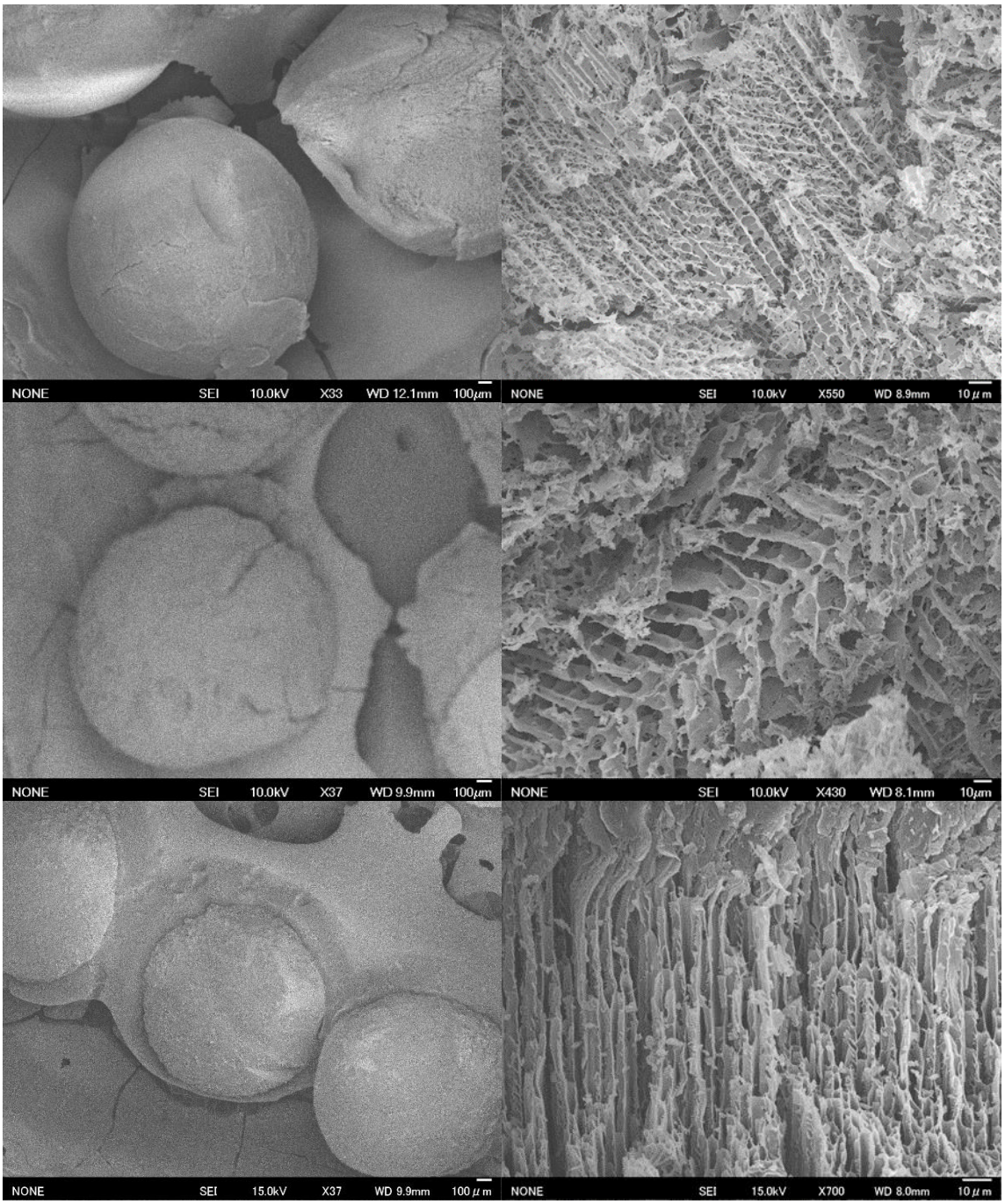

Figure 4.5: SEM images for the three formulation of the particles obtained and their correspondent internal structure. In order solution A, B and C.

As can be noticed from the images the particles obtained with this technique are larger and more spherical. Moreover, the surface is smoother and uniform except for micro-breakage caused while handling the sample. Due to particles dimensions and the limit of the SEM chamber, only a limited number of these particles could be placed in it, it was not possible to obtain a proper distribution due to the insufficient number of measurements. Considering the cross-section, we have a completely different scenario from the previous pores observed. The structure is more ordered, it is possible to distinguish the delimitations for each pore and hence it is possible to calculate the diameter. The pores have an elongated shape like ropes, they are organized in fasces following the same orientation, typical for the dendritic growth of ice (Shimada and Furukawa, 1997). Spray drying performed with the vibrating needle led to the

typical morphology of spherical particles in all tests, while the other method's particles were irregular and angular. Contrary to the spray gun particles morphology, strongly influenced by the parameters of the drying processes, the shape of the SFD powder atomized with the needle was mainly influenced by the cutting and screening processes after drying.

4.2 Specific surface area determination

Beside the pores it is significative to understand the internal morphology of the particles, to have an idea about the internal surface left after ice sublimation. To do so, samples have been analyzed using the gas adsorption measurement of both nitrogen and argon. The first samples analyzed were the one obtained from the mannitol solutions. The results achieved are presented in the Figure 4.6.

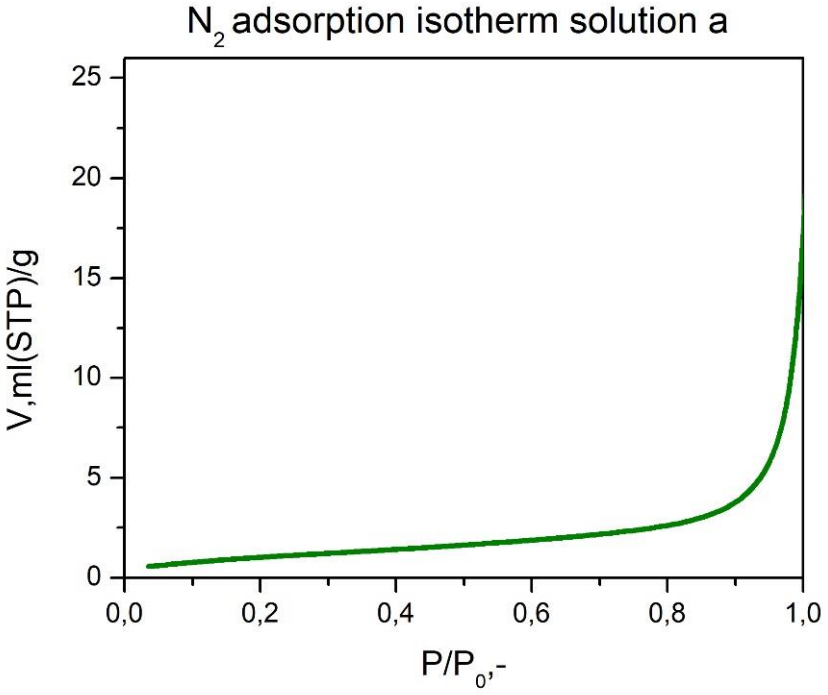

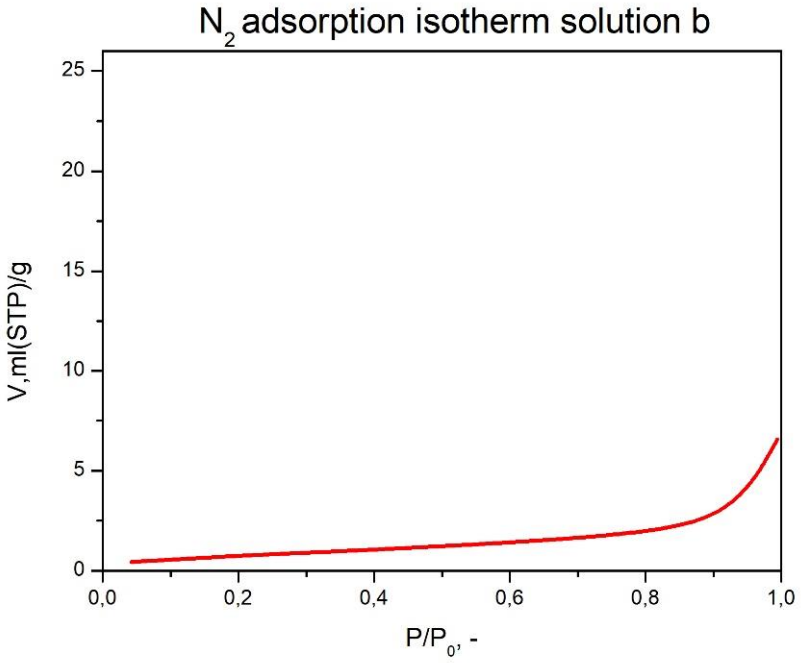

Figure 4.6: Nitrogen adsorption isotherm for solutions a and b.

Since what is measured is the amount of the gas adsorbed on the particles surface, it is important to take into consideration a crucial feature such as the dimension. Hence, beside nitrogen (atomic radius=155pm) we have decided to repeat the measurement maintaining the same conditions and using devices but switching the fed gas to argon (atomic radius=71pm). Being smaller, more than half compared to nitrogen, it is more accountable since argon molecules can more easily access to the porous structure of the dried material. The argon isotherms are shown in Figure 4.7 for the two mannitol-based solutions.

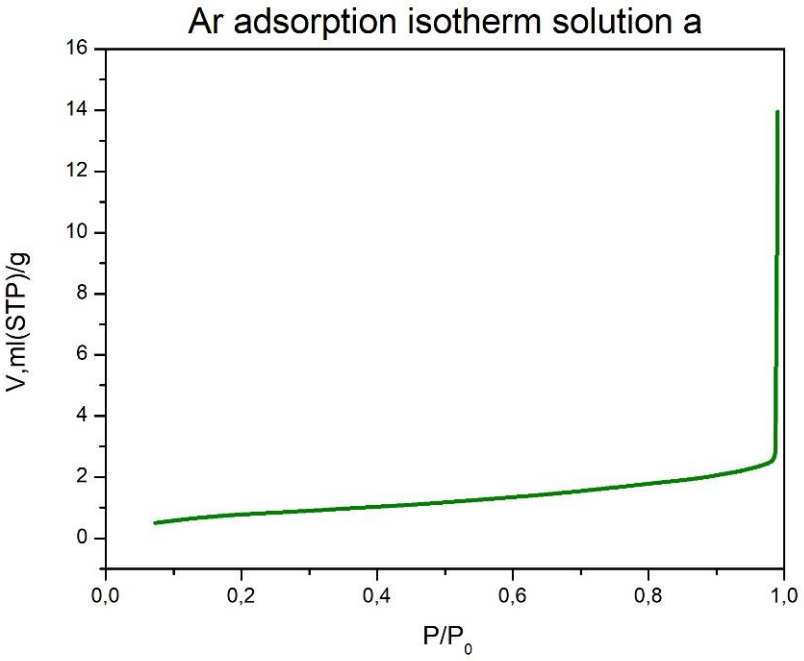

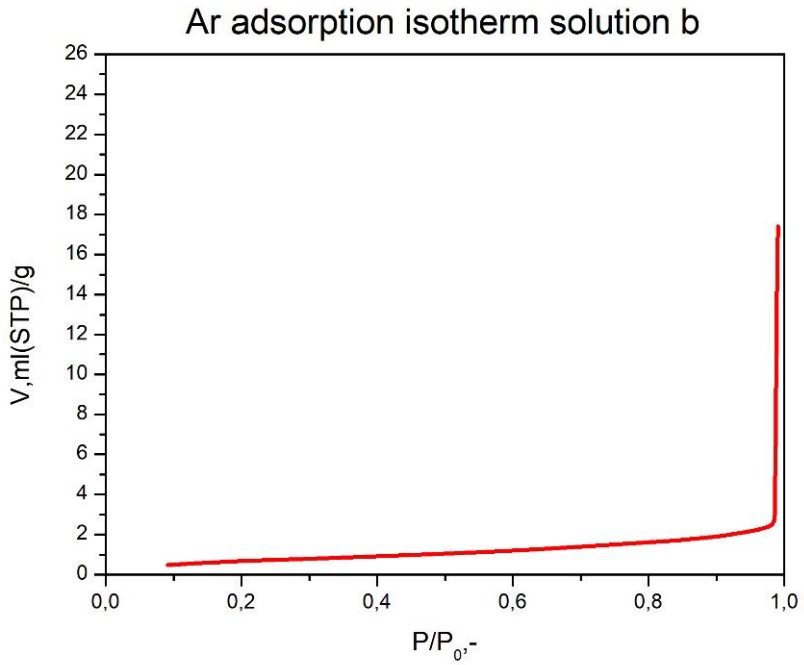

Figure 4.7: Argon adsorption isotherm for solutions a and b.

Despite the theoretical basis of the choice made, comparing both the isotherms and the specific area detected (Table 4.2), the values obtained were not that different.

Table 4.2: Comparison between nitrogen and argon in term of specific surface, m^2/g, for the two mannitol-based formulations studied a and b.

Gas adsorbed	Solution A	Solution B
Nitrogen	3.1	2.9
Argon	3.8	2.7

Once finished analyzing the samples from the mannitol-based solutions, a problem with the results obtained has emerged: due to its crystallinity, mannitol created an internal architecture of pores which are originated by the sugar and not by the ice sublimated. The surface built in this manner is exposed to the gas and then detected. From the surface measurement it is impossible to discern between the two and this infects the reliability of the detection. For this reason, we have decided to change the formulation preparing a solution with trehalose (5% w/w) and albumin (5% w/w) as described in paragraph 3.1. Trehalose is amorphous, for that XRD measurement was not performed on the sample obtained from this specific formulation, avoiding any interference in the analysis. The isotherm obtained with nitrogen and argon and the measurement of the specific area for formulation c are presented in Figure 4.8 and Table 4.3 respectively.

Table 3.3: Comparison between of specific surface area of samples obtained from freeze-drying of solution C using either nitrogen or argon.

Gas adsorbed	Speacific Surface Area, m^2/g
Nitrogen	4.6
Argon	4.7

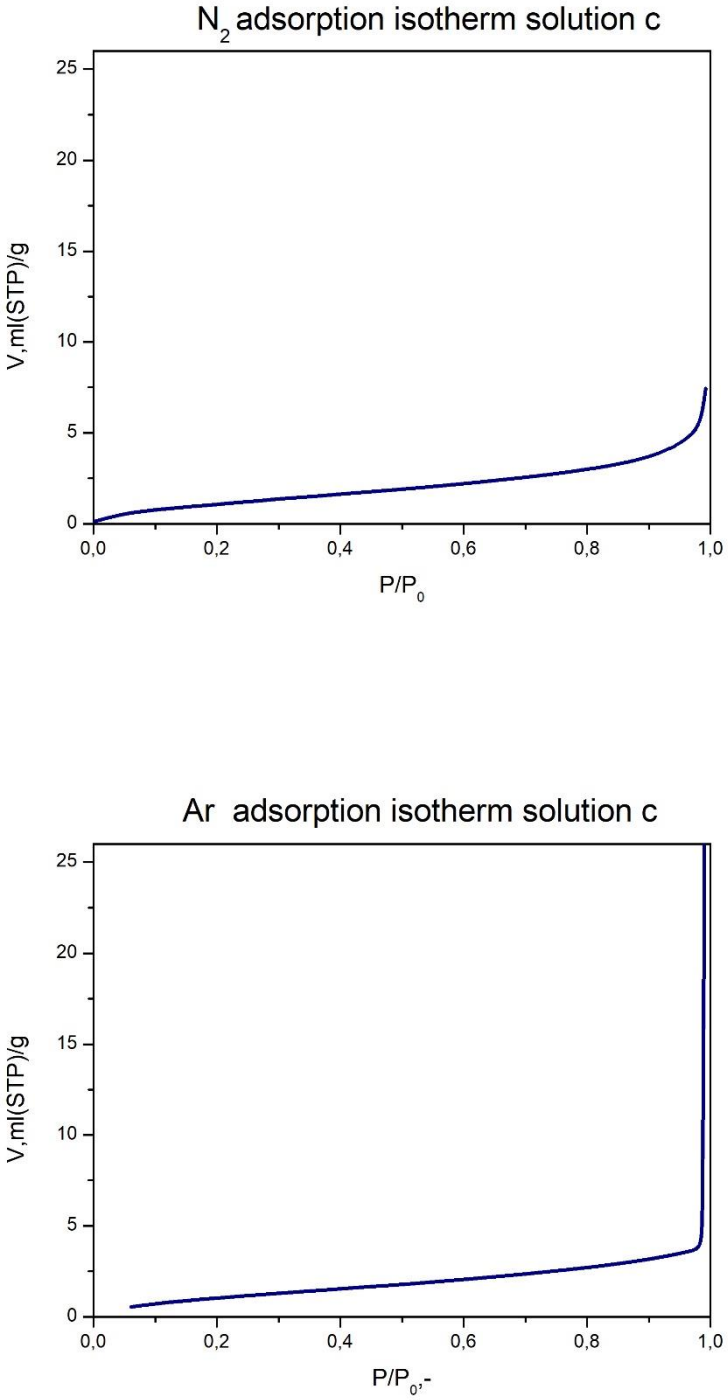

Figure 4.8: Nitrogen and argon adsorption isotherms for solution c.

The adsorption branches for all the formulations and the adsorbed gas at first glance resemble a type II curve (non-porous or macroporous materials) as per the IUPAC classification (Figure 3.23. This type of isotherm suggests capillary condensation typical of mesopores, which are pores measuring 2-50 nm. Mesopores sizes lie between those of the micropores (< 2 nm) and macropores (> 50 nm). The isotherms have a sharp step increment at a relative pressure (P/P0) of ~0.9. Similar isotherms were also reported for other air-dried materials (Kawasaki,

Shimanouchi and Kimura, 2019). The volume of nitrogen adsorbed at ~0.96 was estimated (assumed cylindrical pores) to correspond to a pore diameter of 50 nm (Kawasaki, Shimanouchi and Kimura, 2019). Comparatively, all three samples exhibit the highest adsorption at high relative pressures.

4.3 Average pore size determination

Using SEM images, the average pore size has been determined. The measurements of the void dimension left by the ice were used to calculate an experimental value for comparing with the one evaluated from the model. The pores were not considered on the external surface. Both the morphology and the pore could be affected by multiple factors and not reconnectable to the pore size of particles inner structure (Figure 4.9)

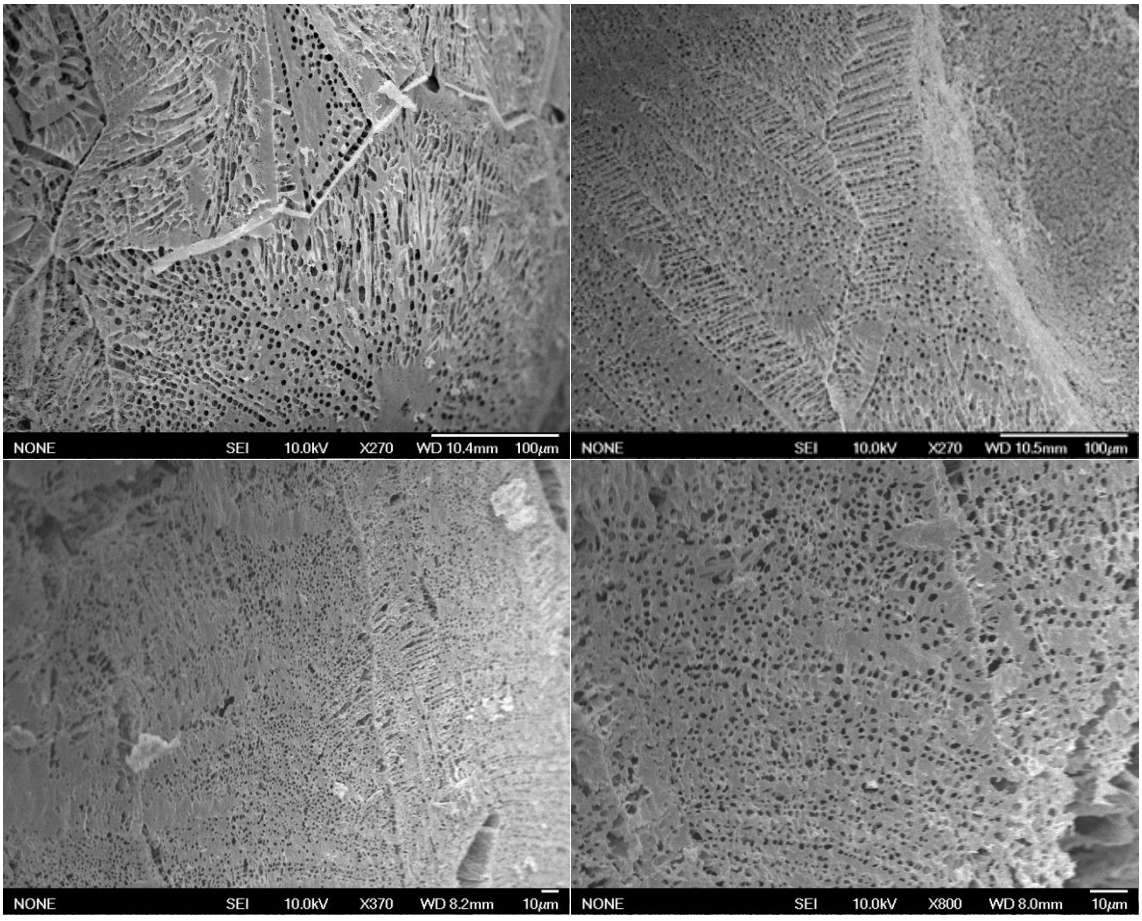

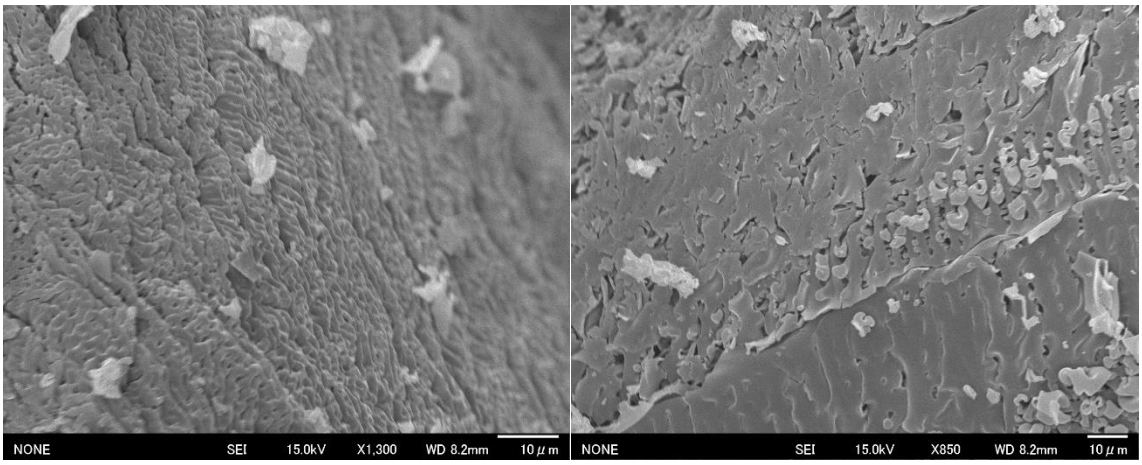

Figure 4.9: SEM images of the external surface from the samples obtained from solution a,b and c respectively.

We then focused on the images of the cross section of the lyophilized particles. We tried to cut the particles into two parts. After that, we used SEM to collect as many pictures as possible, the most significative one is presented in Figures 4.10- 4.12.

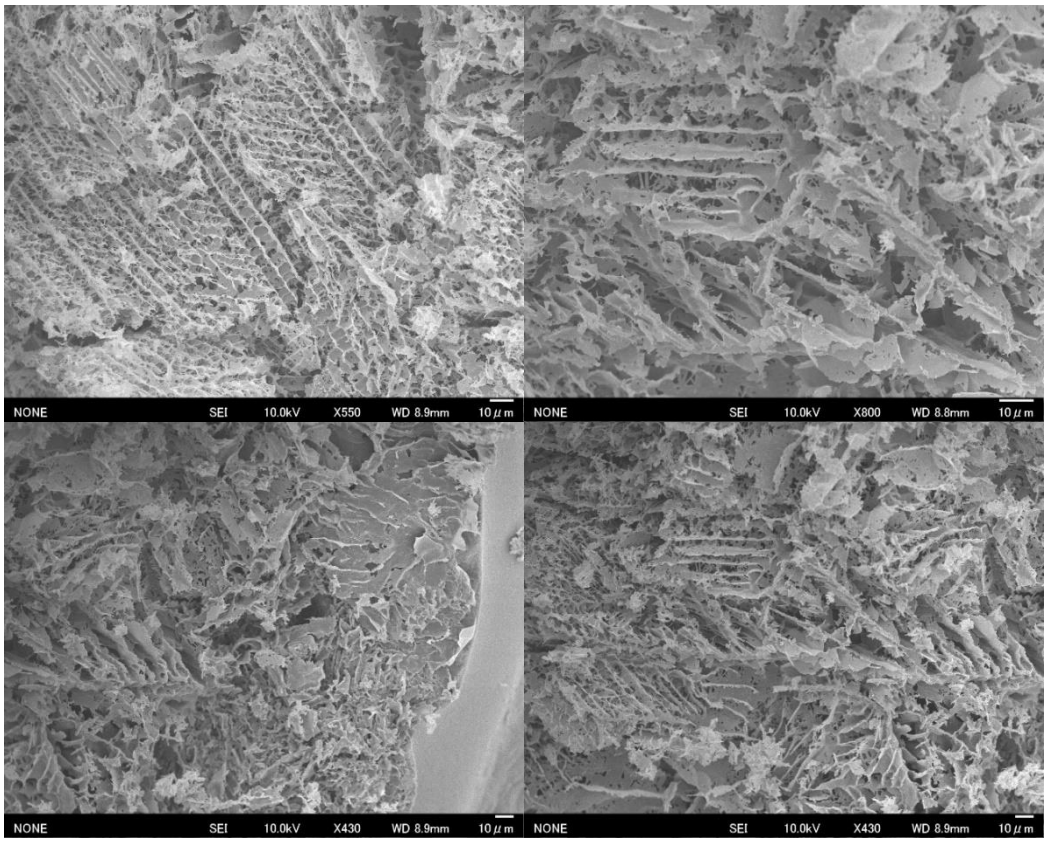

Figure 4.10: SEM images of the cross section from sample a.

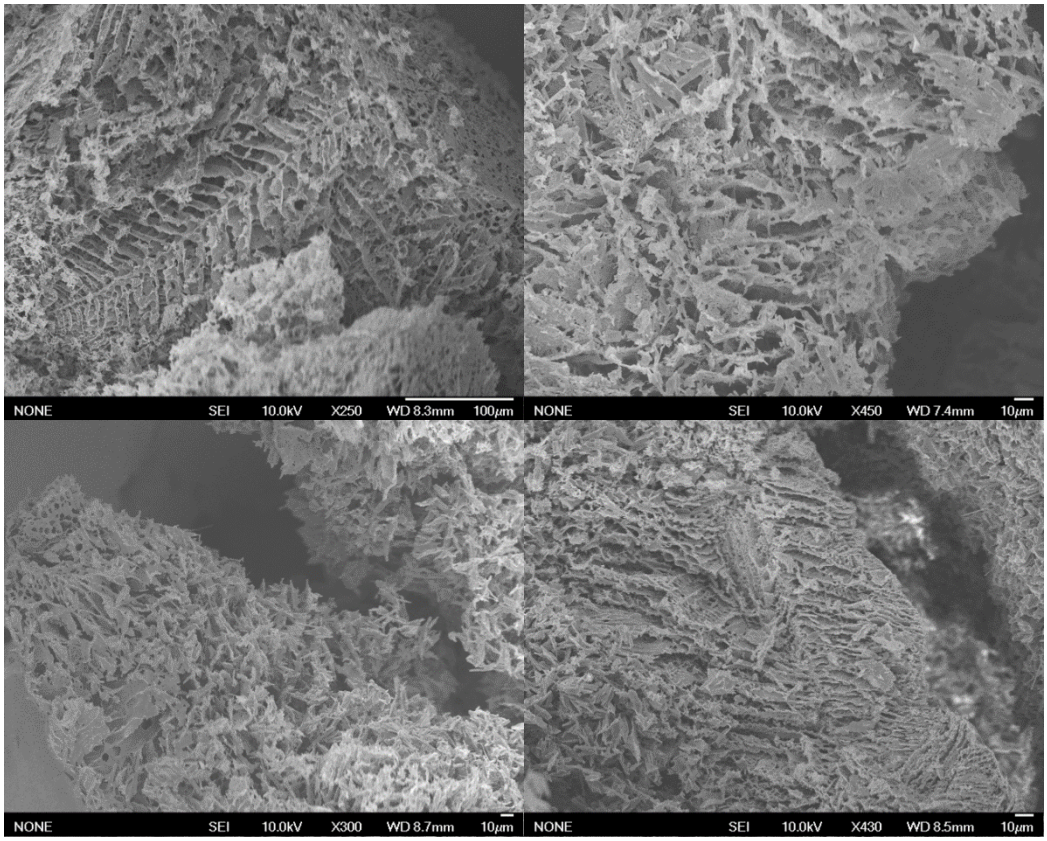

Figure 4.11: SEM images of the cross section from sample b.

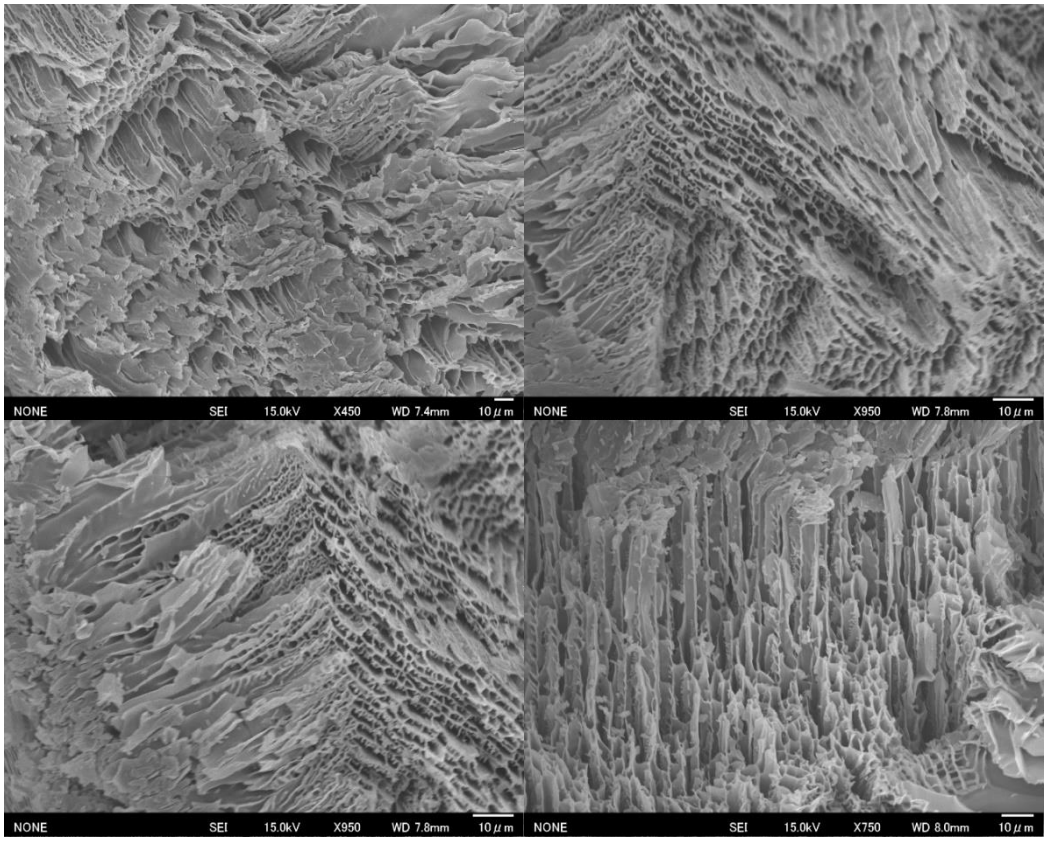

Figure 4.12: SEM images of the cross section from sample c.

From Figures 4.10-4.12, it can be observed how the void left by the ice looks like ropes, organized in bundles with a certain orientation. They suggest the idea, which find a theoretical validation, of the dendritic growth of ice during freezing like the branches of a tree. The pictures were analyzed with *ImageJ* (vers. 1.49). The values of the diameters were collected, and a pore size distribution obtained. These distributions are shown in the Figure 4.13 representing the pores population for each solution prepared.

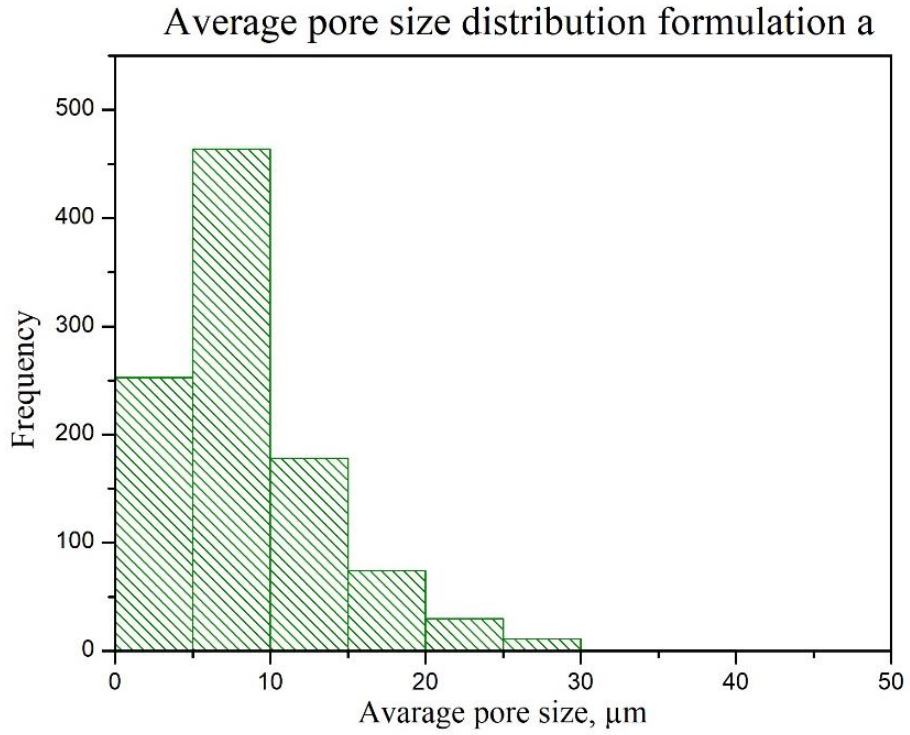

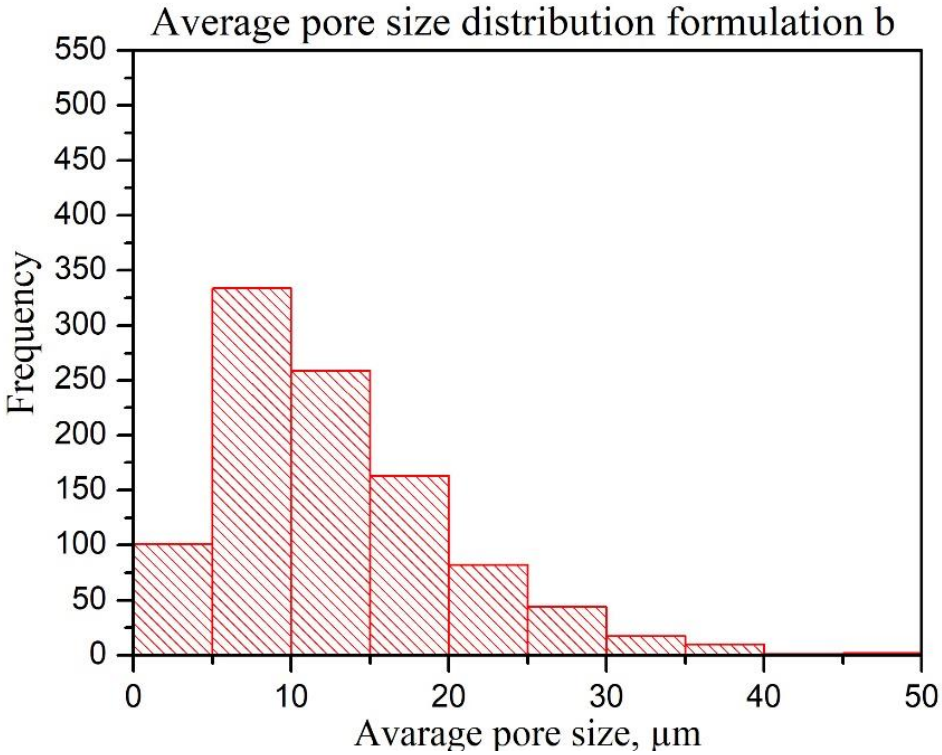

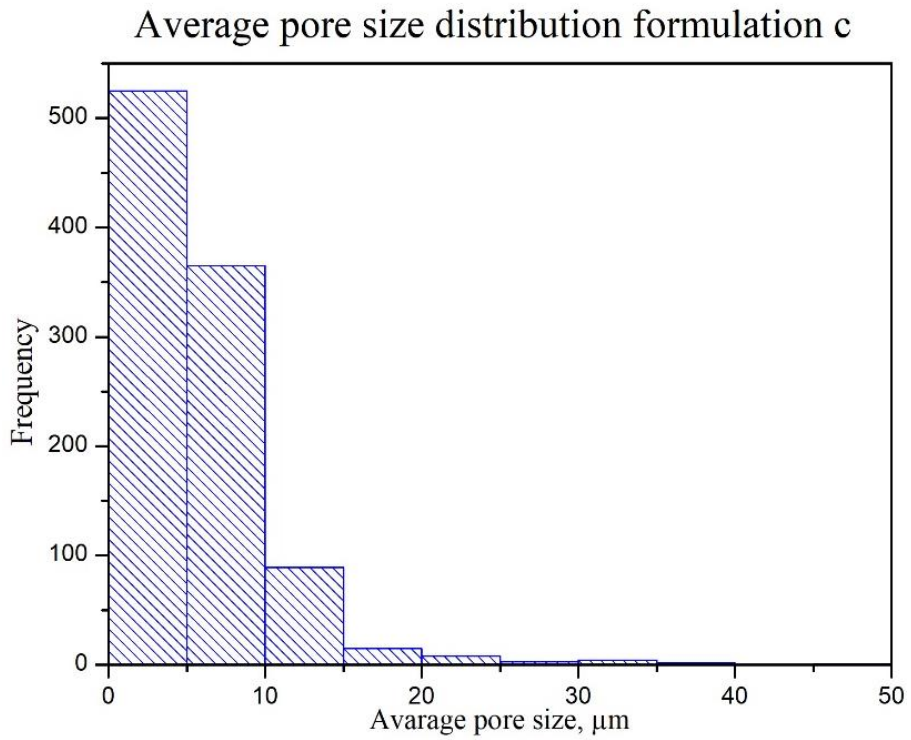

Figure 4.13: pore size distribution for the three formulations

The distributions differ both between formulations with different composition (solution A and B compared to C) that between the ones with the same solute but at different concentration (solution A vs B). From their distribution the pores of solution B appear to be larger than the ones of solution A, in fact a significantly lower proportion of particles of B has a diameter < 5 µm and the bars of the distribution are displaced on the right. Comparing mannitol to the trehalose solutions it is possible to notice how the distribution of solution C, being narrower, suggests a more uniform size of the pores. This is an advantage since it makes easier to tune the homogeneity of size of the final particles obtained, hence having a much higher control on the process outcome. The average size is also smaller than in the other two cases. This is due to the nature of the sugars used: mannitol being crystallin gives a contribute to the pore with the arrangement of its structure, increasing the dimension of the pores and hence the porosity of the material; trehalose is amorphous so the pores detected are created only by water sublimating. For each formulation we calculated a medium value to compare with the one obtained from the model, the results are listed in table 4.4.

Table 4.4: Average pore size values of each formulation tested.

Formulations	Average pore size, µm
A	8.7
B	12.7
C	6.1

To validate the model, equation 2.36 has been used to calculate the correspondent value of D_p for a particle diameter determined with ImageJ from SEM images. A particle has been chosen as representative of sample C (which has given the most convincing results), its diameter has

been measured and resulted of 1.5 mm. Putting this diameter in eq. 2.36 it is possible to calculate the expected D_p (Table 4.5).

Table 4.5: Particle diameter used to evaluate the Dp provided by the equation obtained by the simulation on COMSOL vers 5.3.

Diameter,mm	Dp, µm
2	5.73

The value obtained of D_p (Table 4.6) is very close to one detected experimentally but is understandable considering that the measurements made of the pores diameters with ImageJ could be affected by errors due to the not absolute precision of the program itself.

Table 4.6: Comparison between the theoretical and experimental values referred to sample C.

Theoretical value, µm	Experimental value, µm
5.73	6.1

Considering the difference in operating condition between the simulation made in Turin and the experimental work in Kyoto the model can be consider as valid. On COMSOL the particles were simulated falling into a column full of cryogenic fluid while in the laboratory we used liquid nitrogen in a tray. Moreover, we must consider the possible errors in the detection of the diameters also due to the cut made on the particles which could break the pores affecting the image obtained.

Chapter 5

Conclusion and future developments

This Thesis deals with the problem of spray freeze-drying of pharmaceutical formulation. The study of this unitary operation was carried out with the aim of developing an optimal freeze-drying process in terms of quality of the final product, product dynamics as well as the capacity of additives to preserve the active pharmaceutical ingredient against freezing and drying stresses (testing two mannitol-based solutions and a trehalose-albumin based solution).

These advantages, combined with the exceeding of limits that are typical of existing drying methods, show the superiority of SFD. Therefore, this work focused on the description, modelling and subsequent experimental validation of an SFD process used for a pharmaceutical solution. After describing the salient characteristics, the mathematical model used to describe the freezing phase was illustrated. In this model we used two source terms that, introduced in the enthalpy balance, allow to describe the generation of heat due respectively to nucleation and latent heat of crystallization.

For this reason, the procedure and the results obtained in the prediction, by using the simulation software COMSOL vers 5.3, of the average diameter of the ice crystals and of their distribution when the particle diameter changes were shown. The model developed in this thesis was implemented in COMSOL vers 5.3 during the period carried out at the Polytechnic of Turin and validated using experimental data collected through the freeze-dryer of Kyoto University.

It has been found that the tuning is good, so the mathematical description adopted is adequate and allows to carry out predictive analysis. In order to increase the productivity and the uniformity of the operating conditions in which the solutions are processed, the model developed in this work could provide a valid support to the understanding of the mechanisms involved and to the prediction of the behavior of the process.

There is a wide margin for improvement and experimentation starting from the variation of the solution used and the improvement of both the lyophilizer used and the atomizer available in Kyoto to an industry scale.

Bibliography

Arsiccio, A., Barresi, A. A. and Pisano, R. (2017) 'Prediction of Ice Crystal Size Distribution after Freezing of Pharmaceutical Solutions', *Crystal Growth and Design*, 17(9), pp. 4573–4581.

Banga, J. R. and Paul Singh, R. (1994) 'Optimization of air drying of foods', *Journal of Food Engineering*, 23(2), pp. 189–211.

Berberović, E. *et al.* (2018) 'Computational modeling of freezing of supercooled water using phase-field front propagation with immersed points', *International Journal of Multiphase Flow*. Elsevier Ltd, 99, pp. 329–346.

Claussen, I. C. *et al.* (2007) 'Atmospheric freeze drying - A review', *Drying Technology*, pp. 947–957.

Cleland, J. L., Powell, M. F. and Shire, S. J. (1993) 'The development of stable protein formulations: A close look at protein aggregation, deamidation, and oxidation', *Critical Reviews in Therapeutic Drug Carrier Systems*, pp. 307–377.

Donohue, M. D. and Aranovich, G. L. (1998) 'Classification of Gibbs adsorption isotherms', *Advances in Colloid and Interface Science*. Elsevier, 76–77, pp. 137–152.

Doymaz, I. (2004) 'Drying kinetics of white mulberry', *Journal of Food Engineering*, 61(3), pp. 341–346.

Evans, J. A. (2009) *Frozen Food Science and Technology*, *Frozen Food Science and Technology*. Blackwell Publishing Ltd.

Fissore, D. and Barresi, A. A. (2011) 'Scale-up and process transfer of freeze-drying recipes', *Drying Technology*, 29(14), pp. 1673–1684.

Fissore, D., Pisano, R. and Barresi, A. (no date) *Freeze drying of pharmaceutical products*.

Grace, J. R. *et al.* (1978) *Bubbles, Drops, and Particles*.

Her, J. Y. *et al.* (2010) 'Preparation of kanamycin powder by an optimized spray freeze-drying method', *Powder Technology*, 199(2), pp. 159–164.

Holzwarth, M. *et al.* (2012) 'Evaluation of the effects of different freezing and thawing methods on color, polyphenol and ascorbic acid retention in strawberries (Fragaria×ananassa Duch.)', *Food Research International*, 48(1), pp. 241–248.

Jena, S. *et al.* (2019) 'Stability of lyophilized albumin formulations: Role of excipient crystallinity and molecular mobility', *International Journal of Pharmaceutics*. Elsevier B.V., 569.

Jennings, T. (1999) 'Lyophilization: introduction and basic principles'. Available at: https://content.taylorfrancis.com/books/download?dac=C2009-0-22366-X&isbn=9781439806074&format=googlePreviewPdf (Accessed: 29 November 2019).

Johnson, R. E., Kirchhoff, C. F. and Gaud, H. T. (2002) 'Mannitol-sucrose mixtures - Versatile formulations for protein lyophilization', *Journal of Pharmaceutical Sciences*. John Wiley and Sons Inc., 91(4), pp. 914–922.

Kasper, J. C. and Friess, W. (2011) 'The freezing step in lyophilization: Physico-chemical fundamentals, freezing methods and consequences on process performance and quality attributes of biopharmaceuticals', *European Journal of Pharmaceutics and Biopharmaceutics*, pp. 248–263.

Kawasaki, H., Shimanouchi, T. and Kimura, Y. (2019) 'Recent Development of Optimization of Lyophilization Process', *Journal of Chemistry*. Hindawi Limited, 2019.

Mason, B. J. (1953) 'The growth of ice crystals in a supercooled water cloud', *Quarterly Journal of the Royal Meteorological Society*, 79(339), pp. 104–111.

Mujumdar, A. S., Huang, L.-X. and Dong Chen, X. (2010) 'An overview of the recent advances in spray-drying An overview of the recent advances in spray-drying Article published by EDP Sciences', *Dairy Sci. Technol*, 90(3), pp. 211–224.

Nireesha, G. R. *et al.* (2013) *Lyophilization/Freeze Drying-An Review*. Available at: www.ijntps.com (Accessed: 29 November 2019).
Oetijen, G. W. and Haseley, P. (2004) 'Freeze-drying.', *Freeze-drying.* WILEY-VCH Verlag GMBH & Co. KGaA, (Ed.2).
Oetjen, G.-W. and Haseley, P. (2004) *Freeze-drying.* Wiley-VCH.
Patel, S. M., Doen, T. and Pikal, M. J. (2010) 'Determination of end point of primary drying in freeze-drying process control', *AAPS PharmSciTech*, 11(1), pp. 73–84.
Pikal, M. J. *et al.* (1990) 'The secondary drying stage of freeze drying: drying kinetics as a function of temperature and chamber pressure', *International Journal of Pharmaceutics*, 60(3), pp. 203–207.
Pisano, R. and Capozzi, L. C. (2017) 'Prediction of product morphology of lyophilized drugs in the case of Vacuum Induced Surface Freezing', *Chemical Engineering Research and Design*. Institution of Chemical Engineers, 125, pp. 119–129. d
Prestrelski, S. J. *et al.* (1993) 'Dehydration-induced conformational transitions in proteins and their inhibition by stabilizers', *Biophysical Journal*, 65(2), pp. 661–671.
Sadikoglu, H., Ozdemir, M. and Seker, M. (2006) 'Freeze-drying of pharmaceutical products: Research and development needs', *Drying Technology*, 24(7), pp. 849–861.
Sarciaux, J. M. *et al.* (1999) 'Effects of buffer composition and processing conditions on aggregation of bovine IgG during freeze-drying', *Journal of Pharmaceutical Sciences*. American Chemical Society, 88(12), pp. 1354–1361.
Shimada, W. and Furukawa, Y. (1997) 'Pattern Formation of Ice Crystals during Free Growth in Supercooled Water', *The Journal of Physical Chemistry B*, 101(32), pp. 6171–6173.
Sing, K. (2001) 'The use of nitrogen adsorption for the characterisation of porous materials', in *Colloids and Surfaces A: Physicochemical and Engineering Aspects*. Elsevier, pp. 3–9.
Sonner, C., Maa, Y. F. and Lee, G. (2002) 'Spray-freeze-drying for protein powder preparation: Particle characterization and a case study with trypsinogen stability', *Journal of Pharmaceutical Sciences*. John Wiley and Sons Inc., 91(10), pp. 2122–2139.
Troller, J. A. and Christian, J. H. B. (1978) *Water activity and food*. Academic Press.
Valdenegro M *et al.* (2013) 'The Effects of Drying Processes on Organoleptic Characteristics and the Health Quality of Food Ingredients Obtained from Goldenberry Fruits (Physalis peruviana)'.
Vishali, D. A. *et al.* (2019) 'Spray freeze drying: Emerging applications in drug delivery', *Journal of Controlled Release*. Elsevier B.V., pp. 93–101..

List of symbols

a_w	water activity, -
C_p	specific heat capacity, $JKg^{-1}K^{-1}$
$C_{p,app}$	apparent specific heat capacity, $JKg^{-1}K^{-1}$
$C^*_{p,app}$	average apparent specific heat capacity, $JKg^{-1}K^{-1}$
Cpi	heat capacity of ice, $JKg^{-1}K^{-1}$
$\boldsymbol{C_{pw}}$	heat capacity of water, $JKg^{-1}K^{-1}$
C	solutes mass fraction, -
C'_g	maximally freeze concentrated mass fraction of solutes, -
D_p	size of ice crystals/pores, m
D_s	diffusion coefficient of solutes, m^2 s-1
h	heat transfer coefficient for air natural convection, J s−1m−2 K−1
h_s	heat transfer coefficient between the technical fluid and the shelf, J s−1m−2 K−1
H	enthalpy, J
ΔHf	latent heat of crystallization, J kg−1
k	thermal conductivity, J s−1m−1 K−1
k_{air}	thermal conductivity of air, J s−1m−1 K−1
k_n	rate constant of nucleation, kg s−1m−3 K−1
k_n	rate of nucleation per unit of volume m s^{-1} m^{-3}
m	mass of a water molecule, kg
m_{wn}	mass of water crystallized at nucleation, kg
m_{wf}	mass of freezable water, kg
P_v	equilibrium vapor pressure, Pa
P_{sat}	saturation pressure, Pa
Q_c	heat flux of crystallization, J s−1m−2
Q_e	heat flux of evaporation, J s−1m−2
Q_n	heat flux of nucleation, J s−1m−2
r	radial coordinate, m
S	r-position of the solid–liquid interface, m
S_{ice}	surface of ice crystals, m^2
t	time, s
t_n	freezing time, s
T_0	solution temperature at t=0, K
T_{air}	temperature of the cooling media, K
T_f	equilibrium freezing temperature, K
T_e	eutectic temperature, K
$Tmax$	temperature at the mushy zone–liquid inter face, K
$Tmin$	temperature at the mushy zone–solid interface, K
T_n	nucleation temperature, K
X_{ice}	mass fraction of ice, kg m−3

Greek letters

α	parameter of Eq. (2.15)
β	exponent of Eq. (2.13)
γ	temperature gradient within the frozen zone, K
δ	crystal inclination angle
ε	ratio between the volume of ice and the total volume of the system
θ	temperature gradient within the frozen zone, K m−1
θ, φ	angular coordinate, rad
λ_1	parameter of Eq. (2.15)
λ_2	parameter of Eq. (2.15)
ν	freezing front rate, m s−1
ρ	mass density, kg m−3
ρ^*	average mass density, kg m−3
ϱ_{ice}	density of ice, kg m−3
ϱl	density of the liquid, kg m−3
τ	tortuosity
ϕ	fraction of water which crystallizes, -
ξ	thickness of the undercooled zone, m

Abbreviation

FD	Freeze drying
SPD	Spray freeze drying
SEM	Scanning electron microscopy
BET	Brunauer-Emmett-Teller
XRD	X ray-diffraction